Calhoun: The NPS Institutional Archive

DSpace Repository

Theses and Dissertations | 1. Thesis and Dissertation Collection, all items

2009-06

Hardware model of a shipboard generator

Elkins, Gregory L.

Monterey California. Naval Postgraduate School

http://hdl.handle.net/10945/4300

This publication is a work of the U.S. Government as defined in Title 17, United States Code, Section 101. Copyright protection is not available for this work in the United States.

Downloaded from NPS Archive: Calhoun

http://www.nps.edu/library

Calhoun is the Naval Postgraduate School's public access digital repository for research materials and institutional publications created by the NPS community. Calhoun is named for Professor of Mathematics Guy K. Calhoun, NPS's first appointed -- and published -- scholarly author.

Dudley Knox Library / Naval Postgraduate School
411 Dyer Road / 1 University Circle
Monterey, California USA 93943

Hardware Model of a Shipboard Generator

By
Gregory L. Elkins
B.S. Chemical Engineering
West Virginia Institute of Technology, 1998

SUBMITTED TO THE DEPARTMENT OF MECHANICAL ENGINEERING IN PARTIAL FULFILLMENT OF THE REQUIREMENTS FOR THE DEGREES OF

NAVAL ENGINEER
AND
MASTER OF SCIENCE IN MECHANICAL ENGINEERING

AT THE
MASSACHUSETTS INSTITUTE OF TECHNOLOGY
JUNE 2009

© 2009 Massachusetts Institute of Technology. All rights reserved.

The author hereby grants to the Massachusetts Institute of Technology permission to reproduce and to distribute publicly paper and electronic copies of this thesis document in whole or in part in any medium now known or hereafter created.

Signature of Author_____
Department of Mechanical Engineering
May 19, 2009

Certified by_____
Chris Schantz
Department of Mechanical Engineering
Thesis Reader

Certified by_____
Steven B. Leeb
Professor of Electrical Engineering and Computer Science & Mechanical Engineering
Thesis Supervisor

Accepted by_____
David E. Hardt
Chairman, Department Committee on Graduate Students
Department of Mechanical Engineering

(This Page Intentionally Left Blank)

Hardware Model of a Shipboard Generator

By
Gregory L. Elkins

Submitted to the Department of Mechanical Engineering on May 19, 2009 in Partial Fulfillment of the Requirements for the Degrees of

Naval Engineer
and
Master of Science in Mechanical Engineering

Abstract

A hardware model of the Gas Turbine Generator (GTG) in use on the US Navy's DDG-51 Class Destroyer is constructed for use as a lab apparatus at the Massachusetts Institute of Technology's Laboratory for Electromagnetic and Electronic Systems (LEES). The components of the hardware model include a 5 kilowatt three-phase generator; DC power supplies and motors that function as the prime mover; computer software to implement speed and voltage control; and an input-output interface board that passes measurement and controller signals to and from the software environment.

A numerical Simulink model of the GTG is developed that provides speed response to a change in electrical loading. The GTG model takes into account basic physical characteristics of gas turbine generators and is tuned to provide a response similar to that of the destroyer's Allison 501-K34 GTG. An empirical open-loop model of the tabletop generator is also developed in Simulink and subsequently provided with closed-loop feedback control. Controller gains are adjusted such that the tabletop's Simulink model provides a response likened to the GTG model.

Proportional and Integral (PI) control of the tabletop generator is implemented in the software environment. The tabletop generator's response to a certain electrical transient is compared to the GTG response predicted by the Simulink model. Recommendations to improve the response of the tabletop generator are made based on analysis of actual speed sensor noise.

Thesis Supervisor: Steven B. Leeb
Professor of Electrical Engineering and Computer Science & Mechanical Engineering

Thesis Reader: Chris Schantz
Department of Mechanical Engineering

Acknowledgements

The following are recognized in the accomplishment of this work.

- Dr. Steven Leeb for his guidance and support throughout this effort.
- Dr. Robert Cox for his continued support of the research being conducted at LEES.
- Vanessa Esch's implementation of the control scheme in the software environment while working on an Undergraduate Advanced Project.
- Jacob Osterberg's development of speed and voltage signal conditioning while working through the Undergraduate Research Opportunity Program.
- Chris Schantz for thinking to look on ebay for a small 3-phase generator and his assistance in the lab.
- Warit Wichakool for his knowledge and assistance throughout while he continues research at LEES.
- Jeremy Leghorn and Keith Douglas for their camaraderie as we worked together to progress NILM research field studies being conducted at LEES.
- Naval Sea Systems Command for placing me here to advance my education.
- My family, without which there would not be much point in this effort.

Table of Contents

List of Figures

List of Tables

Chapter 1

Introduction

Research being conducted at the Massachusetts Institute of Technology's Laboratory for Electromagnetic and Electronic Systems (LEES) includes shipboard applications of Non-Intrusive Load Monitoring (NILM) to reliably monitor and track diagnostic conditions of critical systems. The NILM's potential to disaggregate individual loads from bus current and voltage may provide future electrical protection systems with valuable information to protect critical loads [1].

The Multi-Function Monitor (MFM) is currently employed to protect the Zonal Electrical Distribution (ZED) of modern ships. The MFM uses current sensors located on the main busses of the ship. This is considered a natural entry point for NILM to monitor multiple loads from a single point [1]. In addition to its current use on warships, ZED is a central concept in the architecture of the Next Generation Integrated Power System (NGIPS) [2].

Reliable technology is required to implement Power Distribution Modules (PDM) and Power Control (PCON) as called out in the NGIPS roadmap [2]. The power monitoring being demonstrated at MIT is considered critical enabling technology for future PDM and PCON devices [1].

This thesis describes the construction of a hardware model of the Gas Turbine Generator (GTG) in use on the US Navy's DDG-51 Class Destroyer. This hardware model of a ship's generator may be utilized in a scale model of a ship's electrical power distribution system. Subsequent simulations of shipboard electrical faults will allow for the advancement of power monitoring technologies.

The equipment used in the hardware model is briefly described in the first two sections of Chapter 2. Section 2.3 details the characterization of the DC motor and evaluates the best suited gear ratio between the generator and prime mover. A potential gearbox is included

in the gear ratio discussion that may be utilized in lieu of existing timing belt pulleys. Chapter 3 provides an overview of gas turbines. This includes shipboard application of gas turbine generators; the basic design and classification of gas turbines; and discussion of gas turbine control and modeling.

Simulink models of the GTG and the tabletop generator are developed in Chapter 4. The GTG model follows from the control and modeling discussed in Section 3.3. The GTG model is initially tuned to meet response specifications. Minor adjustments are then made to key parameters in the model to match actual response data.

Section 4.2 discusses the empirical development of the open-loop model for the tabletop generator. This system identification is performed in two distinct steps. First, a Simulink model simulates the response to a change in electrical loading while terminal voltage to the DC motor is held constant. This captures the self regulating aspect of a DC motor as discussed in Section 2.3. Building on this model, the second step incorporates the effect that a change in terminal voltage has on speed. In this open-loop test, a change in terminal voltage drives the speed response with the generator's electric load held constant.

Following the open-loop modeling of Section 4.2, closed-loop feedback control of the tabletop generator is modeled in Section 4.3. The closed-loop model is tuned to provide a response similar to the GTG model for a specific change in electrical loading. The closed-loop model is then evaluated for the following: sensitivity to a key parameter that showed deviation in open-loop modeling; exclusion of estimated power losses; and variation in step changes of the electric load.

A physical description of the hardware model is provided in Chapter 5 along with response testing results. Recommendations to improve the response of the tabletop generator are made based on analysis of actual speed sensor noise. Conclusions and future work are discussed in Chapter 6.

Implementation of the control scheme in the software environment was conducted by Vanessa Esch while working on an Undergraduate Advanced Project. Signal conditioning of speed and voltage measurements was developed by Jacob Osterberg while working through the Undergraduate Research Opportunity Program. Their work is shown in its entirety in the Appendices. Though some information is duplicated and conflicts may exist, no attempt was made to modify or summarize their reports. This preserves the insight of three observers involved on one project.

Chapter 2

Initial Design Considerations

The equipment used in the hardware model is briefly described in the first two sections of Chapter 2. Section 2.3 details the characterization of the DC motor and evaluates the best suited gear ratio between the generator and prime mover. A potential gearbox is included in the gear ratio discussion that may be utilized in lieu of existing timing belt pulleys.

2.1 Generator

Obtaining a reasonably sized three phase AC generator was the starting point for creating the tabletop model of a shipboard generator. Some initial effort was put forth in utilizing a large truck alternator which produces a three phase current prior to its rectification for use in the truck's DC power system. However, given that alternators are intended to produce DC power and are thus not restricted in their speed; operation of the alternator at a speed to provide a frequency of 60 Hz results in an undesirably low power output. Alternator conversion kits exist that provide reasonable 60 Hz power output. Conversion of an alternator requires additional windings on the armature to provide more power at a slower speed. This was deemed impractical, removing the alternator from further considerations.

Three phase generators are typically associated with large industrial applications and are not readily available in smaller power ratings. The search for a smaller three phase generator resulted in the purchase of the 5 KW machine shown in Figure 1. Generator nameplate data is shown in Figure 2. These generators are primarily intended for use in remote or otherwise underserved areas where electrical power is either not available or unreliable. Typically, these machines would be driven by a tractor's Power Take-Off (PTO) drive or any other available combustion engine and utilized where exacting control of frequency is not required. Additional specification is included in Appendix C and purchase information is listed in Appendix D.

Figure 1: Generator Head

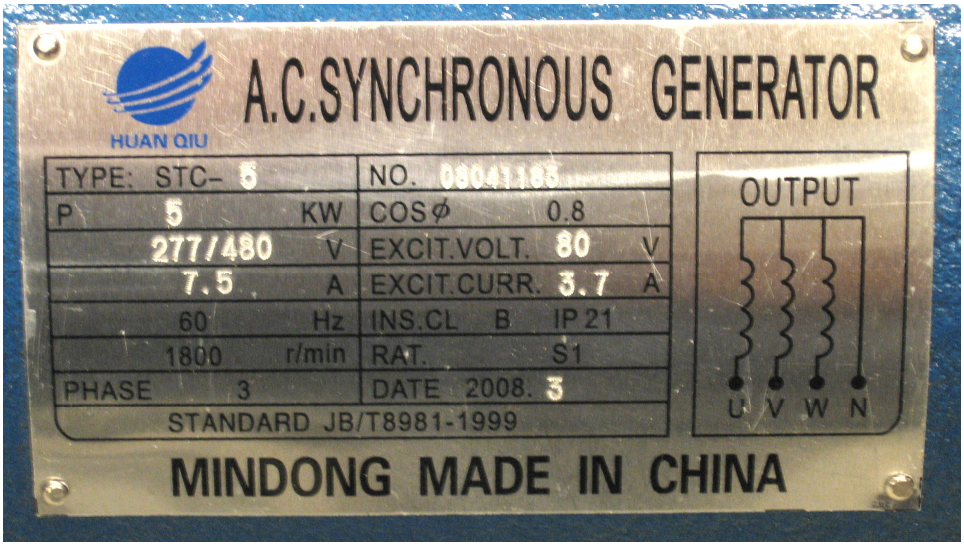

Figure 2: Generator Nameplate

2.2 Prime Mover

A direct current motor was chosen to act as the generator's prime mover due to its inherent controllability as discussed in Section 2.3. Two permanent magnet DC motors chosen from lab inventory are shown coupled together in Figure 3. Each motor is rated at 2 HP as indicated on the nameplate shown in Figure 4. The motors have a drive shaft that extends outward from either side of the motor housing which allows the motor to be centered between two driven loads such as on a treadmill. Rigidly coupling two motors together and connecting them in series electrically provides a rated capacity of 4 HP.

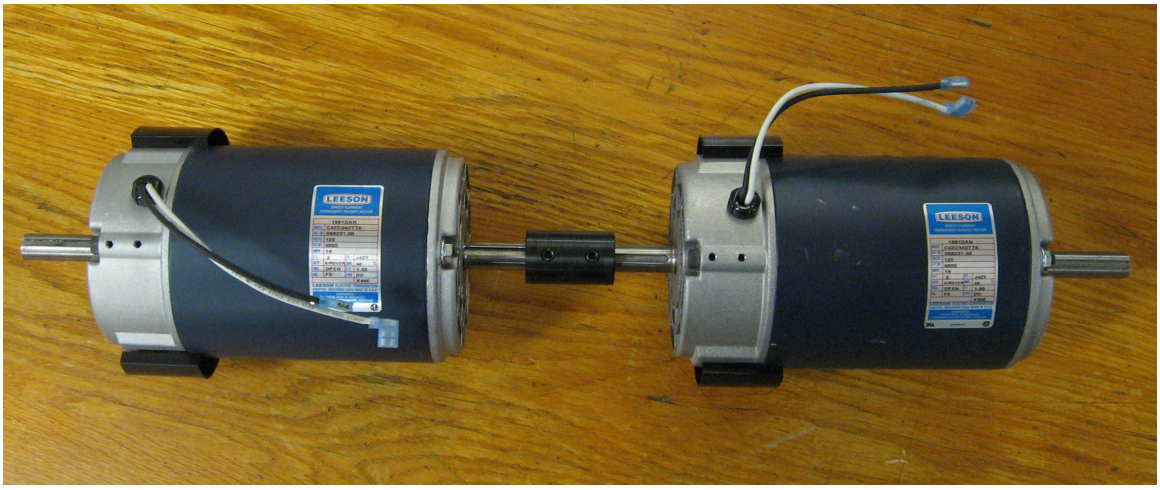

Figure 3: Coupled Motors

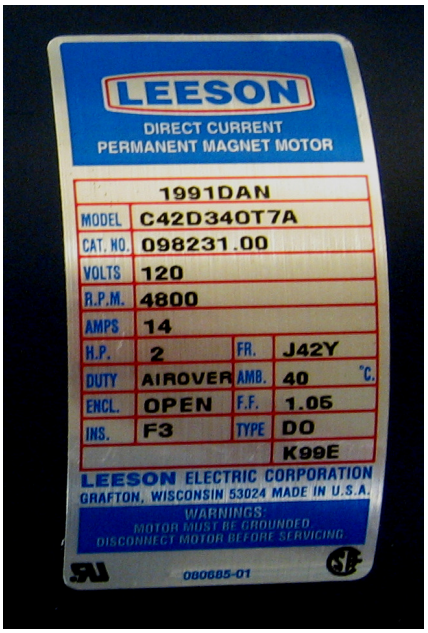

Figure 4: Motor Nameplate

Remote output control of a DC power supply was required to implement speed control of the prime mover. The remote output control feature of a power supply allows a small voltage input, such as from a PC, to direct the voltage output from the power supply to the motor. Two XHR 1000 Watt Series programmable DC power supplies were chosen from lab inventory to meet this requirement. The power supplies were placed in a parallel master-slave configuration to provide a rated output of 150 volts and 14 amps.

2.3 DC Motor Characteristics

The circuit diagram for a permanent magnet DC motor is shown in Figure 5. The inductance of the armature windings is typically neglected in the study of simple DC motors. Kirchhoff's Voltage Law leads directly to the basic equation of a DC motor as shown in Equation 1 [3]. This is the starting point to develop the equations necessary to characterize the DC motor. The equations that follow are utilized in the identification of the best suited gear ratio at the end of this section. The DC motor characteristics and equations are also used in Sections 4.2 and 4.3 where Simulink modeling of the tabletop generator includes the mechanical loading of the motor.

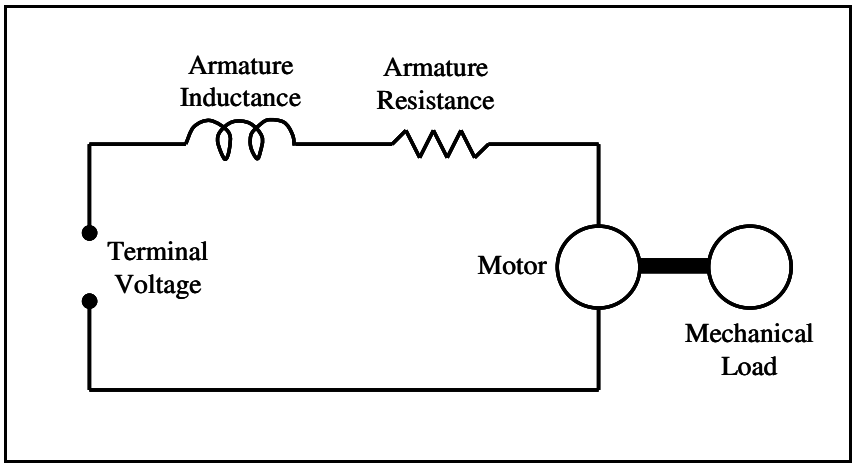

Figure 5: DC Motor Circuit Diagram

Voltage applied to the terminals of the DC motor produces a current on the armature windings. This current is within the influence of a magnetic field produced from either permanently installed magnets or field windings. The current carrying conductor within a magnetic field satisfies the requirements for motor action, producing a force that acts orthogonal to the current flow. A commutator maintains the orientation of the armature current to ensure this force results in motor rotation. Upon rotation of the motor, the conductor travelling within a magnetic field satisfies the requirements for generator action, producing a voltage that counters the applied voltage [3].

$$V_{Term} = I_M R_M + V_C \quad (1)$$

Where: V_{Term} = terminal voltage

I_M = armature current

R_M = armature resistance

V_C = counter voltage (back electromotive force)

If the magnetic field is maintained constant through the use of permanent magnets or by a constant current applied to field windings, then the counter voltage of a DC motor is a linear function of its speed as shown in Equation 2 [3].

$$V_C = K\omega \quad (2)$$

Where: K = motor constant

ω = rotational speed (radians/sec)

The value of the motor constant was determined by mechanically joining two motors as shown previously and applying a range of voltages to the terminals of one of the two motors. With one motor driving the other, the counter voltage of the second at various speeds may be measured directly at its terminals with no current on the armature. Linear regression of the counter voltage data plotted as a function of rotational speed results in a straight line with a slope equal to the motor constant. The result for one of the motor constants is shown in Figure 6 to be 0.215 volt*sec. The second motor tested produced a similar value with a motor constant of 0.217 volt*sec.

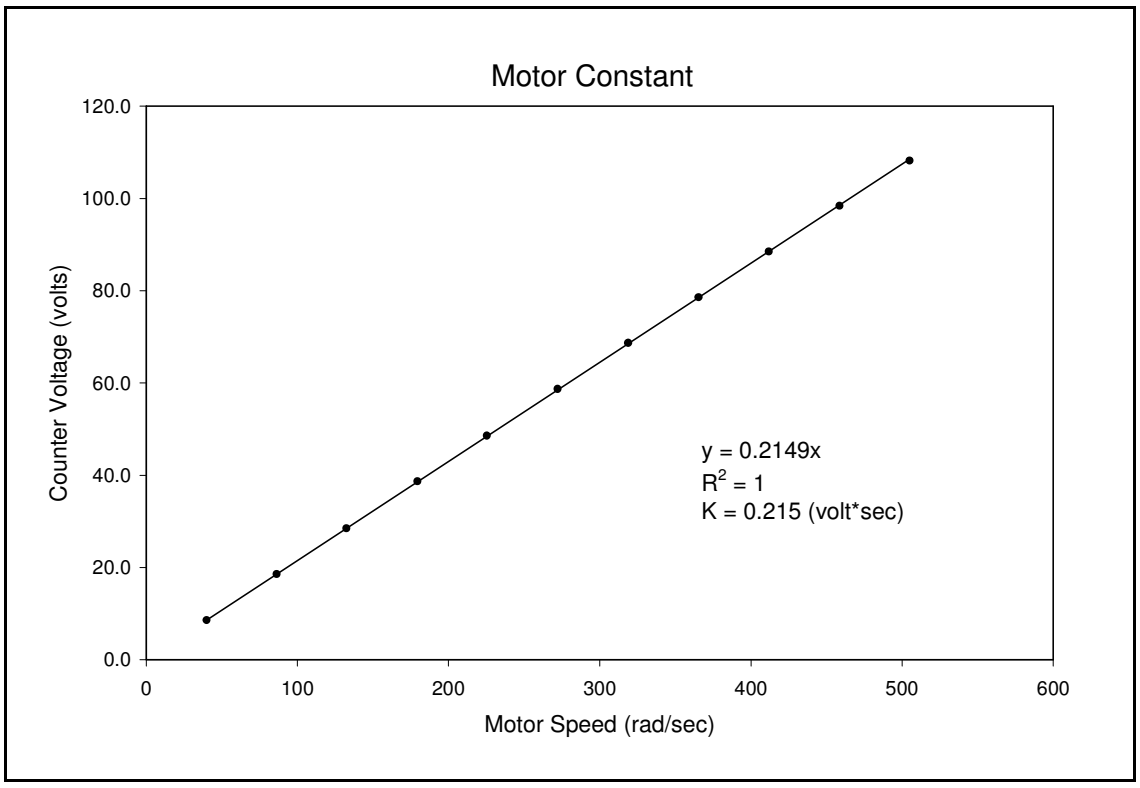

Figure 6: Motor Constant

Power in a simple DC circuit is the product of current and voltage. The voltage drop associated with the armature resistance shown in Equation 1 results in some power lost to heat in the motor. Neglecting frictional heating, the useful mechanical power of the motor (P_M) becomes the product of armature current and counter voltage and may be written as:

$$P_M = K\, I_M\, \omega \quad (3)$$

This result may also be obtained by considering the armature torque that is produced from the interaction of the field and armature flux [3]. This torque is a result of the motor action force mentioned earlier acting at some distance from the center of rotation. Given the constant field flux of the permanent magnet motor, the torque of the motor (T_M) may be written as:

$$T_M = K\, I_M \quad (4)$$

Mechanical power in its simplest form arises from force acting over some distance for some period of time. For rotating machinery, power is the product of torque and rotational speed as shown in Equation 5.

$$P_M = T_M\, \omega = K\, I_M\, \omega \quad (5)$$

Direct current motors have long been utilized in applications requiring speed control. The linear nature of the equations presented above attest to the controllability and inherent stability of the DC motor [3]. For example, increasing the mechanical loading on the motor will initially slow the machine and decrease its counter voltage. Since armature resistance is typically very small, any decrease in counter voltage results in a pronounced increase in armature current. This balances out until a new steady state is reached where the power of the motor equals the mechanical loading at some lowered speed with an increased armature current. In order for the DC motor to return to its initial speed, some operator or automatic control function must occur to raise terminal voltage.

After obtaining the motor constant, a torque-speed curve was developed to further classify the DC motor and provide insight into acceptable motor speeds. Combining Equations 1 and 2, solving for current, and substitution into Equation 4 results in the following:

$$T_M = \frac{K}{R_M} V_{Term} - \frac{K^2}{R_M} \omega \quad (6)$$

Motor resistance was determined at the same time as the motor constant with one motor driving the other. For motor resistance, the counter voltage developed on the slowly driven motor was measured at a specific speed. Shorting the driven motor's terminals through a DC meter and readjusting speed provided the current flow corresponding to the previously measured voltage. Dividing voltage by current resulted in a motor resistance of 0.957 and 0.912 ohms for the two motors tested. With motor constant (K) and motor resistance (R_M) known, Equation 6 was utilized to show how motor torque changes with speed for a given applied terminal voltage. The resulting torque-speed curve for both motors mechanically joined and operating in series electrically is shown in Figure 7.

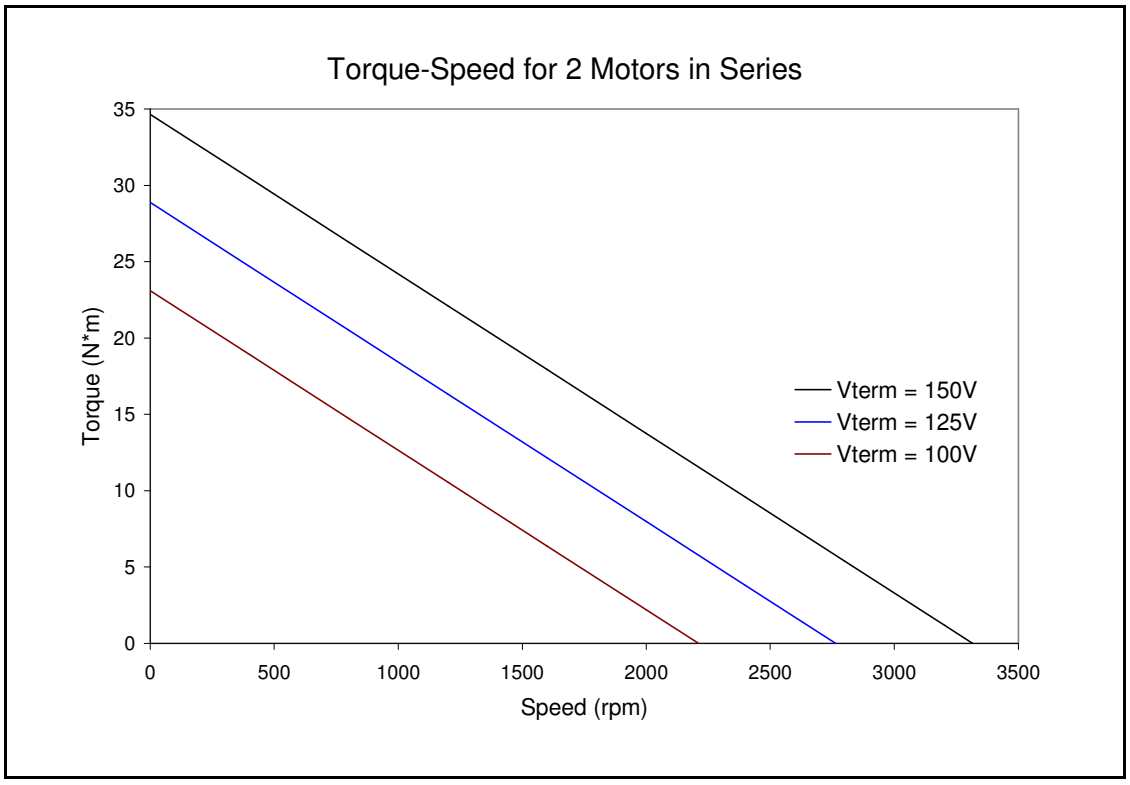

Figure 7: Motor Torque-Speed

The two motors operating in series have a rating of 4800 rpm at 240 volts; however, the power supply is limited to 150 volts. The torque-speed curve was plotted at 100, 125, and 150 volts to allow for evaluation of motor speed given this constraint. From Equations 1 and 2, the motor speed corresponding to a power supply of 150 volts and 14 amps was determined to be 2737 rpm.

$$\omega = \frac{V_{Term} - I_M R_M}{K} \quad (7)$$

Thus, the best suited motor speed would be 2737 rpm to properly deliver power to the prime mover from the power supply. The torque-speed curve indicates that the motor will operate satisfactorily at this speed between 125 and 150 volts. Interpolation of unloaded speed data collected at the same time of motor constant testing indicates the unloaded motors should operate very near 125 volts at 2737 rpm drawing 0.7 amps.

Given the generator must rotate at 1800 rpm to produce power at 60 Hz; the best suited gear ratio is 1.52. Any deviation from this gear ratio will limit the maximum output of the power supply. From Equation 7, in order for the motor to operate at a higher speed, given that the terminal voltage is limited in value, the motor current must decrease. Thus, for a larger gear ratio, the power supply will become voltage limited, reaching 150 volts at a current less than the rated peak. Conversely, a smaller gear ratio will result in a current limited power supply where 14 amps is reached prior to 150 volts.

For the purposes of this work, essentially a thorough feasibility study, the motor and generator were mounted aside one another on a rigid platform. The motor was mechanically coupled to the generator via L Series timing belt pulleys and a 1/2 inch timing belt. This is later shown in Chapter 5 with the physical description of the hardware model. Given the initial purchase of a generator pulley with 32 teeth from preliminary work involving one 1.5 HP motor, the readily available gear ratios were either 1.6 or 1.4545 corresponding to a new motor pulley with 20 or 22 teeth respectfully.

By fixing either terminal voltage at 150 volts for ratios larger than 1.52 or current at 14 amps for smaller ratios, Equation 7 can be used to show how various gear ratios limit the use of the power supply. Table 1 compares the two ratios above for this initial design and includes two variations. The first variation is the use of HTD Series pulleys available with 34 and 22 teeth corresponding to a gear ratio of 1.5454. The second variation is an angled Howse Gearbox with a ratio of 1.47 that is included for future consideration.

The Howse Gearbox is designed for a tractor's PTO driven M60 Rough Cut Mower. A tractor's PTO drive operates at 540 rpm to drive a wide assortment of attachments. As such, the intended speed range of this gearbox is approximately 1/5 that of the tabletop motor driven generator. However, it is rated at 55 HP, more than 10 times the power driving the generator, and is designed to withstand significant backlash associated with objects hit by a large tractor pulled mower. Given the gearbox's splined shafting and its angled design, it is expected that a fair amount of machining and alignment work would be required for its incorporation.

Specifications and ordering information is included in Appendix D for both the hardware utilized to achieve a gear ratio of 1.4545 and the Howse Gearbox that may be incorporated in future work.

	Gear Ratio	Motor Speed (rpm)	Max Power Supply Output (watts)
L Series (32/20)	1.6	2880	1581
HTD Series (34/22)	1.5454	2782	1938
Best Suited Ratio and Speed	1.52	2736	2100
Howse Gearbox	1.47	2646	2042
L Series (32/22)	1.4545	2618	2025

Table 1: Gear Ratio Comparison

The gear ratios shown in Table 1 that are less than the best suited ratio of 1.52 represent the current limited power supply as discussed previously. This table identifies that it is more advantageous to operate below the best suited speed with regard to utilization of the given power supply. Operation at a slower speed is also beneficial from a torque-speed standpoint as shown in Figure 7. As such, the L Series 22 tooth timing belt pulley was installed on the motor shaft to drive the 32 tooth pulley on the generator. Table 1 also shows that the Howse Gearbox has a well suited gear ratio for this application.

Chapter 3

Gas Turbine Generators

Chapter 3 provides an overview of gas turbines. This includes shipboard application of gas turbine generators; the basic design and classification of gas turbines; and discussion of gas turbine control and modeling. The modeling of a GTG control system discussed in Section 3.3 leads directly to the Simulink model of the Allison 501-K34 GTG shown in Section 4.1.

3.1 Shipboard Application

As will be discussed throughout Sections 3.2 and 3.3, single-shaft gas turbines are inherently better suited for constant speed applications and are typically preferred for production of electrical power when compared to two-shaft gas turbines. The Allison 501-K34 GTG installed on US Navy DDG-51 Class Destroyers is a single-shaft gas turbine with a compression ratio of 10.5 operating at a speed of 14,340 rpm. It is rated to provide a usable output of 4328 HP without bleed air in use and 3523 HP while supplying 2.37 lb/sec of bleed air [4]. Bleed air is air that may be removed from the compressor to provide compressed air to various auxiliary systems throughout the ship.

Given the specifications above, the Allison 501-K34 would be classified as a light industrial gas turbine engine with a high power-to-weight ratio as described at the beginning of Section 3.2. The power ratings correspond to 3227 KW and 2627 KW respectfully. This variation in power rating, dependant on the utilization of bleed air, accounts for discrepancies seen in early literature review where some documents rate the Allison 501-K34 at 3 MW while others identify its rating as 2.5 MW.

The governing system of the shipboard GTG is required to provide isochronous control while allowing for load sharing with other generators operating in parallel with similar governing systems [4]. This is the normal mode of operation with two or three generators

providing power to the ship. An additional droop control mode is included to allow the shipboard GTG to load share with pier side shore-power.

In addition to providing isochronous governing with load sharing capability, the Allison 501-K34 Specification requires the governing system to handle full power load excursions. That is, without bleed air in use, the GTG must withstand the application or removal of its full rated load without exceeding a 2% deviation from its base speed and must recover within 1.5 seconds to stay within 1% of its base speed [4]. The strict speed control placed on the Allison 501-K34 driven generator along with its high power-to-weight ratio attest to the demanding requirements of naval warship machinery.

3.2 Basic Design

Gas turbines are commonly classified based on their intended use and typically fall into one of the following categories: aerospace, light industrial, or heavy industrial. Light industrial gas turbines have high power-to-weight ratios obtained through operation at high combustion and exhaust temperatures along with relatively high compression ratios that typically exceed 7. Structural weight is minimized which generally implies more frequent maintenance. To offset this, light industrial turbines are designed as a single module for easy removal and installation. Thus, a malfunctioning unit may be quickly swapped for a functional gas turbine and sent out for repair. Light industrial gas turbines are limited in their power output to about 10 MW [5].

Gas turbines are also classified based on their physical construction. In a single-shaft gas turbine, the compressor and power turbine share a common shaft. Two-shaft gas turbines have a compressor turbine that drives the compressor located on a common shaft while the power turbine resides on a separate shaft to drive the load. The basic arrangement of a single and a two-shaft gas turbine are shown below [5].

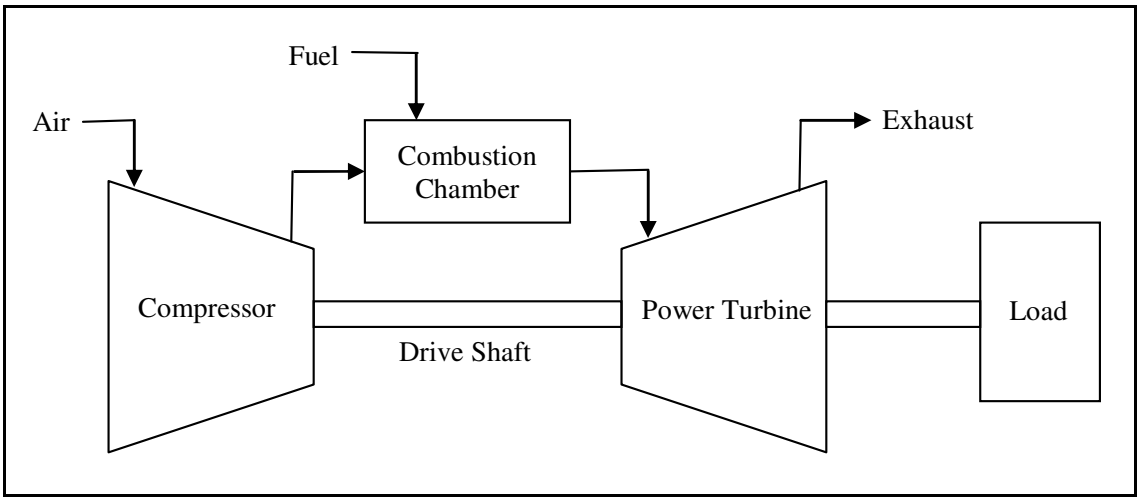

Figure 8: Basic Arrangement of a Single-Shaft Gas Turbine

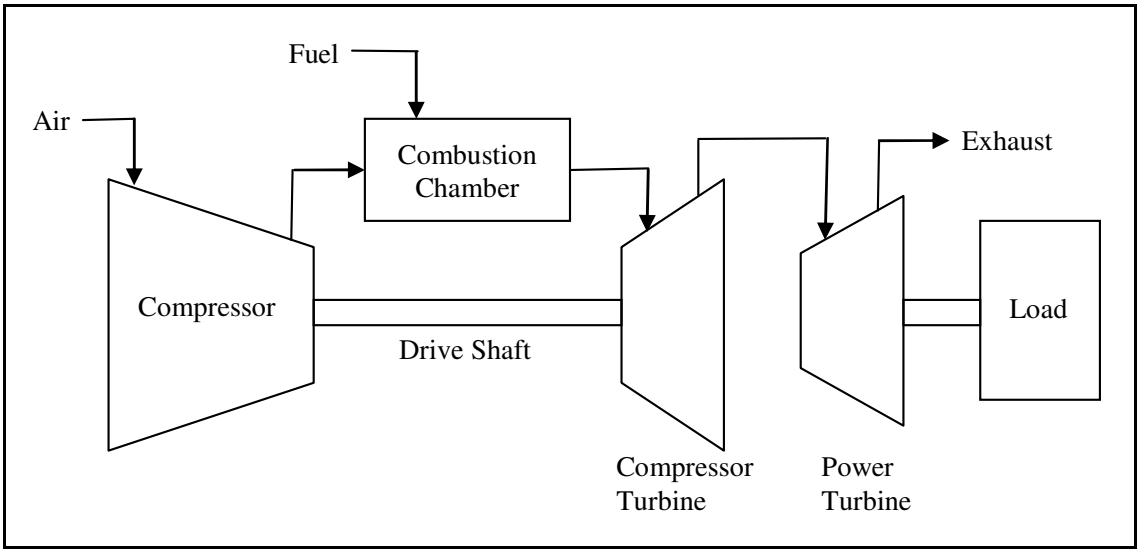

Figure 9: Basic Arrangement of a Two-Shaft Gas Turbine

Two-shaft gas turbines allow both the compressor and the power turbine to operate at their most efficient speeds, allowing for better thermodynamic performance. However, two-shaft gas turbines are slower to respond and are not suitable to drive a generator that must operate in synchronism with other generators [5].

The basic operation of the gas turbine is best described by the Ideal Brayton Cycle that consists of two isobaric and two isentropic processes. Figure 10 shows the applicable Pressure-Volume (P-V) and Temperature-Entropy (T-S) diagrams that describe the thermodynamics of a single-shaft gas turbine [6].

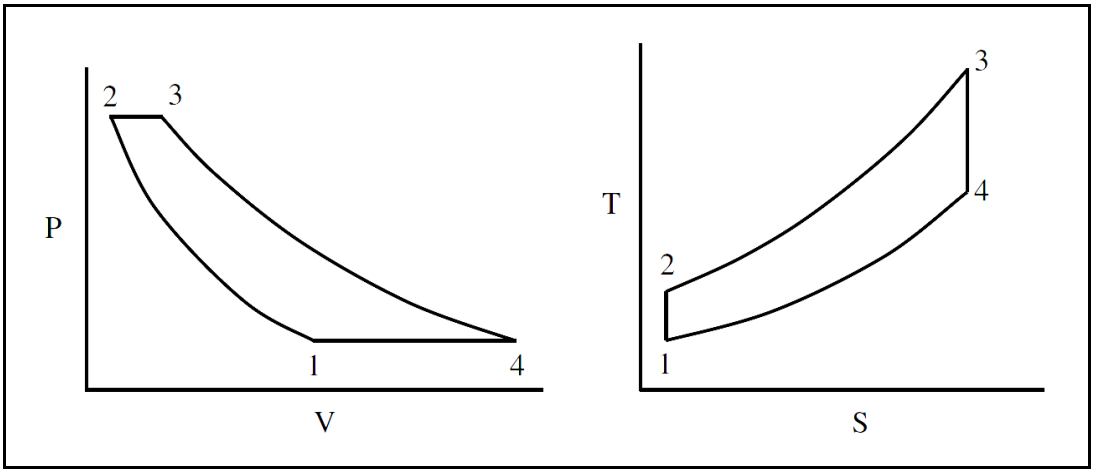

Figure 10: Ideal Brayton Cycle

Referring to Figure 8 and Figure 10, the compressor works on the fluid from 1 to 2, increasing pressure and temperature while decreasing volume at constant entropy. Combustion occurs from 2 to 3, increasing temperature, entropy, and volume at a constant pressure. The compressed and heated fluid expands through the power turbine to perform work from 3 to 4 at constant entropy with an associated decrease in pressure and temperature. Heat is removed from the system from 4 to 1 via the exhaust. Regenerative cycles are often included to capture some of the heat lost through the exhaust [6].

3.3 Basic Control

Control systems ensure a system produces a desired output and are comprised of control loops that may be categorized as either open or closed. In an open loop control system, the input is independent of the output and there usually exists an offset between the output and set point. In the closed loop system, the offset from the open loop response is input to the closed loop controller to moderate the output by adjusting the input. The

closed loop control systems predominately found in use incorporate some combination of proportional (P), integral (I), and derivative (D) action [7].

Proportional control produces a signal proportional to the error between the measured system output and the desired set point. Proportional control alone will result in a steady-state error known as proportional offset if the set point is adjusted. The offset may be alleviated either through operator action (manual reset) or by the inclusion of integral action in the closed loop controller [7].

Integral action occurs as a result of the error being integrated continuously and effectively provides an automatic reset that removes proportional offset. One drawback to inclusion of integral control is the possibility of integral wind-up that may occur if conditions are met such that controller action no longer affects the system output. This may result from actuator saturation where some physical limitation is reached that prevents further response. The resulting steady error will be summed up by the integral action and force unnecessary control when the system re-enters a controllable range [7].

Derivative control looks at the rate of change of the error and is useful to improve transient response when the system is inherently very slow. Derivative action will not counter proportional offset or integral wind-up given these occur with a non-changing error. Derivative control is often omitted in gas turbine control systems. A controller utilizing all three terms (PID) is represented below [7].

$$OP = Er \cdot Kc + \frac{Kc}{Ti}\int Er \cdot dt + Kc \cdot Td\frac{d(Er)}{dt} \quad (8)$$

Where: OP = controller output
Er = error between process output and set point
Kc = controller gain
Ti = integral time
Td = derivative time constant

Gas turbine control systems must also protect the engine from exceeding design limits. This is accomplished with the incorporation of signal selection where additional error signals are generated from the comparison of operating limit set points with current values. Two examples of operating limits that preclude engine damage are Exhaust Gas Temperature (EGT) limit and power turbine speed limit. Signal selection may also be employed to avoid operation near critical speeds where a significant increase in vibration occurs, typically 50 to 70% of design speed for a gas turbine [7].

Single-shaft gas turbines are most suited for fixed speed applications with a resistance to over-speeding resulting from the high power requirements of the compressor. They are typically equipped with Variable Inlet Guide Vanes (VIGV) on the compressor to reduce starting power requirements by reducing airflow through the compressor. The position of the variable guide vanes are adjusted based on EGT. Two schemes exist where one maintains EGT below the operational limit and the other maintains it at the limit during reduced power output. The second is typically employed with combined cycle plants where the hot exhaust gas from the gas turbine is utilized to operate or supplement a steam cycle power plant. In either case, another control scheme is required in addition to that maintaining speed or power [7].

The open-loop or uncontrolled speed-torque characteristic of a gas turbine is not suitable for power generation. Without closed-loop feedback control, the initial speed response to a change in electrical loading is predominately a function of the generator's inertia. A closed-loop gas turbine governor measures and amplifies deviation in speed, sending a response signal to the fuel valve that regulates gas turbine power. At this point, there is an inherent variation between the response of single-shaft and two-shaft gas turbines. Two-shaft gas turbines have an additional finite delay in that the compressor responds prior to the power turbine. As such, single-shaft gas turbines are considered to have superior speed performance, able to accept sudden changes in electrical power with less deviation and faster recovery [5].

A generator's output frequency is determined by its speed. In all power systems, frequency deviation must be minimized for incremental changes in power demand, some of which could be quite large. There are two methodologies used predominately to control the speed of gas turbine generators. These are droop governing and isochronous governing [5].

Droop governing, also referred to as proportional control, allows a drop in speed to occur as a result of increased electrical loading. Droop governing is commonly used in power systems since it provides a simple and reasonably accurate load sharing capability amongst a group of generators [5]. This method reflects the proportional offset discussed earlier that occurs from proportional only control.

Isochronous governing, also referred to as integral control, drives the steady state speed error to zero, resulting in a constant frequency. Accurate power sharing and constant speed control involves load measurement of each generator, power system frequency measurement, and a control sub-system that drives power mismatches to zero [5]. For a single generator, isochronous governing may be implemented through proportional and integral control with a relatively large gain placed on the integral action. Accurate load sharing amongst two or more isochronous generators is beyond the scope of this work.

A basic block diagram is shown in Figure 11 that represents the elements of the equation of motion that are most associated with gas turbine control. Rotational friction and windage are often ignored since they have little influence on the performance of the control system. The complexity of a gas turbine control block diagram is dependent on available data and the nature of the study. Simplifications are usually acceptable, for example, engine protection sub-systems are not required for basic response analysis [5].

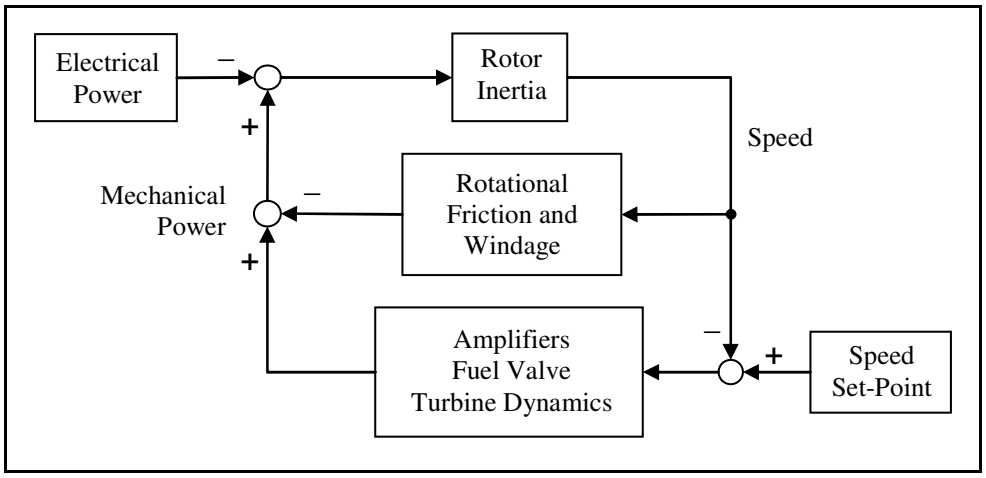

Figure 11: Basic GTG Control Block Diagram

A model representing the droop governing of a single-shaft gas turbine is shown in Figure 12. Electrical power is the actual load demand on the power turbine shaft and mechanical power is the useful power output of the gas turbine. Electrical power is subtracted from mechanical power such that an increase in electrical loading initially results in a decrease in speed as determined by the inertia of the system. The system inertia includes the gas turbine, couplings, gearbox, and generator. The term representing this inertia as shown in the model is defined as [5]:

$$Gh = \frac{1}{2H} \quad (9)$$

Where: Gh = inverted inertia term

H = inertia constant (seconds)

The inertia constant (H) is typically used in electrical engineering to convert the moment of inertia of the rotating system to a base of electrical volt-amps. It was developed specifically for solving differential equations describing generator shaft dynamics and is defined as the energy stored in the rotating mass divided by the volt-amp rating of the generator [5].

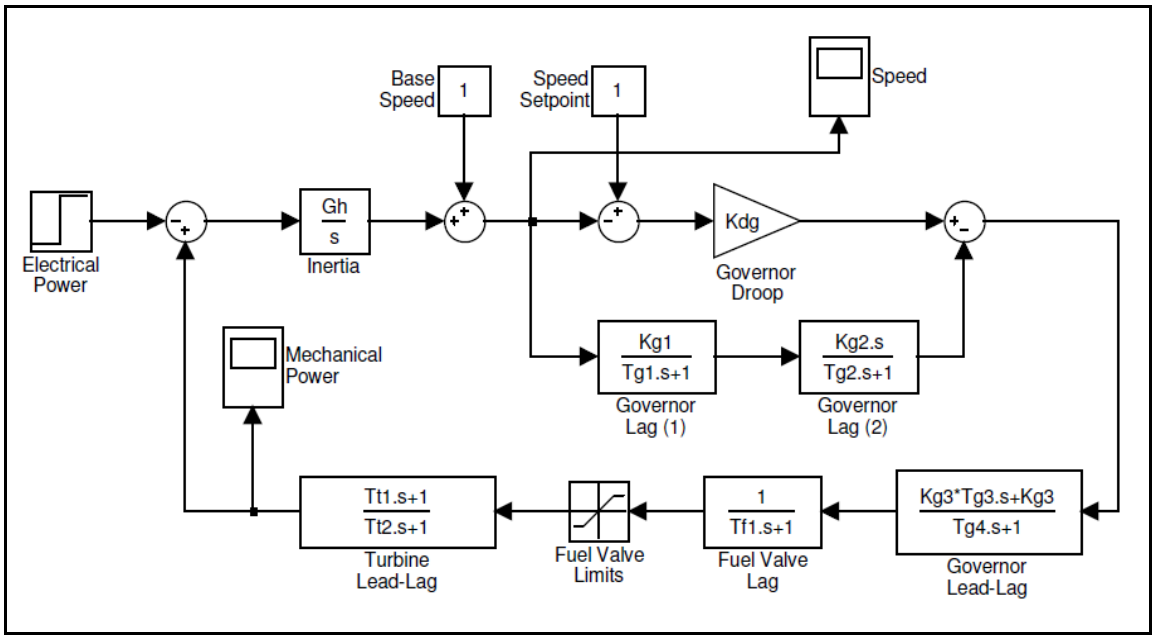

Figure 12: Droop Governing of a Single-Shaft Gas Turbine

All values in the model are normalized to a per unit system which allows for evaluation of machines with widely varying capacities. Power is normalized to the rating of the generator and speed to that which corresponds to a frequency output of 60 hertz. The speed change from the inertia transfer function is summed with the per unit base speed. The resulting turbine speed is then subtracted from the setpoint to provide an error signal to the droop governor. Governor lags 1 and 2 represent delays inherently present in electronic circuits and contain the derivative damping gain Kg2 which is often adjustable. A compensation circuit, used in some controllers to improve speed response, is represented by the governor lead-lag block [5].

The output signal from the controller directs the fuel valve position which adds an additional delay associated with the valve stem response. The fuel valve has physical limits represented in a saturation block that prevents the model from demanding a greater change in fuel than what is achievable. An artificial negative value for the minimum fuel flow represents the fact that the valve is initially open to about 15% of its travel while the gas turbine generator is operating at speed with no electrical loading [5].

There is a finite burning rate the associated with complete combustion of the fuel as it travels through the combustion chamber. Additionally, there is a delay as the heated gas transfers energy through the power turbine to produce usable mechanical power. The turbine lead-lag approximates this conversion of a change in fuel flow to a change in power [5].

A range of typical values found in the gas, oil, and petrochemical industry is provided in Table 2. The values shown in this table are based on per unit modeling of the gas turbine control system [5]. Applicable parameters are utilized in the modeling of the Allison 501-K34 GTG as presented in Section 4.1. Values shown here serve as the starting point for the Simulink model of a shipboard GTG.

Parameter	Low	Typical	High
Gh	0.25	0.33	0.42
Kdg	0.02	0.04	0.08
Kg1	1.0	1.0	1.0
Tg1	0.015	0.01	0.05
Kg2	10.0	20.0	40.0
Tg2	0.02	0.04	0.15
Kg3	1.0	1.0	1.0
Tg3	0.25	0.50	0.75
Tg4	1.0	1.50	1.75
Tf1	0.01	0.02	0.05
fmax	1.2	1.35	1.5
fmin	-0.2	-0.15	0.0
Tt1	0.3	0.6	0.9
Tt2	1.2	1.4	2.0

Table 2: Typical GTG Parameters for the Gas, Oil, and Petrochemical Industry

Chapter 4

Model Development

Simulink models of the GTG and the tabletop generator are developed in Chapter 4. The GTG model follows from the control and modeling discussed in Section 3.3. The GTG model is initially tuned to meet response specifications. Minor adjustments are then made to key parameters in the model to match actual response data.

Section 4.2 discusses the empirical development of the open-loop model for the tabletop generator. This system identification is performed in two distinct steps. First, a Simulink model simulates the response to a change in electrical loading while terminal voltage to the DC motor is held constant. This captures the self regulating aspect of a DC motor as discussed in Section 2.3. Building on this model, the second step incorporates the effect that a change in terminal voltage has on speed. In this open-loop test, a change in terminal voltage drives the speed response with the generator's electric load held constant.

Following the open-loop modeling of Section 4.2, closed-loop feedback control of the tabletop generator is modeled in Section 4.3. The closed-loop model is tuned to provide a response similar to the GTG model for a specific change in electric loading. The closed-loop model is then evaluated for the following: sensitivity to a key parameter that showed deviation in open-loop modeling; exclusion of estimated power losses; and variation in electric loading.

4.1 Numerical Simulink Model of Allison 501-K34 GTG

The numerical Simulink model developed to simulate the response of the shipboard generator is shown in Figure 13. This model is similar to that shown in Figure 12 with the notable difference that the droop governing control blocks are replaced with a PI controller. As discussed in Section 3.3, a large gain placed on the integral action of a PI

controller invokes isochronous control. Thus, the modeled controller represents the constant speed governor of the GTG during normal shipboard operations.

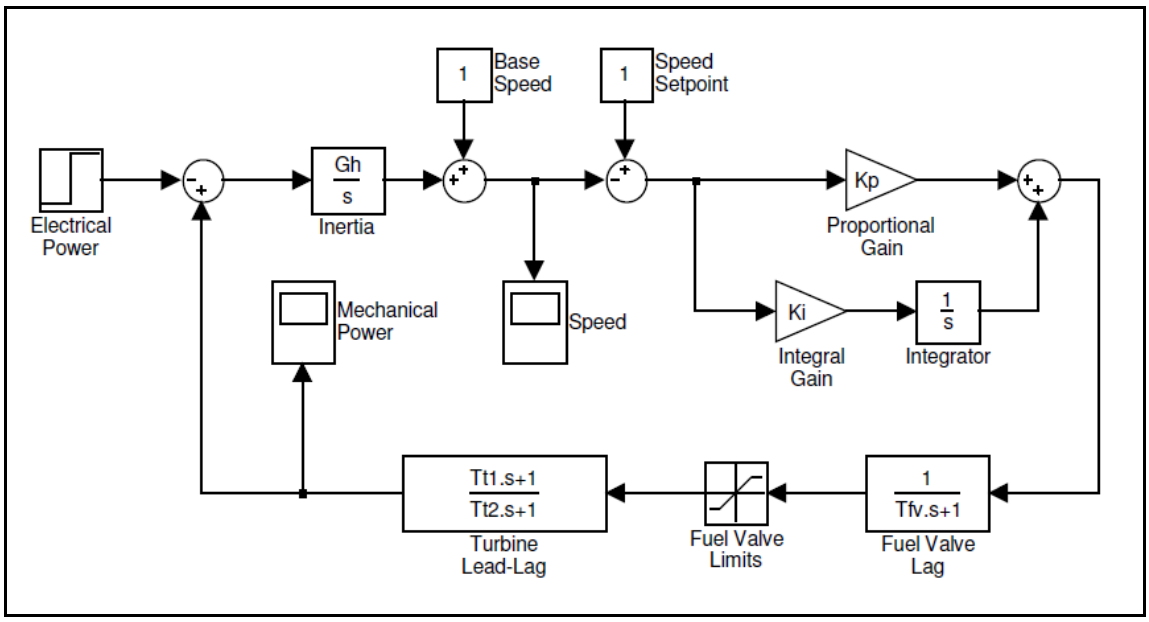

Figure 13: Simulink Model of Allison 501-K34

As with the droop governed model, per unit values are utilized to allow for comparison with machines of significantly different ratings. Aside from the governor, the core characteristics and signal flows are the same as that discussed in Section 3.3. The inertia term (Gh), as defined in Equation 9, was estimated from the inertia of the gas turbine and generator. The mass moment of inertia for the gas turbine was taken from the Allison 501-K34 Specification [4]. The generator's inertia was obtained via correspondence with Naval Surface Warfare Center, Carderock Division (NSWCCD) [8].

Initially, typical values from Table 2 were used in the model to test its response to a step increase in electrical power from 0 to 1 per unit, representing the instantaneous application of the machine's full rated load from 0 to 3000 KW. Controller gains were increased and time constants adjusted until the speed response met the GTG Specification criteria discussed in Section 3.1. Table 3 shows typical ranges of the applicable parameters taken from Table 2 along with the values utilized in this model to meet speed response criteria. As with Table 2, the parameters are based on per unit modeling of the

speed control of a GTG typically found in the gas, oil, and petrochemical industry. They are included here to provide some validation of the shipboard GTG model.

Parameter	Typical Values	Simulink Model
Gh	0.25 to 0.42	0.55
Kp	-	40
Ki	-	40
Tf1	0.01 to 0.05	0.01
fmax	1.2 to 1.5	1.35
fmin	-0.2 to 0	-0.15
Tt1	0.3 to 0.9	1.2
Tt2	1.2 to 2.0	0.9

Table 3: Initial GTG Simulink Model Parameters

Although the governor of the shipboard GTG is not precisely modeled and it is not known whether the turbine lead and lag time constants are truly representative; the model does include the fundamental dynamic aspects of gas turbine generators and values utilized in the model are typical or near typical as shown in Table 3.

A larger value of the inertia term (Gh) represents a machine that has less stored rotational energy given the same power rating. Given space and weight limitations of naval vessels, shipboard machinery often has larger than normal power densities and it is not surprising that this value is outside the typical range. However, the inertia of the gearbox was not specifically included with the value obtained for the generator and while the inertia of the generator (3550 $lb \cdot ft^2$) clearly dominates when compared to the gas turbine (61 $lb \cdot ft^2$); the gearbox may represent a reasonable percentage of the system's inertia. If the inertia of the gearbox is not included in the generator's value, and assuming the gearbox accounts for 10% of the system's inertia, then the value for Gh becomes 0.50 which is closer to but still outside the typical range.

Given that exact model parameters are unknown and the intent was to provide a response similar to the GTG, the model was deemed acceptable given its ability to meet response criteria as shown in Figure 14.

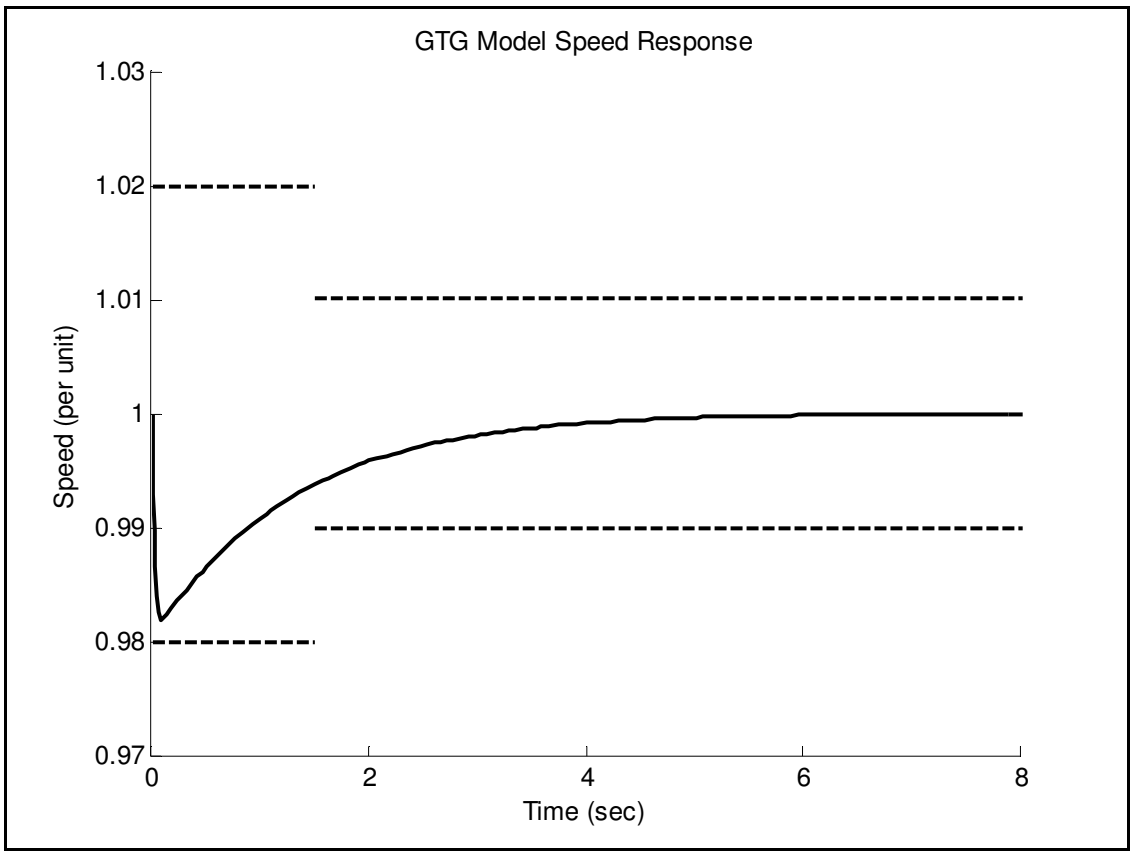

Figure 14: Initial GTG Model, Response to Rated Load Step Increase

Following the development of the model above, actual full load power excursion data was received from NSWCCD [8]. As tested, the Allison 501-K34 response to removal and application of its full rated load is shown in Figure 15. The associated electrical transient is shown in Figure 16.

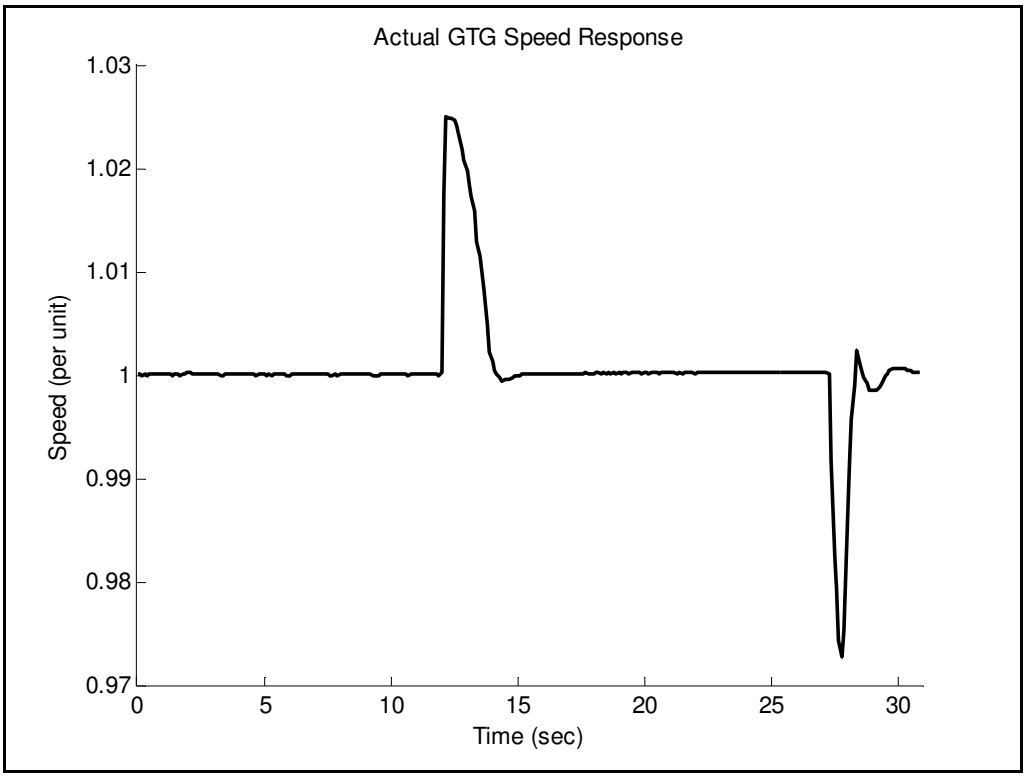

Figure 15: Actual GTG Response to Full Rated Power Excursions

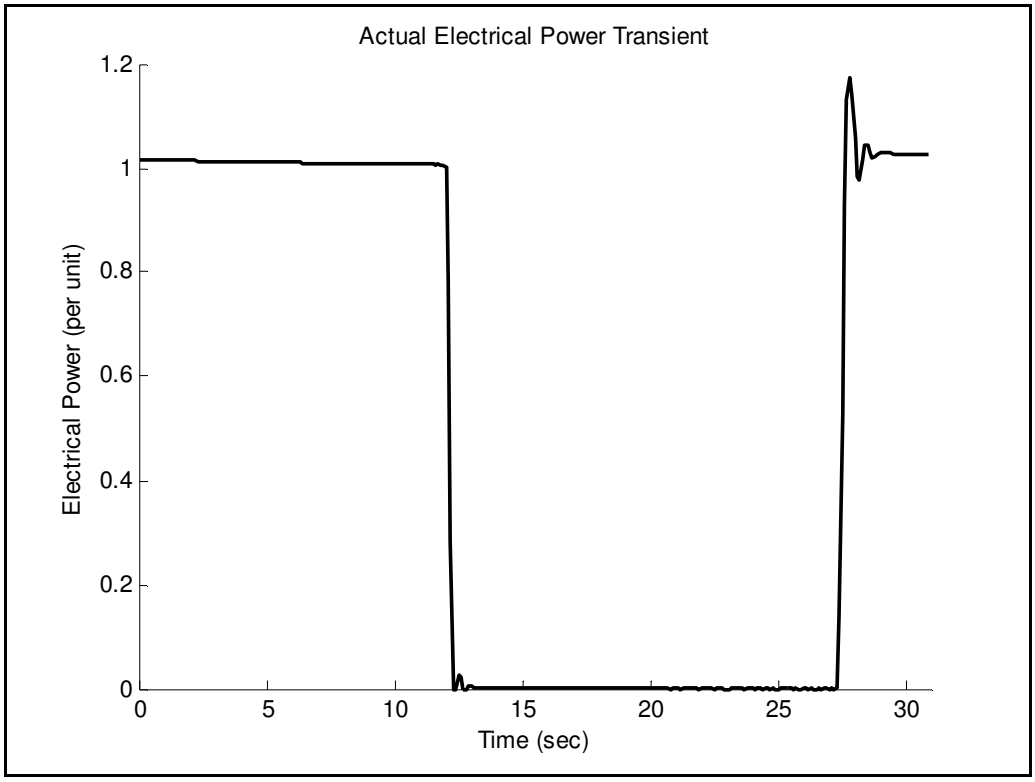

Figure 16: Actual Full Rated Electrical Power Transient

Utilizing the provided data, the actual full rated electrical power transient was input to the GTG model vice an idealized step input. The comparison of the model's speed response with actual data is shown in Figure 17.

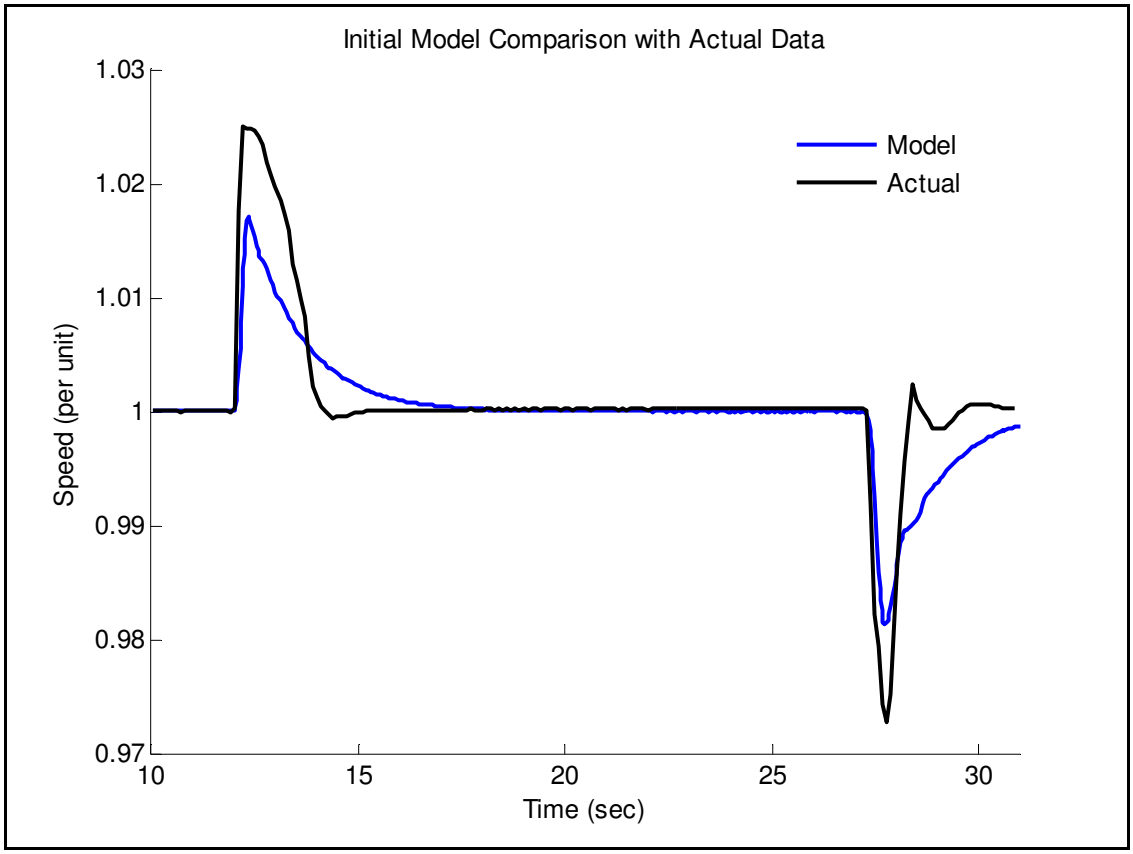

Figure 17: Initial GTG Model Comparison

As seen in Figure 17, the actual response exceeds the 2% deviation initially suggested by the 1987 Model Specification. This is most likely attributable to variations found on ships constructed later in the class (DDG-91 and beyond). Modifications were made to the model parameters to more closely approximate the actual response. The model is most sensitive to small changes in the turbine lead and lag time constants Tt1 and Tt2 respectfully. Some improvement was also noted utilizing a smaller value for the inertia term (Gh). The inertia term was reduced in value to that mentioned earlier, accounting for the inertia of the gearbox, with further reduction showing little affect. No changes were made to the modeled controller gains or fuel valve dynamics. The modified

parameters are shown in Table 4. The response of the finalized model of the GTG as compared to the actual response data is presented in Figure 18. Although the model does not correctly identify the overshoot seen in the actual data, it does adequately describe the peak response and settling time. This model becomes the basis for the tabletop generator's empirical model developed in Section 4.2.

Parameter	Typical Values	Initial Value	Final Value
Gh	0.25 to 0.42	0.55	0.50
Kp	-	40	40
Ki	-	40	40
Tf1	0.01 to 0.05	0.01	0.01
fmax	1.2 to 1.5	1.35	1.35
fmin	-0.2 to 0	-0.15	-0.15
Tt1	0.3 to 0.9	1.2	0.96
Tt2	1.2 to 2.0	0.9	1.14

Table 4: Modified GTG Simulink Model Parameters

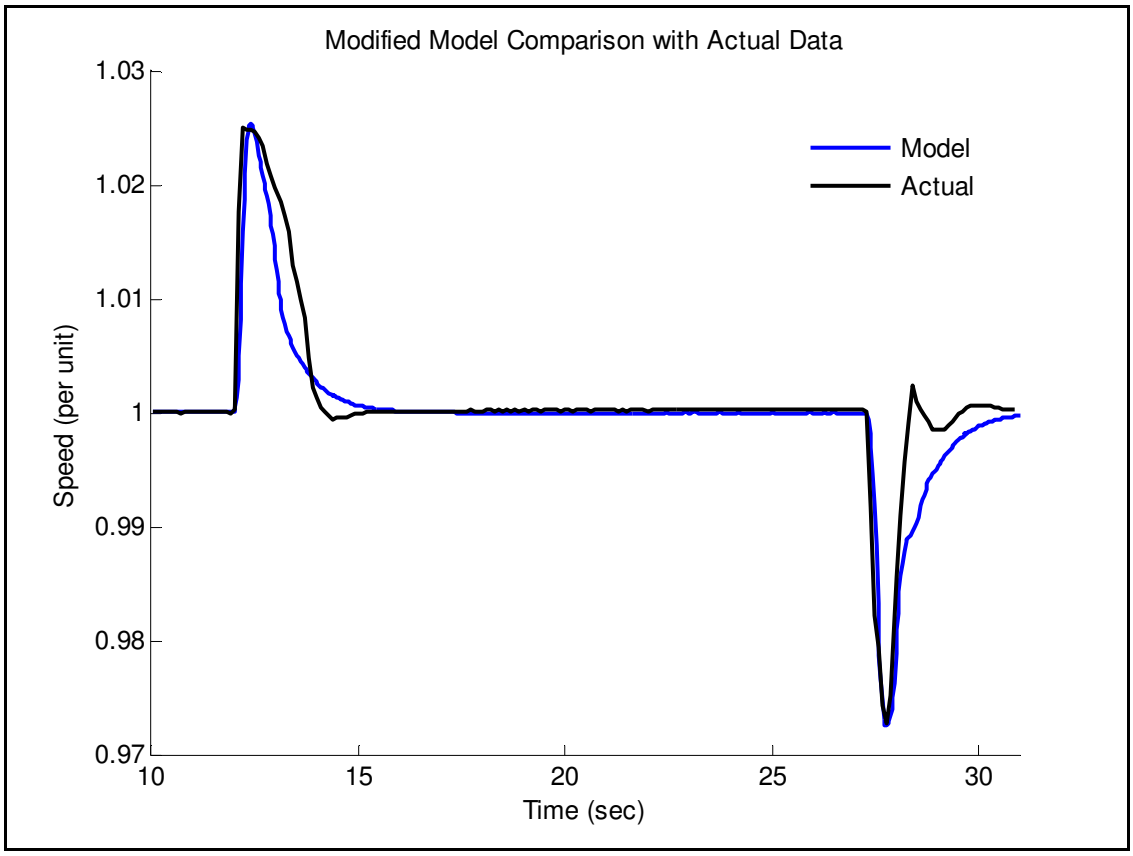

Figure 18: Finalized GTG Simulink Model

4.2 Empirical Open-Loop Modeling of Tabletop Generator

Open-Loop response testing was performed for the following conditions: increased electrical loading from 0.045 to 0.135 per unit, decreased electrical loading from 0.135 to 0.045 per unit, and increased terminal voltage by 5.2 volts while supplying 0.045 per unit power near operational speed and output voltage. The per unit changes in power correspond to the readily available 225 to 675 watt step loading of the tabletop generator rated at 5 KW. The empirical model of the tabletop generator's speed response to a change in electrical load as developed in Simulink is shown in Figure 19.

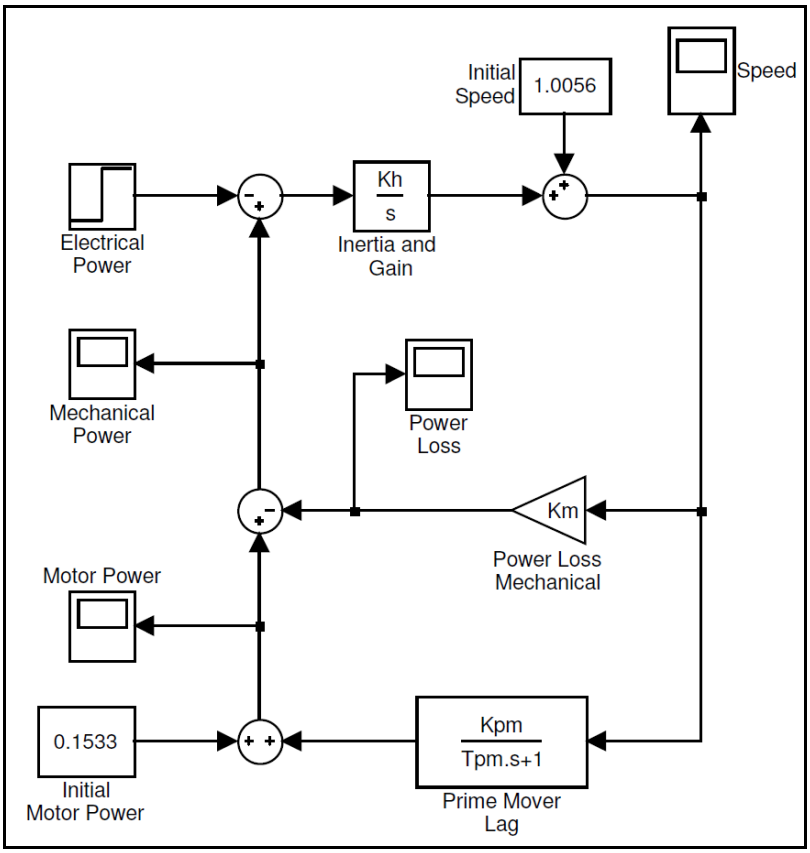

Figure 19: Open-Loop Response Model to a Change in Loading

The model was designed in a fashion similar to the GTG model developed in Section 4.1 where a mismatch between electrical and mechanical power results in an initial change in speed as determined primarily by the inertia of the machine. The tabletop generator presents a fair amount of vibration throughout all speeds in addition to pronounced vibration that occurs at a number of critical speeds. The sideward loading associated with the prime mover pulley arrangement may exacerbate this condition. The power loss approximates this loss of energy and allows for a more direct observation of motor power within the model. The lagging transfer function describes how a change in speed affects the motor's power output. This self regulation, within the uncontrolled or open-loop model, attests to the DC motor's inherent stability as discussed in Section 2.3.

Figure 19 shows initial values for power and speed immediately prior to a step increase in electrical loading. Initial motor power was determined from Equation 3, utilizing measured values for motor current and speed. Initial estimates for the prime mover's time

constant and gain (Tpm and Kpm) were made utilizing techniques most valid for a system dominated by a primary lag. The time constant was taken as the time required for the response to reach 63% of the total change in speed. The gain was estimated as shown below. Figure 20 provides a graphical representation [9].

$$Kpm = \frac{\Delta\omega}{\Delta u} \quad (10)$$

Where: $\Delta\omega$ = completed response change in speed

Δu = straight line change in speed

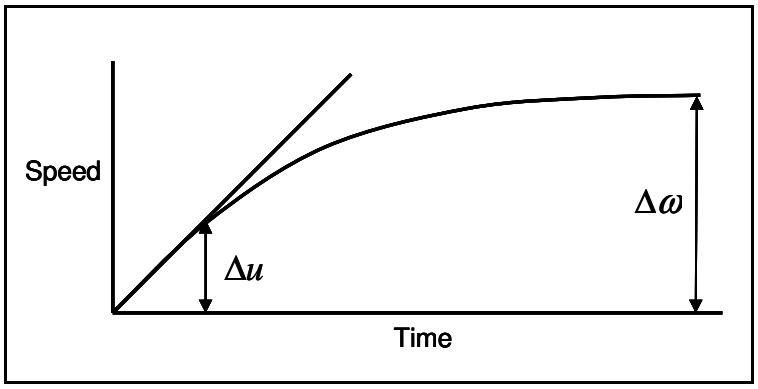

Figure 20: Initial Estimation of Prime Mover Gain

Using these estimated values, the inertia term (Kh) was adjusted until the modeled response curve obtained the correct shape. Adjustment was then made to the lagging time constant and gain until the modeled motor power obtained a steady state value corresponding to that observed during the response testing. Final adjustment was made to the time constant to provide the response shown in Figure 21.

The final value for the modeled motor power is near but not equal to that observed. Some of this variation results from the linear estimation of the mechanical power loss. The ideal power loss due to rotational damping is given as [10]:

$$P_{Loss} = B\omega^2 \quad (11)$$

Utilizing per unit values and considering small speed fluctuations near a value of 1, the power loss was assumed to behave in a linear fashion with the constant B approximated as the average of the two power losses observed during the up-power and down-power response testing.

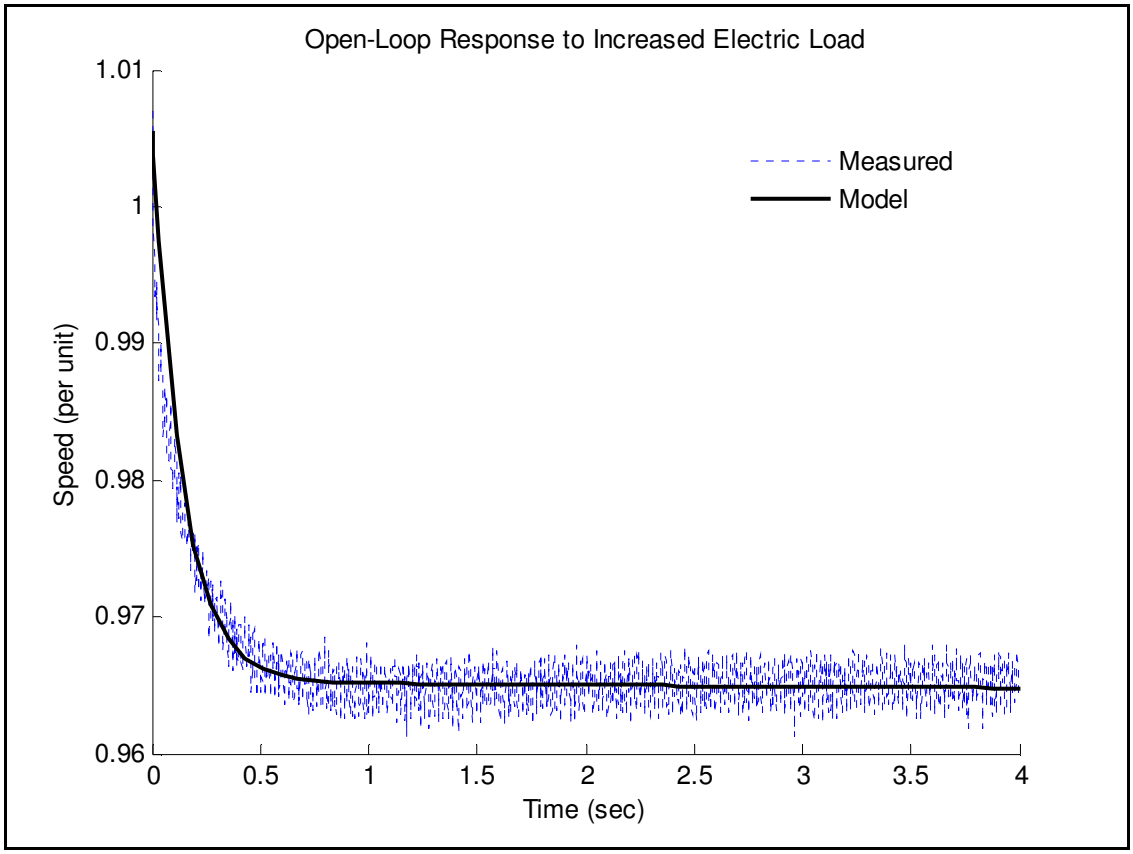

Figure 21: Uncontrolled Response to Increased Loading

Utilizing values identified from the up-power response, the model shown in Figure 19 was utilized to describe the speed response to a decrease in electric loading. The one notable difference between these two events is the sign of the prime mover gain (Kpm). For a sudden drop in loading, the increasing motor speed results in a greater counter voltage and subsequent drop in armature current. The prime mover gain is negative in this case to account for the decrease in power that occurs. Additionally, some adjustment to the magnitude of the prime mover gain was required to obtain the response shown in Figure 22. Values utilized in the open-loop response models are provided in Table 5.

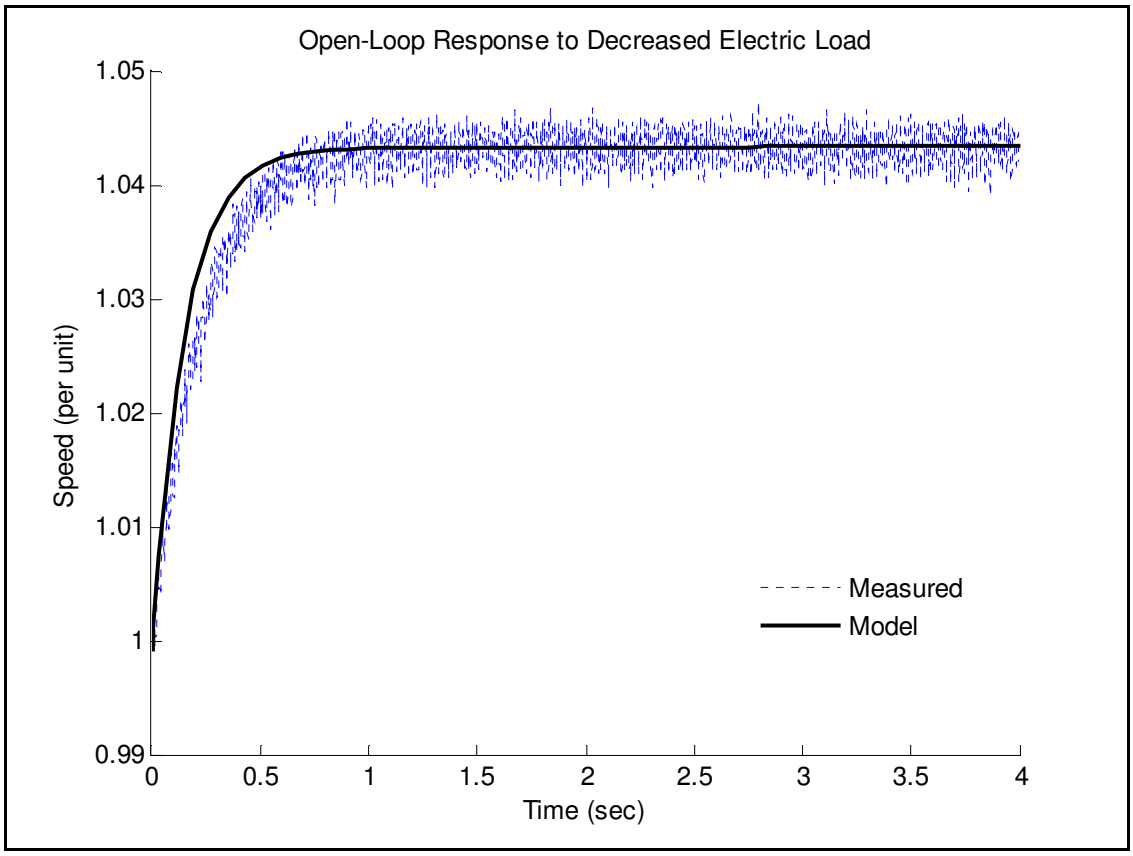

Figure 22: Uncontrolled Response to Decreased Loading

The open-loop response to a change in electric loading represents the self regulating aspect of the DC motor as discussed in Section 2.3 where the changing speed affects counter voltage and subsequently armature current. Adjustment of terminal voltage is required in order to maintain motor speed under varying loading conditions. From Equations 5 and 6, the power of the DC motor may be written as:

$$P_M = \left[\frac{K}{R_M} V_{Term}\ \omega\right] - \left[\frac{K^2}{R_M}\omega^2\right] \quad (12)$$

The second term of Equation 12 is accounted for in the open-loop response model to a change in loading shown in Figure 19. The first term is included to model the uncontrolled response to a change in terminal voltage as shown in Figure 23.

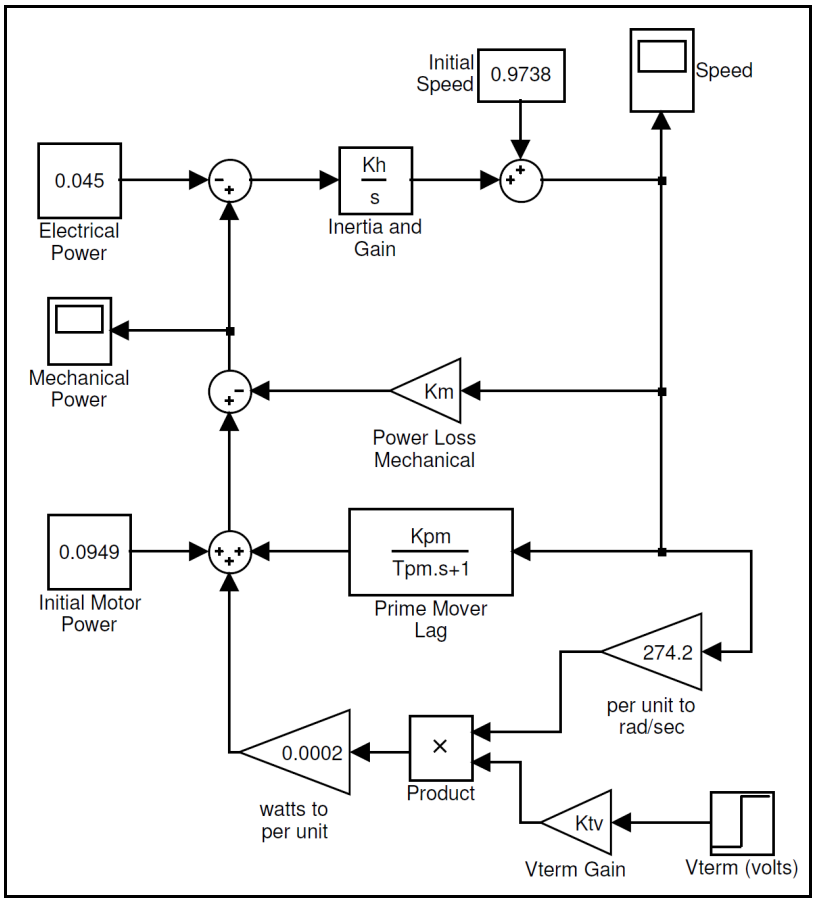

Figure 23: Open-Loop Response Model to a Change in Terminal Voltage

The affect that a change in terminal voltage has on motor power is modeled directly as the product of terminal voltage, constant (Ktv), and speed. Units were introduced in this area of the model to assist with proper identification of the closed-loop controller gains developed in Section 4.3. The initial estimate for the terminal voltage gain (Ktv) was taken directly from Equation 12 as the motor constant divided by armature resistance.

The power loss gain (Km) was calculated for this model as that loss actually observed at the beginning of the test run. Remaining parameters were assigned preliminary values based on those used to model the up-power transient since both of these response tests have the same initial electrical loading. Adjustment was then made to the prime mover gain (Kpm) to maintain the shape of the response curve while the terminal voltage gain (Ktv) was manipulated to obtain the correct change in speed. The resulting response curve is shown in Figure 24.

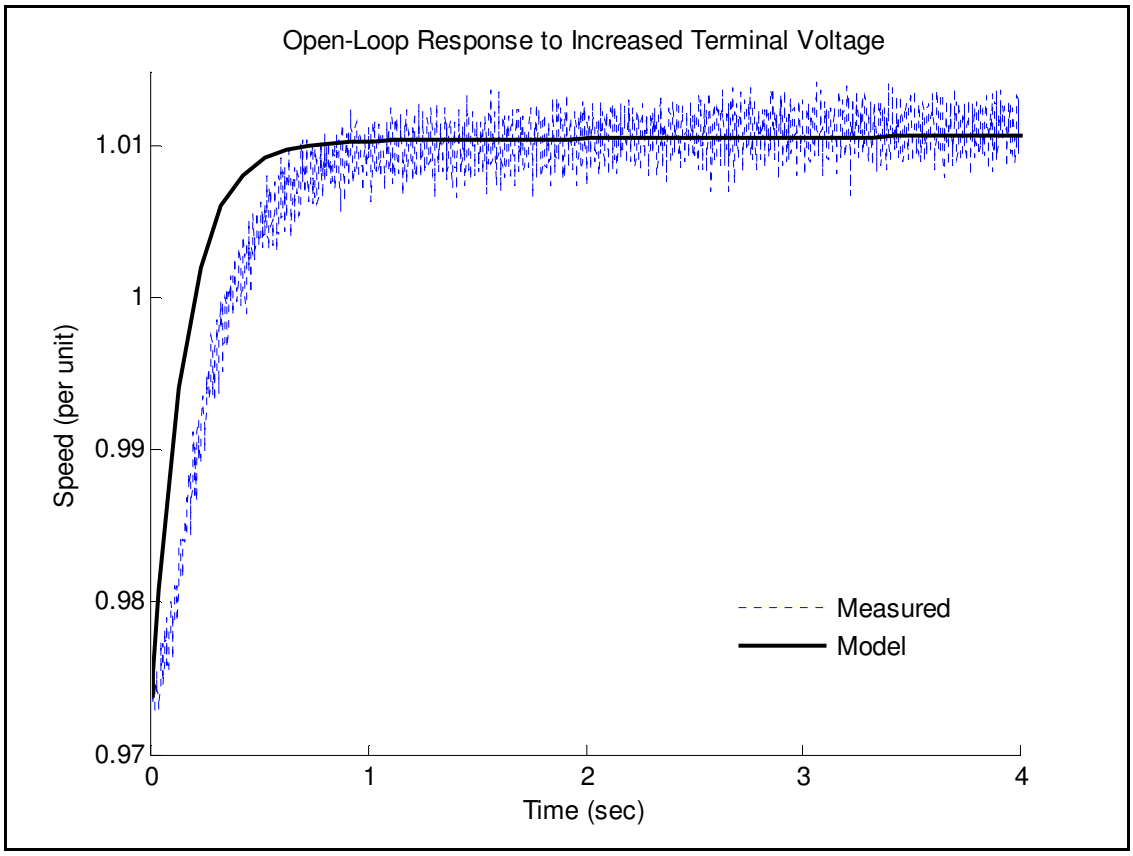

Figure 24: Uncontrolled Response to Change in Terminal Voltage

Table 5 shows parameter values utilized in the three open-loop response models. The power loss gain for the step change in terminal voltage was significantly different from that observed for step changes in power. This may be a result of variation in the armature's interaction with the field given the generator output voltage was initially 118 volts line to neutral vice the 120 volts established at the beginning of the change in power experiments. It is expected that the power loss term will remain near constant with speed and voltage control in place.

Parameter	Increased Electric Load	Decreased Electric Load	Increased Terminal Voltage
Kh	3.3	3.3	3.3
Km	0.1062	0.1062	0.0499
Kpm	0.0872	-0.0805	-0.0741
Tpm	0.144	0.144	0.144
Ktv	-	-	0.262

Table 5: Open-Loop Model Parameters

The power loss term (Km) is not actually needed for the model to describe speed response; it was included to provide insight into the behavior of modeled motor power to assist with the empirical modeling. In lieu of estimating power loss and observing motor power, the model could have been constructed utilizing an initial mechanical input equal to the initial electrical power. Additionally, as mentioned in Section 3.3, rotational friction and windage are often ignored in modeling since they have little influence on the performance of the control system. As such, variation in power loss is not considered a hindrance to establishing speed and voltage control.

As shown in Table 5, the inertia term (Kh) and prime mover time constant (Tpm) were found to be consistent throughout the three models. The much larger value for Kh, when compared to Gh used in the GTG model, indicates that either the machine maintains very little energy in an inertial capacitive form as discussed in Section 3.3 or some other system dynamic is included in this parameter. Given the large amount of energy lost to rotate the generator while maintaining voltage, some of this discrepancy may attest to the general imbalance of the tabletop generator. Variation may also be attributed to the inherent differences between the DC motor and gas turbine prime movers. For example, removal of power from the operational DC motor results in the inertia of the generator acting to rotate the motor and in turn causes the motor to behave as a generator with an associated counter torque.

The variation in the prime mover gain (Kpm) required to fit all three response curves presents some concern for the modeling and subsequent implementation of closed-loop control. This is addressed in Section 4.3 by evaluating how deviation in this term affects the response of the closed-loop system.

4.3 Closed-Loop Model of Tabletop Generator

Incorporating what was learned from the open-loop response modeling, closed-loop feedback control of the tabletop generator was included and adjustment made such that the closed-loop response approximates that of the GTG model developed in Section 4.1. The model, shown in Figure 25, follows directly from the open-loop model shown in Figure 23 with the addition of a speed error signal input to a PI controller that adjusts terminal voltage to drive the speed error to zero.

Units were included in the modeled controller to assist with exporting gains to the software controller. As developed, the product of the frequency error and controller gain results in a fractional change in terminal voltage. This fractional change, multiplied by the voltage range of the power supply, identifies the desired change in terminal voltage.

The speed derivative is evaluated in the determination of the sign of the prime mover gain (Kpm). As discussed in Section 4.2, this parameter is positive when speed is decreasing and negative with increasing speed. This introduces a discontinuity such that the default Ordinary Differential Equation (ODE) solver would not converge for a wide range of controller gains. In lieu of Simulink's default variable step Domand-Prince (ODE-45) solver, the fixed step Runge-Kutta (ODE-4) solver was used with a step size of 0.001 and a run time of 5 seconds during adjustment of controller gains.

Utilizing parameters indentified in Table 5 for an increase in electric loading from 0.045 to 0.135 per unit and the terminal voltage gain (Ktv), controller gains were adjusted until the response resembled that of the GTG model as shown in Figure 26. After reaching the desired response, the terminal voltage and controller gains were adjusted correspondingly

to provide a fractional change in terminal voltage matching that observed during similar response testing. Values utilized in this model are shown in Table 6.

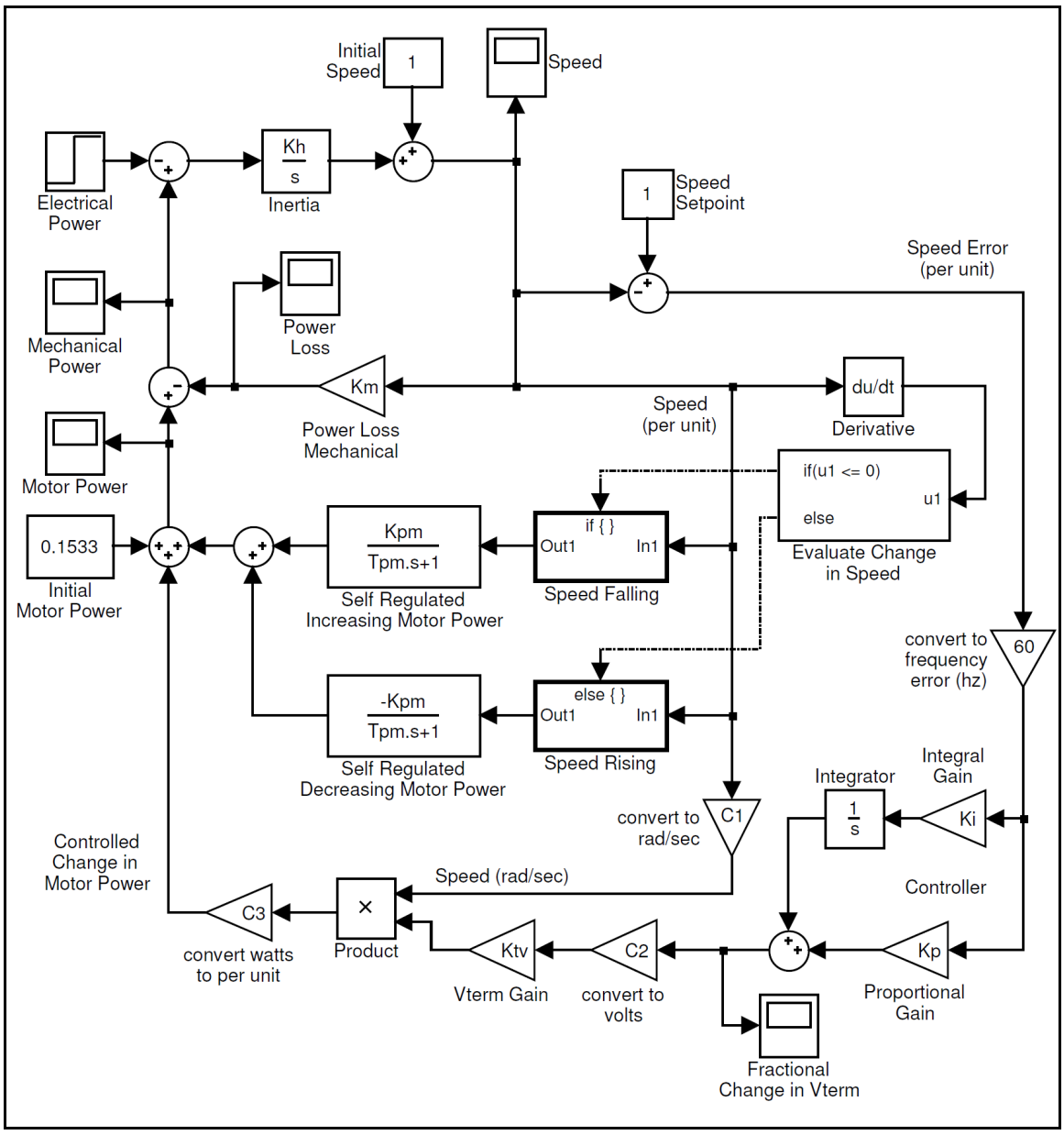

Figure 25: Tabletop Closed-Loop Response Model

Parameter	Value
Kp	0.165
Ki	0.215
Kh	3.3
Km	0.1062
Kpm	0.0872
Tpm	0.144
Ktv	0.36
C1	274.2
C2	150
C3	0.0002

Table 6: Tabletop Closed-Loop Parameters

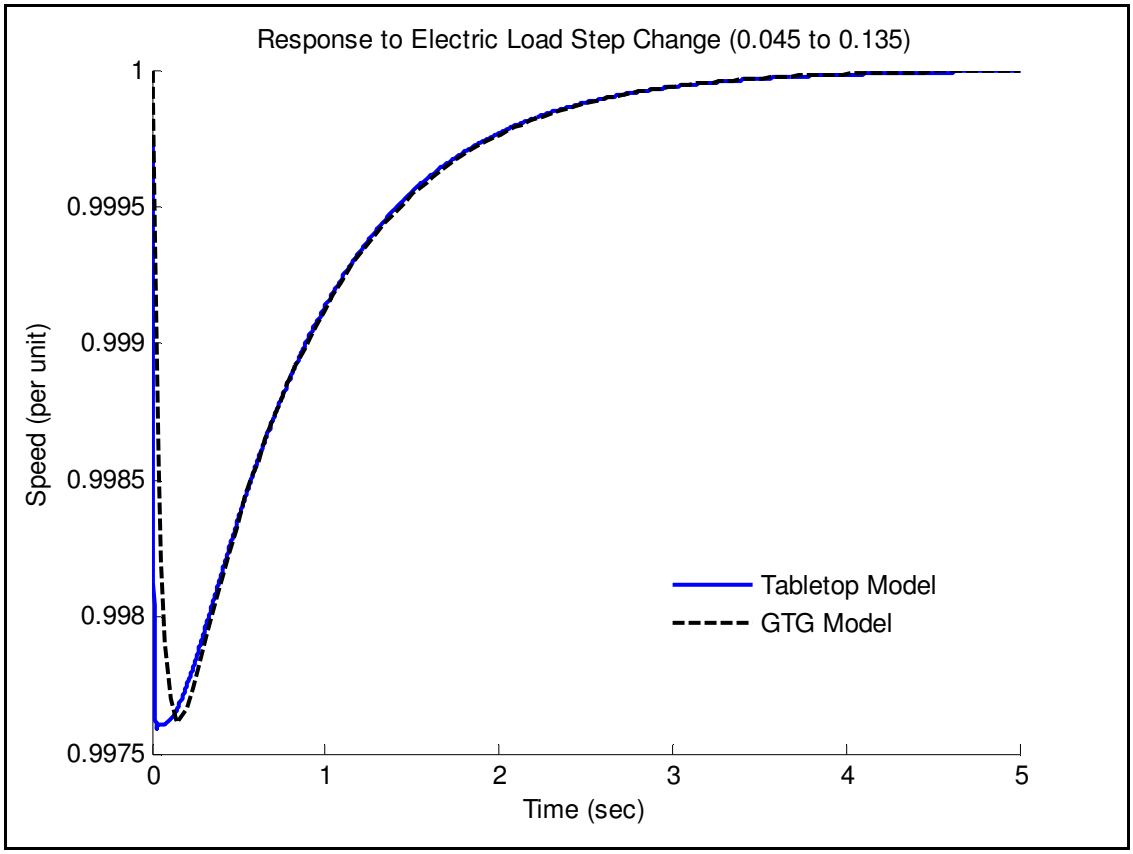

Figure 26: Tabletop Model Closed-Loop Response

Given the uncertainty in the estimation of the power loss and the variation in the prime mover gain seen in open-loop modeling, the closed-loop model was revised as shown in Figure 27. With estimation of power loss removed from the model, the initial steady state condition was established by including an initial mechanical power such that the power mismatch is zero at time equal to zero. Using the same 0.045 to 0.135 step change, the prime mover gain was adjusted upward and downward 15% to observe how sensitive the response is to deviations in this parameter. Results of this analysis are shown in Figure 28.

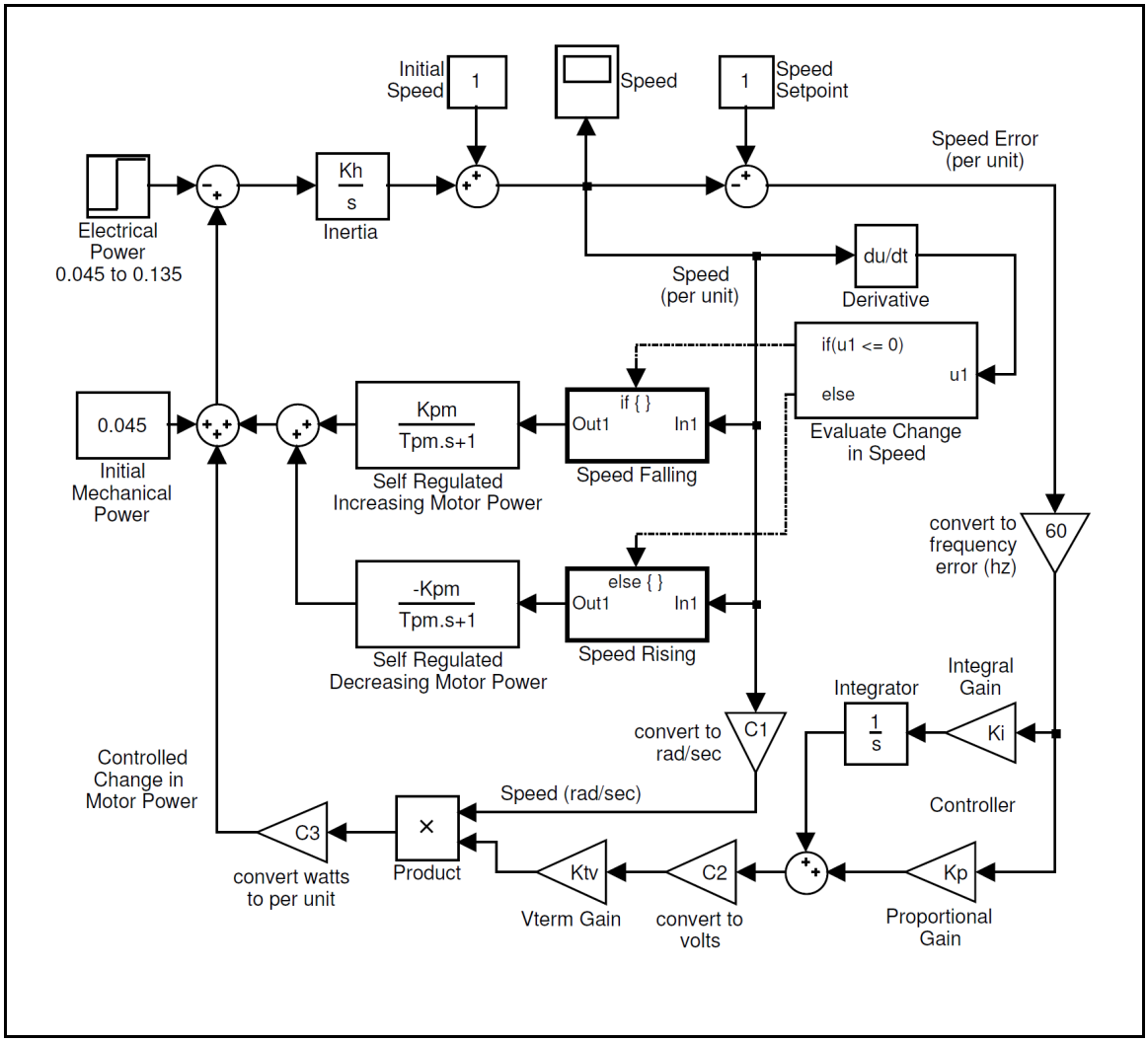

Figure 27: Tabletop Closed-Loop Model without Estimation of Power Loss

Comparison of the response curve for the non-deviated prime mover gain (1.0 Kpm) shown in Figure 28 with that shown in Figure 26 provides validation that rotational energy losses (windage, friction, etc.) need not be included in the closed-loop model since they have little affect on the controlled response. The slight variation in modeled response, given a 15% deviation in the prime mover gain, attests to the stability and robustness of the closed-loop feedback control.

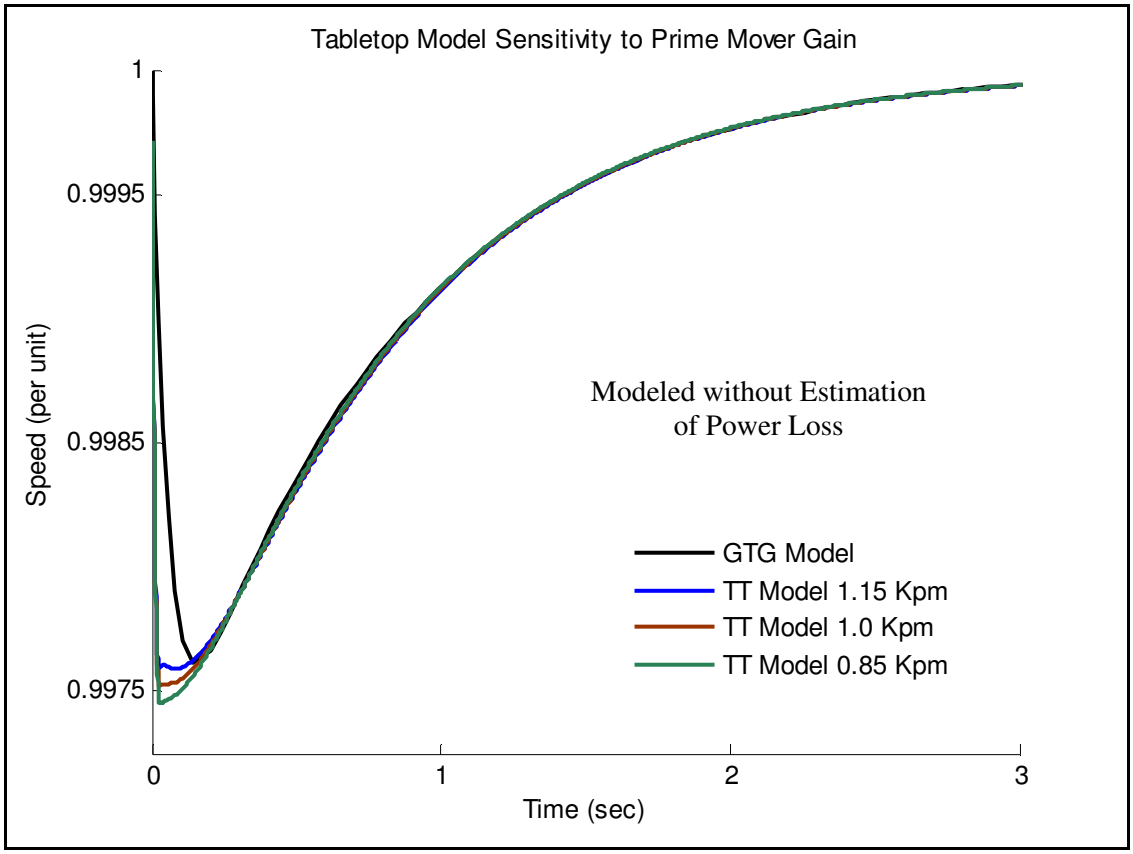

Figure 28: Tabletop Model Sensitivity to Prime Mover Gain

The tabletop model evaluation to this point has been focused on the response to a specific change in electrical loading of 0.045 to 0.135 per unit. This was set as the design point to correspond to the readily available 225 to 675 watt step loading of the tabletop generator rated at 5 KW. Using the Simulink model with no estimation of power loss, the response to a step change in electric loading from 0 to 0.225 is shown in Figure 29. This step in power represents the uppermost power excursion for the tabletop generator which is limited in its useable power output to a little more than 1125 watts.

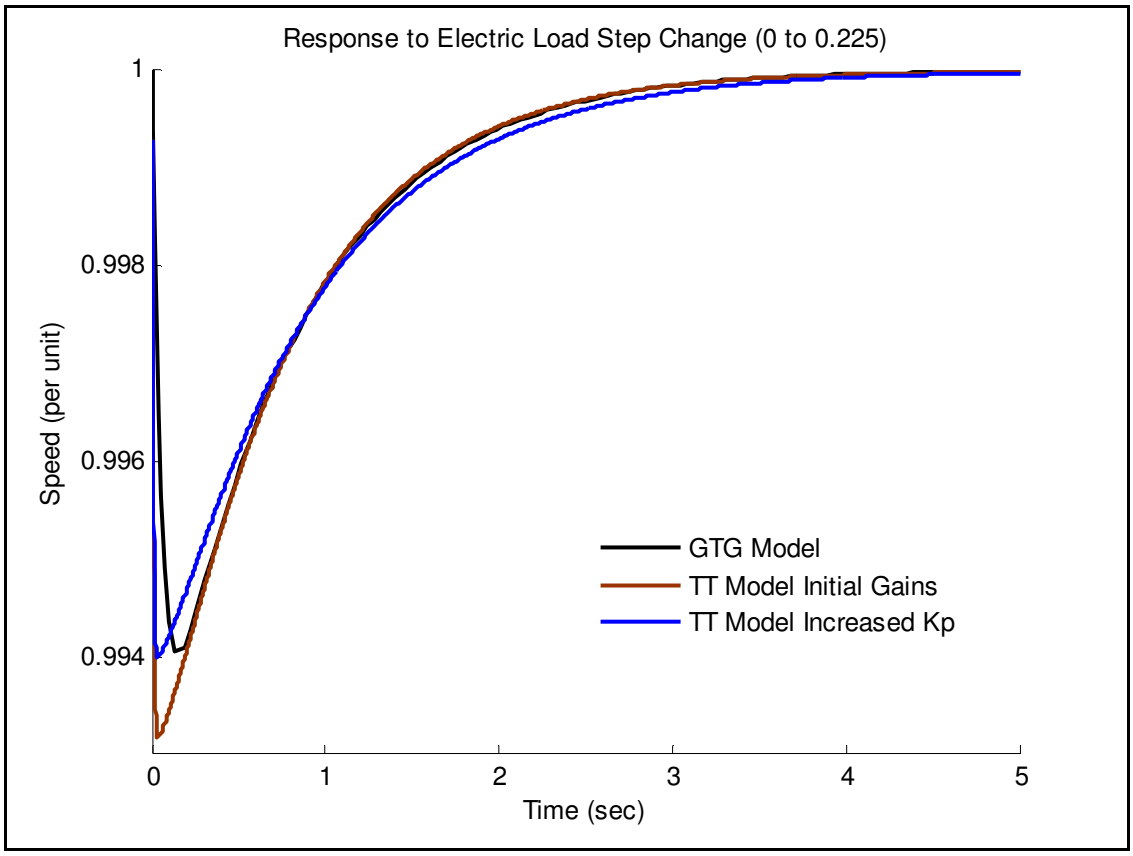

Figure 29: Closed-Loop Response to a Larger Step Input

As shown, utilizing controller gains identified for the step change in power from 0.045 to 0.135 per unit does not provide the same level of agreement when a larger step change of 0.225 per unit is applied to the gas turbine and tabletop models. Adjustment of the tabletop controller's proportional gain from 0.165 to 0.19 improves the correlation between peak values.

Chapter 5

Hardware Model

A physical description of the hardware model is provided in Chapter 5 along with response testing results. Appendix D provides a listing of parts, including specifications and purchasing information. Recommendations to improve the response of the tabletop generator are made based on analysis of actual speed sensor noise.

5.1 Physical Description

The hardware model of a shipboard generator as constructed is pictured in Figure 30. The 3-phase 5 KW generator is side driven by a timing belt with a 32 tooth pulley mounted on the generator shaft and a 22 tooth pulley on the motor. Two DC motors, in series electrically and mechanically coupled, provide a rated capacity of 4 HP to serve as the prime mover. Not seen in the picture is a small cooling fan that provides forced circulation to the motors and a Hall Effect speed sensor rigidly mounted adjacent to a 14 tooth sprocket set on the furthermost motor shaft. Two XHR 1000 Watt Series programmable DC power supplies provide a rated 14 amps and 150 volts to the DC motors. The additional power supply pictured provides manual control of current to the generator's field windings in order to maintain an output voltage of 120 V line to neutral (208 V across phases). A programmable power supply for voltage control was not in use at the time of this photo.

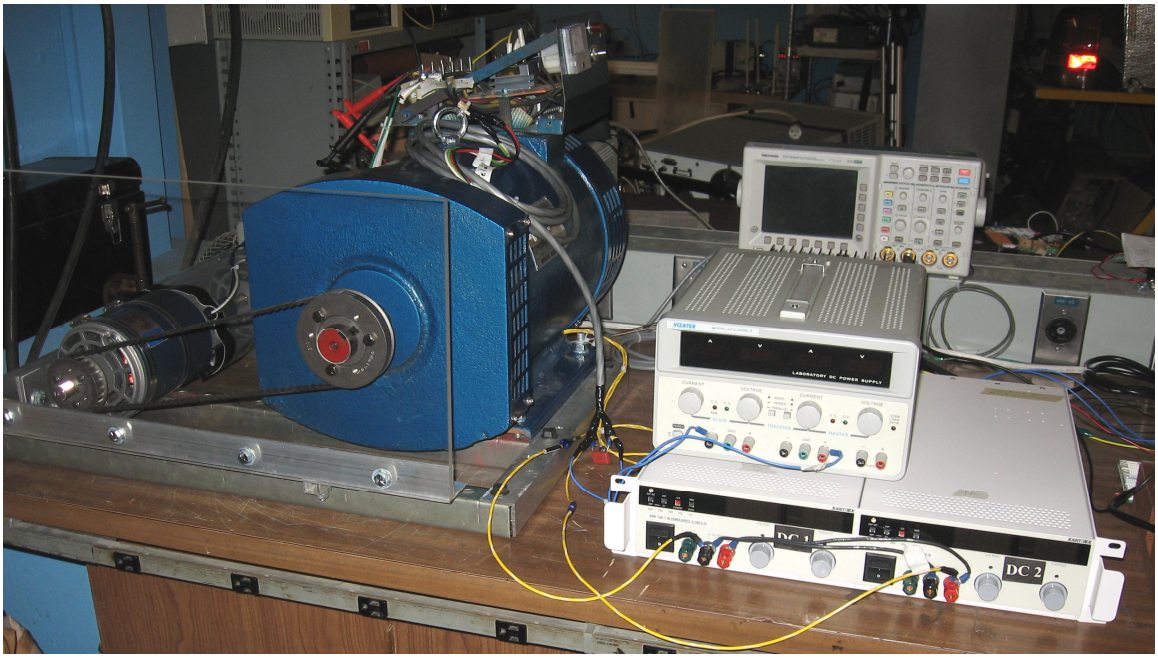

Figure 30: Tabletop Generator as Constructed

The analog / digital USB interface board used to pass measured and controlling signals to and from the software environment is shown in Figure 31. Additional circuit boards were constructed as necessary to modify speed and voltage measurements prior to the USB interface. Labview was utilized to implement speed and voltage control.

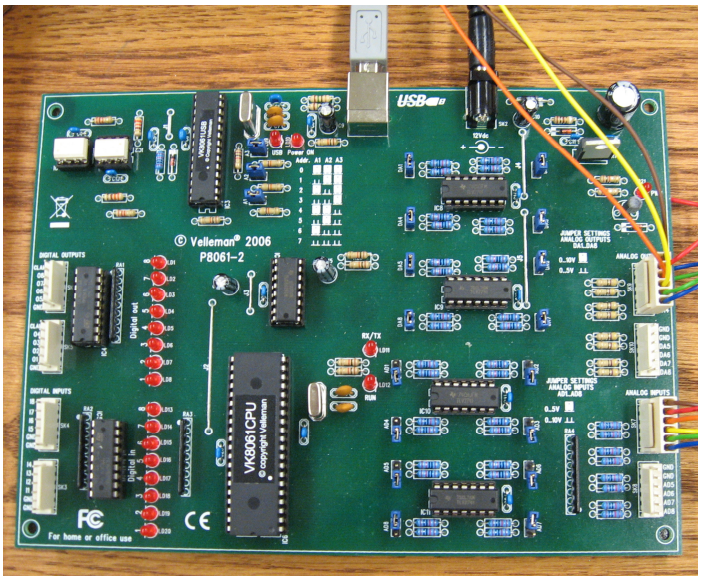

Figure 31: USB Interface Board

Implementation of the control scheme in the software environment was conducted by Vanessa Esch while working on an Undergraduate Advanced Project. Signal conditioning of speed and voltage measurements was developed by Jacob Osterberg while working through the Undergraduate Research Opportunity Program. Their work is shown in its entirety in the Appendices. Though some information is duplicated and conflicts may exist, no attempt was made to modify or summarize their reports. This preserves the insight of three observers involved on one project.

The loading scheme utilized for response testing is shown in Figure 32. A bank of 9 light fixtures allows for some number of variations in electric loading. Though the resistance of a light bulb changes to some degree with temperature, the purely resistive loading was preferred for its ease and reasonable representation of step changes in power. The fixtures are wired in a Y configuration with each light seeing a voltage of 120 V line to neutral. Each column of fixtures is supplied power from one phase.

The first row of lights is operated via the three rightmost switches. Operation of these switches, as near to simultaneous as possible to minimize unbalanced loading, allows for establishment of an initial loading condition if desired. The second and third rows are provided power via the three relays pictured in the left corner. Operation of the leftmost switch energizes the relays to provide instantaneous loading in order to model a step change in power.

Figure 32: Loading Scheme for Response Testing

General characteristics of the tabletop generator are summarized in Table 7. The inclusion of a saturation block in the closed-loop modeling of Section 4.3 was considered but deemed impractical. The saturation represents the limitation of the power supply and was initially thought to be a simple limit placed on the terminal voltage in the model. As observed, a sudden increase in terminal voltage, as required to maintain speed for a large up-power transient, drives the power supply to a current limited condition for some period of time. This occurs while increasing power from 225 watts to some value near 750 watts. As such, there is some limit on up-power transients that may be conducted while maintaining good speed response behavior.

Parallel Power Supply Rating:	2100 watts (14A, 150V)
Power Supply Usable:	2025 watts (current limited)
Motor Speed:	2618 rpm
Motor Constant:	0.432 volt*sec (motors coupled)
Motor Resistance:	1.87 ohms (motors coupled)
Power Lost to Heat:	365 watts
Motor Power:	1660 watts
Generator Speed:	1800 rpm
Power Loss:	~ 525 watts
Generator Output:	~ 1135 watts (tested up to 1125 watts)

Table 7: General Characteristics of Tabletop Generator

The power loss of the generator is significant. About half of this value is attributed to windage and rotational friction. The remaining loss is observed upon energizing the field windings from an external source to provide required output voltage. Utilization of the generator's installed voltage regulator vice an external power source exacerbates the power loss.

5.2 Response Testing

Response testing proved to be very time consuming and did not yield desired results. Electromagnetic interference introduced significant fluctuations in the speed sensor signal. This occurred after the generator was electrically loaded for a short period of time. Relocation and shielding of the speed sensor wiring alleviated this problem. The best response of the tabletop generator is not similar to the GTG model as shown in Figure 33.

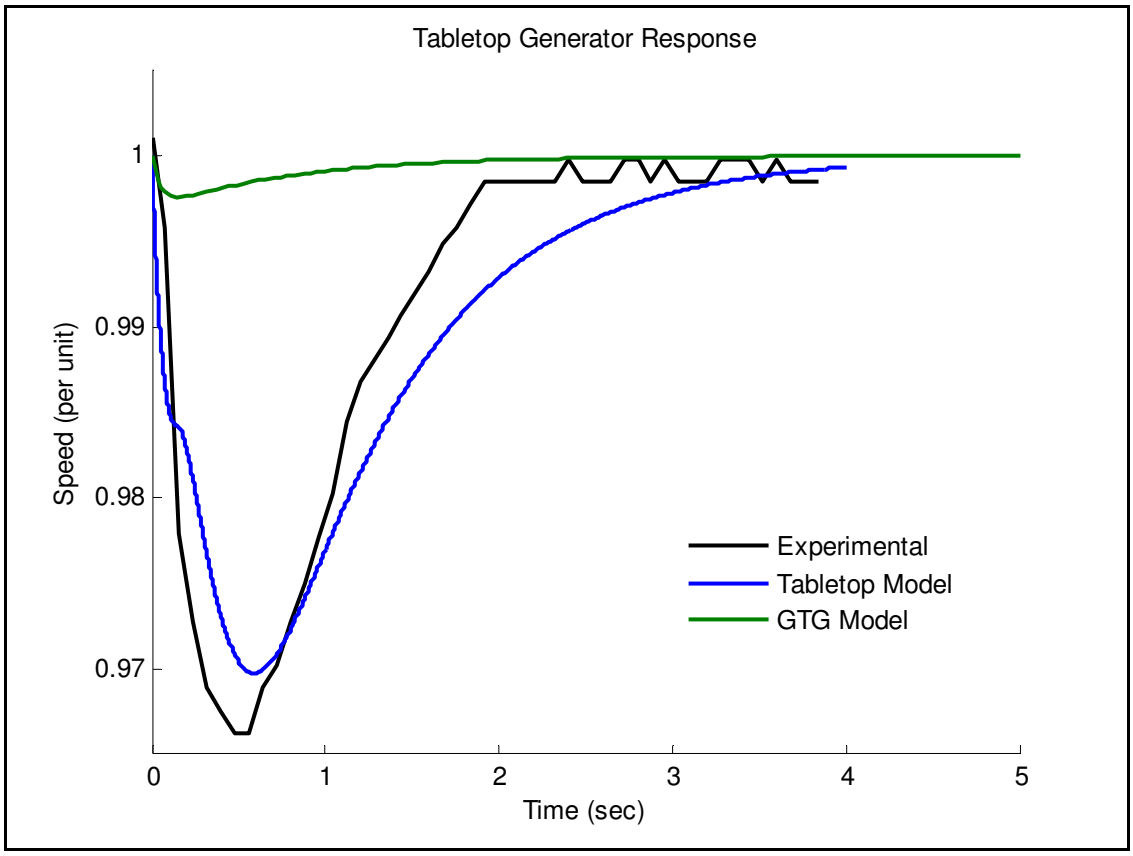

Figure 33: Response of Tabletop Generator

The proportional and integral gains in the software controller were set to 0.0012. Values higher than this resulted in significant oscillation. As shown previously in Table 6, modeled proportional and integral gains to match the GTG response are 0.165 and 0.215. The proportional and integral gains of the tabletop model were set at 0.012 to match the experimental response as shown in Figure 33. Given the similar response obtained with gains 10 times greater than those actually used, it is possible that a factor of 10 error exists between the Simulink model and the Labview controller.

Speed signal noise is a likely contributor in the significant oscillation that occurs with increased controller gains. The filtered speed signal is compared to raw data in Figure 34 and Figure 35. The effect of the signal's 8-bit resolution is shown in Figure 36.

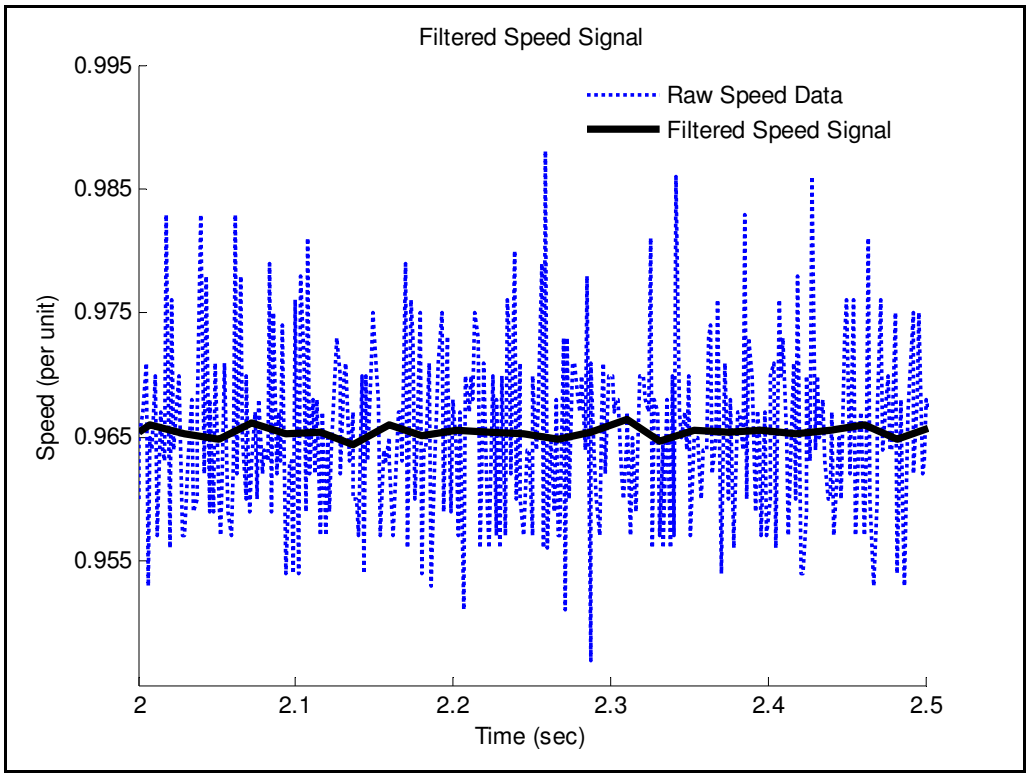

Figure 34: Filtered Speed Signal

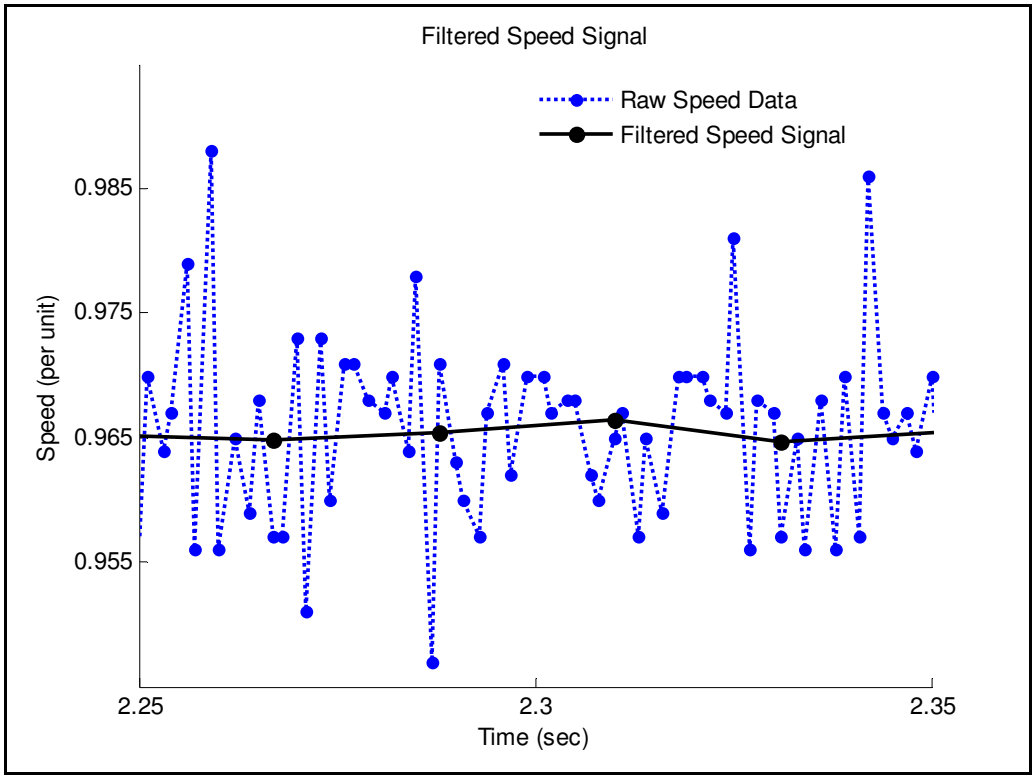

Figure 35: Magnified View of Filtered Speed Signal

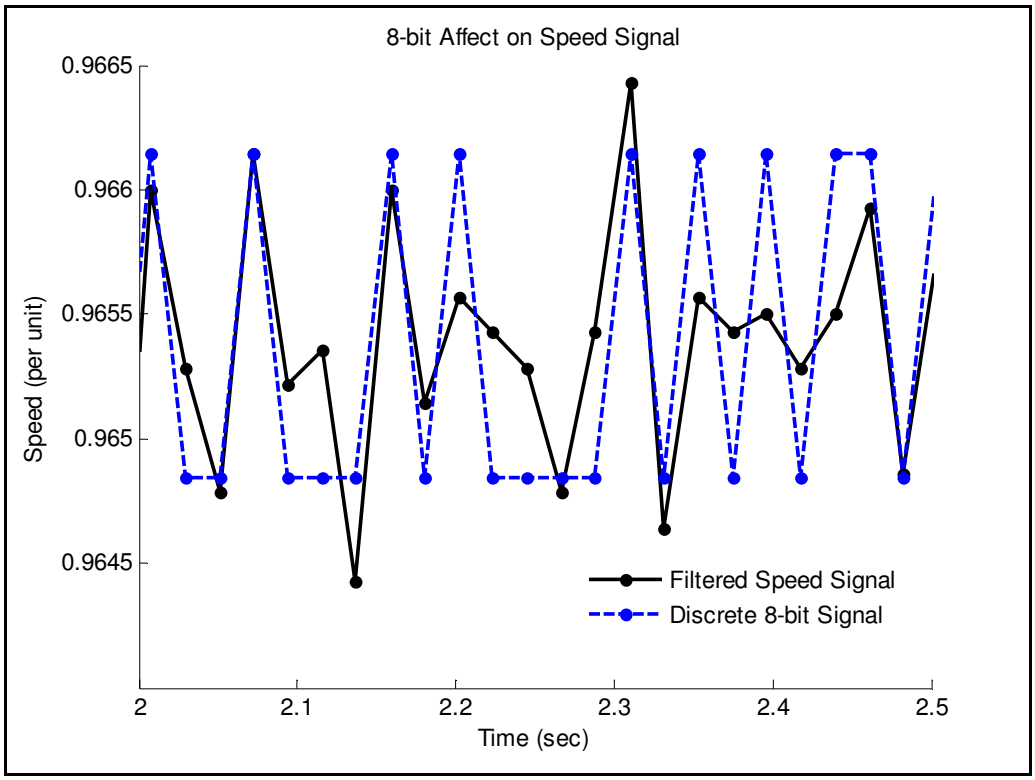

Figure 36: 8-bit Resolution of Speed Signal

The 8-bit resolution of the speed signal results in a non-uniform oscillation of the speed error where one value tends to be favored. As shown above, the signal is artificially low. The amplitude of the filtered speed noise is slightly greater than the 8-bit signal but shows more centered values. The 8-bit signal noise was introduced to the tabletop model as a repeating sequence similar to that shown in Figure 36 where one value is favored over another. The modeled response is shown in Figure 37 with the required controller gains to match the GTG model.

The oscillations predicted by the model occur at a rate faster than the speed sensor data rate. Currently, 14 data points are averaged to represent each motor revolution. This results in approximately 43 signals per second or one signal every 0.023 seconds. The steep oscillations predicted by the model suggest a significant change in speed may occur over this duration. The modeled affect of increasing controller gains is shown in Figure 38 and Figure 39.

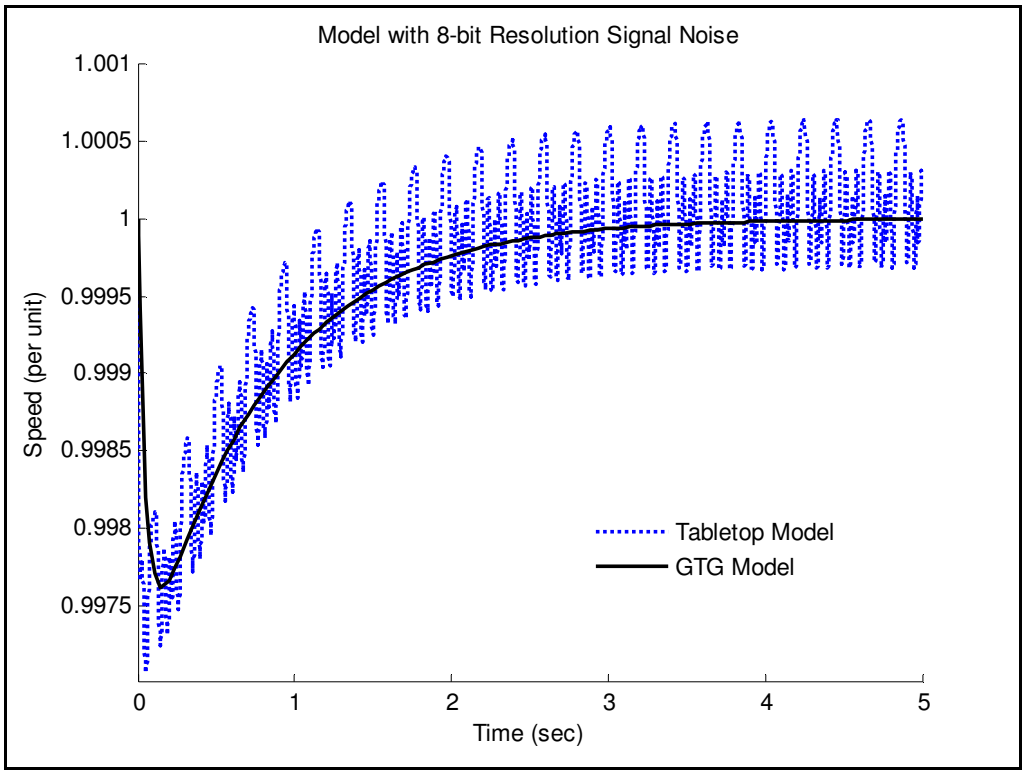

Figure 37: Tabletop Model with 8-bit Signal Noise

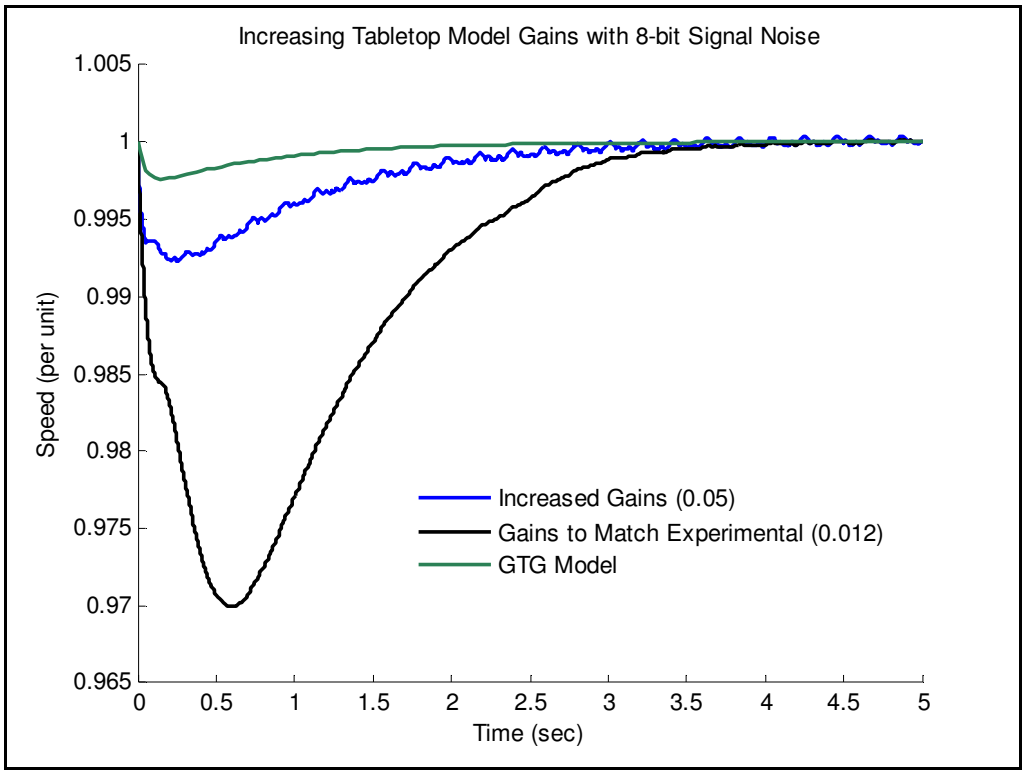

Figure 38: Increasing Controller Gains

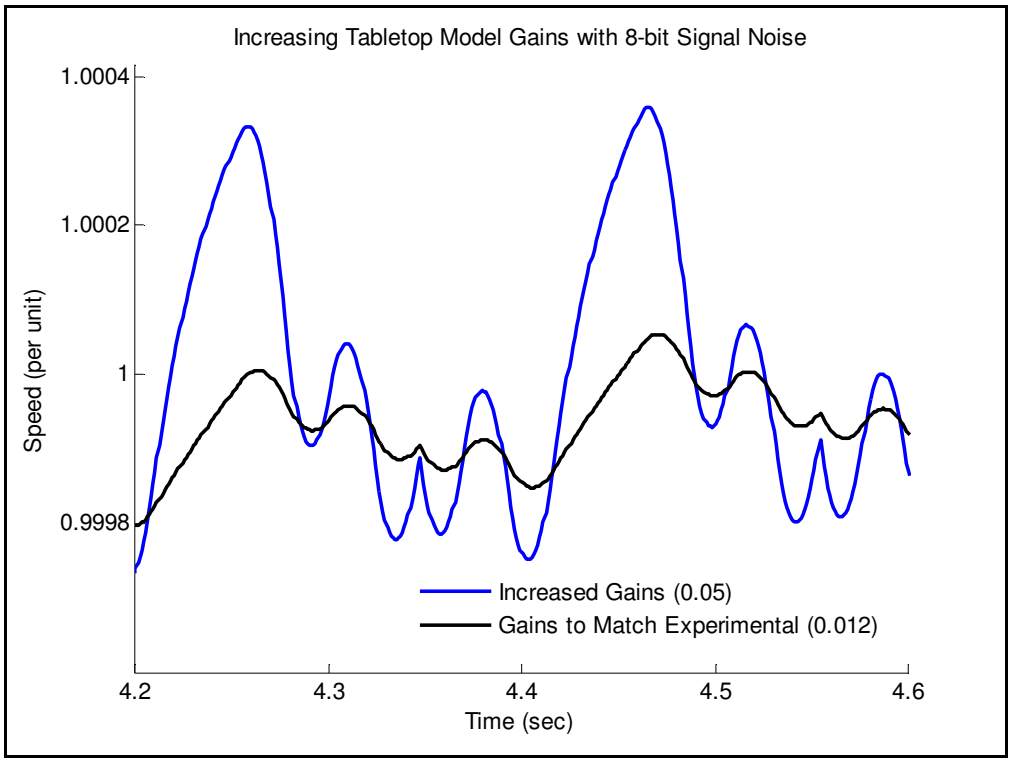

Figure 39: Increasing Controller Gains, Magnified

As gains are increased, the modeled response to speed signal noise shows steep oscillations that may not be seen by the controller until a significant change in speed has occurred. As such, speed sensor noise must be reduced while increasing speed data rate. The 14 tooth sprocket currently installed is not designed specifically to interface with the Hall Effect speed sensor. Construction of a 'speed sensor sprocket' may reduce noise and increase data rate.

Increased resolution of the speed signal may also improve response. However, it is possible that the 8-bit resolution may provide acceptable performance if signal noise is adequately reduced. Inclusion of gain scheduling is another option for consideration. Sensing a change in electrical loading, larger controller gains would be utilized during the transient while smaller gains are used during steady state operation.

Chapter 6

Conclusions and Future Work

The numerical model developed to describe the response of the Allison 501-K34 gas turbine generator provides the key characteristics of the actual response. It accurately describes the peak values reached during a transient and the time required to reach steady state. It does not precisely model the transition from the peak value to steady state.

The closed-loop feedback control modeling of the tabletop generator strongly suggests that the tabletop generator driven by a DC motor may be controlled in a fashion to resemble the speed response of a gas turbine generator. The best agreement occurs when the controller gains are adjusted for a specific change in loading. Deviations from this step change in electric power results in a modeled response of the tabletop generator that reaches a peak value slightly different than that predicted by the gas turbine model.

The response of the tabletop generator as realized is not similar to the GTG model. Controller gains utilized are significantly lower than those suggested by the modeling to match the GTG. As gains are increased, the modeled response to speed signal noise shows steep oscillations that may not be seen by the controller until a significant change in speed has occurred.

The model gains required to match the actual response of the tabletop generator are off by one order of magnitude. A factor of 10 error may exist between the model and software controller.

Speed sensor noise must be reduced while increasing speed data rate. The 14 tooth sprocket currently installed is not designed specifically to interface with the Hall Effect speed sensor. Construction of a 'speed sensor sprocket' may reduce noise and increase data rate.

Increased resolution of the speed signal may also improve response. However, it is possible that the 8-bit resolution may provide acceptable performance if signal noise is adequately reduced.

Gain scheduling is another option for consideration. Sensing a change in electrical loading, larger controller gains would be utilized during the transient while smaller gains are used during steady state operation.

Future work for this project includes that necessary to model a shipboard electrical distribution system. This includes developing a control system that provides accurate load sharing amongst two or more isochronous generators and establishing a methodology to parallel these generators in phase.

Additional work may also include the incorporation of an angled Howse Gearbox that has a well suited gear ratio for this application. This may reduce some power lost to rotational friction associated with the side loading of the generator shaft by the timing belt drive.

References

1. **Leeb, Steven B and Cox, Robert.** Role of the Combat Power Monitor in Zonal Electrical Distribution in the NGIPS. *Whitepaper.* Boston : MIT/Laboratory for Electromagnetic and Electronic Systems, 2008.

2. *Next Generation Integrated Power Systems (NGIPS) for the Future Fleet.* **Doerry, Norbert.** Baltimore : Naval Sea Systems Command, 2009.

3. **Drury, Bill.** *The Control Techniques Drives and Controls Handbook.* London : The Institution of Electrical Engineers, 2001.

4. Industrial Gas Turbine Engine Model 501-K34. *Specification.* Indianapolis : Allison Gas Turbine, 1987.

5. **Sheldrake, Alan L.** *Handbook of Electrical Engineering For Practitioners in the Oil, Gas and Petrochemical Industry.* West Sussex : John Wiley & Sons Ltd, 2003.

6. **Boyce, Meherwan P.** *Gas Turbine Engineering Handbook.* Burlington : Gulf Professional Publishing, 2006.

7. **Razak, A.M.Y.** *Industrial Gas Turbines Performance and Operability.* Boca Raton : CRC Press LLC, 2007.

8. Naval Surface Warfare Center, Carderock Division (NSWCCD). *Correspondance.* Philadelphia Site : Ship Systems Engineering Station (SSES), 2009.

9. **Green, Don W.** *Perry's Chemical Engineers' Handbook.* New York : McGraw-Hill, 1997.

10. **Kutz, Myer.** *Mechanical Engineers' Handbook.* New York : John Wiley & Sons, 1998.

Appendix A: Nomenclature, Data, and Calculations

1) Nomenclature as used in this thesis is listed below.

C1	conversion constant, per unit speed to rad/sec
C2	conversion constant, fractional change in V_{Term} to volts
C3	conversion constant, watts to per unit power
Er	error
fmax	maximum fuel flow
fmin	minimum fuel flow
Gh	inertia term, GTG model
H	inertia constant
I_M	motor current
K	motor constant
Kc	controller gain
Kdg	governor droop
Kg1	governor gain
Kg2	governor gain
Kg3	governor gain
Kh	inertia term, tabletop model
Ki	integral control gain
Km	mechanical power loss gain
Kp	proportional control gain
Kpm	prime mover gain
Ktv	terminal voltage gain
OP	controller output
P_M	motor power
R_M	motor resistance
Td	derivative time constant
Tf1	fuel valve time constant
Tg1	governor time constant
Tg2	governor time constant
Tg3	governor time constant
Tg4	governor time constant
Ti	integral time
T_M	motor torque
Tpm	prime mover time constant
Tt1	turbine leading time constant
Tt2	turbine lagging time constant
V_C	counter voltage
V_{Term}	terminal voltage
ω	rotational speed (rad/sec)

2) Data used in the determination of motor constants. Counter voltage was plotted as a function of speed (rad/sec) where the slope of the resulting line equals the motor constant K (volt*sec) as discussed in Section 2.3.

Motor 2 Driving Motor 1

Voltage (V)	Current (A)	Speed (rpm)	Counter Voltage (V)	Speed (rad/sec)
10	1.14	382	8.6	40.0
20	1.21	824	18.6	86.3
30	1.29	1265	28.5	132.5
40	1.34	1714	38.7	179.5
50	1.38	2152	48.6	225.4
60	1.42	2599	58.7	272.2
70	1.48	3044	68.7	318.8
80	1.53	3489	78.6	365.4
90	1.54	3932	88.5	411.8
100	1.55	4380	98.4	458.7
110	1.59	4822	108.2	505.0

Motor 1 Driving Motor 2

Voltage (V)	Current (A)	Speed (rpm)	Counter Voltage (V)	Speed (rad/sec)
10	1.22	371	8.6	38.9
20	1.34	814	18.6	85.2
30	1.42	1250	28.5	130.9
40	1.48	1691	38.6	177.1
50	1.53	2137	48.8	223.8
60	1.58	2579	58.9	270.1
70	1.64	3026	68.9	316.9
80	1.70	3467	79.0	363.1
90	1.70	3919	89.2	410.4
100	1.74	4366	99.3	457.2
110	1.69	4817	109.5	504.4

Resulting Motor Constants: $K_1 = 0.215$ (volt*sec)
$K_2 = 0.217$ (volt*sec)

3) Terminal voltage and speed data collected from both motors operating in series with no mechanical loading. Note that a 200 volt power supply was initially used for some testing prior to utilizing the 150 volt programmable power supplies.

Motor 1 and 2 in Series, No Load

Voltage (V)	Current (A)	Speed (rpm)	Speed (rad/sec)
20	0.57	418	43.8
40	0.59	862	90.3
60	0.62	1309	137.1
80	0.65	1750	183.3
100	0.67	2200	230.4
120	0.70	2650	277.5
140	0.72	3096	324.2
160	0.73	3546	371.3
180	0.74	3995	418.4
190	0.77	4226	442.5

4) Motor Resistance

Motor 2 Driving Motor 1

	Voltage to Drive Motor (V)	Speed (rpm)	Driven Motor Counter Voltage (V)	Driven Motor Current (A)
Driven Motor Open	5	166	3.79	-
Driven Motor Shorted	8.1	166	-	3.96

Motor 1 Driving Motor 2

	Voltage to Drive Motor (V)	Speed (rpm)	Driven Motor Counter Voltage (V)	Driven Motor Current (A)
Driven Motor Open	5	166	3.83	-
Driven Motor Shorted	8.6	166	-	4.2

$$R_{M1} := \frac{3.79}{3.96} \quad R_{M1} = 0.957$$

$$R_{M2} := \frac{3.83}{4.2} \quad R_{M2} = 0.912$$

5) Torque-speed curve for both motors operating in series electrically while mechanically joined via a rigid coupling.

		Vterm (volts):	100	125	150
	Speed (rpm)	Speed (rad/sec)	Torque (N*m)	Torque (N*m)	Torque (N*m)
K (V*sec)	0	0.0	23.1	28.9	34.7
0.432	400	41.9	18.9	24.7	30.5
	800	83.8	14.7	20.5	26.3
Rm (ohms)	1200	125.7	10.6	16.3	22.1
1.87	1600	167.6	6.4	12.2	17.9
	2000	209.4	2.2	8.0	13.8
	2400	251.3	-2.0	3.8	9.6
	2800	293.2		-0.4	5.4
	3200	335.1			1.2
	3600	377.0			-3.0

Sample Calculation:

$K := 0.432 \ (\text{volt*sec})$

$R_M := 1.87 \ (\text{ohms})$

$V_{Term} := 100 \ (\text{volts})$

$$\omega := \begin{pmatrix} 0 \\ 41.9 \\ 83.8 \\ 125.7 \\ 167.6 \\ 209.4 \\ 251.3 \end{pmatrix} \ (\text{rad/sec}) \qquad T_M := \left(\frac{K}{R_M}\right) \cdot V_{Term} - \left(\frac{K^2}{R_M}\right) \cdot \omega$$

$$T_M = \begin{pmatrix} 23.1 \\ 18.9 \\ 14.7 \\ 10.6 \\ 6.4 \\ 2.2 \\ -2 \end{pmatrix} \ (\text{N*m})$$

6) Best Suited Motor Speed and Gear Ratio

$V_{Term} := 150\ (volts)$ $K := 0.432\ (volt*sec)$

$I_M := 14\ (amps)$ $R_M := 1.87\ (ohms)$ $\omega := \frac{V_{Term} - I_M \cdot R_M}{K}$

$\omega = 286.6\ (rad/sec)$

$Speed := \omega \cdot \left(\frac{60}{2 \cdot \pi}\right)$ $Speed = 2737\ (rpm)$

$Gear\_Ratio := \frac{2737}{1800}$ $Gear\_Ratio = 1.52$

7) Analysis of Available Gear Ratios

Power Supply Voltage Limited

$Gear\_Ratio := \begin{pmatrix} 1.6 \\ 1.5454 \\ 1.52 \end{pmatrix}$ $\omega := Gear\_Ratio \cdot 1800 \cdot \left(\frac{2 \cdot \pi}{60}\right)$ $\omega = \begin{pmatrix} 301.6 \\ 291.3 \\ 286.5 \end{pmatrix}$ (rad/sec)

$V_{Term} := 150\ (volts)$ $I_M := \frac{V_{Term} - K \cdot \omega}{R_M}$ $I_M = \begin{pmatrix} 10.5 \\ 12.9 \\ 14 \end{pmatrix}$ (amps)

$Pwr\_Sup := I_M \cdot V_{Term}$ $Pwr\_Sup = \begin{pmatrix} 1581 \\ 1938 \\ 2104 \end{pmatrix}$ (watts)

Power Supply Current Limited

$Gear\_Ratio := \begin{pmatrix} 1.52 \\ 1.47 \\ 1.4545 \end{pmatrix}$ $\omega := Gear\_Ratio \cdot 1800 \cdot \left(\frac{2 \cdot \pi}{60}\right)$ $\omega = \begin{pmatrix} 286.5 \\ 277.1 \\ 274.2 \end{pmatrix}$ (rad/sec)

$I_M := 14\ (amps)$ $V_{Term} := I_M \cdot R_M + K \cdot \omega$ $V_{Term} = \begin{pmatrix} 150 \\ 145.9 \\ 144.6 \end{pmatrix}$ (volts)

$Pwr\_Sup := I_M \cdot V_{Term}$ $Pwr\_Sup = \begin{pmatrix} 2099 \\ 2042 \\ 2025 \end{pmatrix}$ (watts)

8) Determination of the Inertia Constant (H) and the inverted inertia term (Gh) utilized in the Simulink model of the Allison 501-K34 GTG.

The inertia constant is defined as the Kinetic Energy of the rotating system divided by the Volt-Amp rating of the generator. It represents the amount of time that the generator may supply power at its full rating utilizing the capacitive nature of the inertia with no additional mechanical input.

Note that the shipboard generator is a 4 pole machine that operates at 1800 rpm and it is not known if the inertia of the generator includes the associated gearbox.

$I_{GT} := 61\ (lb*ft^2)$ $I_{Gen} := 3550\ (lb*ft^2)$ $I_{sys} := (I_{GT} + I_{Gen})\cdot(0.04214)$

$I_{sys} = 152.2\ (kg*m^2)$ $\omega := 1800\cdot\left(\frac{2\cdot\pi}{60}\right)$ $\omega = 188.5$ (rad/sec)

$KE_{sys} := \frac{1}{2}\cdot I_{sys}\cdot\omega^2$ $VA\_Rating := 3\cdot10^6$ (volt·amps)

$H := \frac{KE_{sys}}{VA\_Rating}$ $H = 0.9$ (sec) $Gh := \frac{1}{2\cdot H}$ $Gh = 0.555$ (sec^{-1})

9) Tabletop Open-Loop Response Testing

Note that at the time of this testing, the prime mover gear ratio was less than optimum with a 32 tooth pulley on the generator and a 20 tooth pulley on the motor resulting in a gear ratio of 1.6 and a motor speed of 301.6 rad/sec to provide 60 Hz. As discussed at the end of Section 2.3, a better choice of a 22 tooth pulley was later installed on the motor resulting in the finalized motor speed of 274.2 rad/sec utilized elsewhere. Determination of initial motor power and power loss follows.

Supplying 225 watts at 60 hz and 120 volts (line to neutral)

$K := 0.432$ (volt*sec) $I_M := 5.85$ (amps) $\omega := 1.0056\cdot(301.6)$ (rad/sec)

$P_M := K\cdot I_M\cdot\omega$ $P_M = 766$ (watts) $P_{loss} := P_M - 225$ $P_{loss} = 541$ (watts)

$P_M := \frac{P_M}{5000}$ $P_M = 0.1533$ (per unit)

Supplying 675 watts at 60 hz and 120 volts (line to neutral)

$K := 0.432$ (volt*sec) $I_M := 9.21$ (amps) $\omega := 0.9991 \cdot (301.6)$ (rad/sec)

$P_M := K \cdot I_M \cdot \omega$ $P_M = 1199$ (watts) $P_{loss} := P_M - 675$ $P_{loss} = 524$ (watts)

$$P_M := \frac{P_M}{5000} \quad P_M = 0.2398 \quad \text{(per unit)}$$

Supplying 225 watts at 58.2 hz and 118 volts (line to neutral)

$K := 0.432$ (volt*sec) $I_M := 3.74$ (amps) $\omega := 0.9738 \cdot (301.6)$ (rad/sec)

$P_M := K \cdot I_M \cdot \omega$ $P_M = 475$ (watts) $P_{loss} := P_M - 225$ $P_{loss} = 250$ (watts)

$$P_M := \frac{P_M}{5000} \quad P_M = 0.0949 \quad \text{(per unit)}$$

The raw speed data required filtering to provide a reasonable response curve. Averaging the forward 10 data points in Excel resulted in the following improvement.

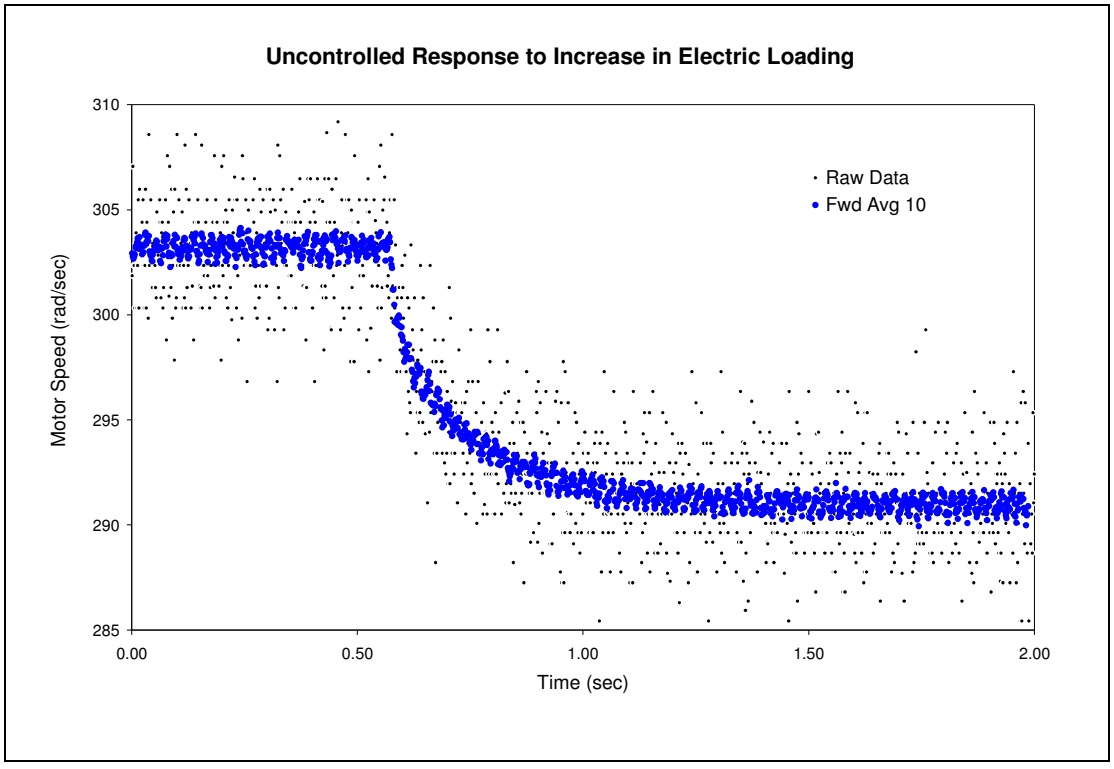

Sample data from open-loop response testing is provided below. The actual measured parameter is the frequency of the square wave generated as a sprocket mounted on the motor shaft interacts with the speed sensor fixed in close proximity. The inverse of the measured frequency is the period or pulse duration. Summation of the pulse durations provide the indicated time. With 14 teeth on the sprocket, the following converts sensor frequency to motor speed:

$$Speed = Freq \cdot \left(\frac{2\pi}{14} \right)$$

Speed Sensor Frequency	Pulse Time	Time	Motor Speed (rad/sec)	Filter (fwd avg 10)
686.44	0.00146	0.5521	308.0718	303.93
669.16	0.00149	0.5536	300.3205	303.26
671.32	0.00149	0.5551	301.2882	303.41
679.53	0.00147	0.5566	304.9735	303.36
676.04	0.00148	0.5581	303.4065	303.25
680.64	0.00147	0.5595	305.4717	303.46
683.06	0.00146	0.5610	306.5567	303.25
676.04	0.00148	0.5625	303.4065	302.58
671.50	0.00149	0.5640	301.3692	303.10
678.24	0.00147	0.5655	304.3943	303.10
671.50	0.00149	0.5669	301.3692	303.21
672.59	0.00149	0.5684	301.8556	303.62
670.24	0.00149	0.5699	300.8036	303.46
677.14	0.00148	0.5714	303.8996	303.72
680.64	0.00147	0.5729	305.4717	303.45
676.04	0.00148	0.5743	303.4065	302.64
668.09	0.00150	0.5758	299.8390	302.38
687.57	0.00145	0.5773	308.5801	302.23
671.50	0.00149	0.5788	301.3692	301.20
680.64	0.00147	0.5803	305.4717	301.19
680.64	0.00147	0.5817	305.4717	300.48
669.16	0.00149	0.5832	300.3205	299.66
675.86	0.00148	0.5847	303.3245	299.71
671.32	0.00149	0.5862	301.2882	299.61
662.43	0.00151	0.5877	297.2966	299.61
670.24	0.00149	0.5892	300.8036	299.86
664.72	0.00150	0.5907	298.3242	299.51
664.72	0.00150	0.5922	298.3242	299.96
671.32	0.00149	0.5937	301.2882	299.86
664.72	0.00150	0.5952	298.3242	299.46
662.43	0.00151	0.5967	297.2966	299.06
670.24	0.00149	0.5982	300.8036	299.41
673.67	0.00148	0.5997	302.3437	298.97
671.32	0.00149	0.6012	301.2882	298.77

Sample Data from Increased Electric Loading

Data collected prior to and after the desired response was removed after close examination of the areas of interest. The following shows how the data was shifted from when the data was collected (time stamp) to the actual response time. Also shown is the determination of initial speed which comes from the averaging of data points prior to the response time of zero.

		Fwd Avg 10			
Time Stamp	**Response Time (sec)**	**Speed (rad/sec)**	**Speed (per unit)**		
0.5714	0.0000	303.72	1.0070	**Initial Speed**	
0.5729	0.0015	303.45	1.0061	303.28	1.0056
0.5743	0.0029	302.64	1.0034	303.05	1.0048
0.5758	0.0044	302.38	1.0026	304.30	1.0089
0.5773	0.0059	302.23	1.0021	303.63	1.0067
0.5788	0.0074	301.20	0.9987	303.78	1.0072
0.5803	0.0089	301.19	0.9986	304.23	1.0087
0.5817	0.0103	300.48	0.9963	303.71	1.0070
0.5832	0.0118	299.66	0.9936	303.49	1.0063
0.5847	0.0133	299.71	0.9937	302.82	1.0041
0.5862	0.0148	299.61	0.9934	302.44	1.0028
0.5877	0.0163	299.61	0.9934	302.74	1.0038
0.5892	0.0178	299.86	0.9942	303.03	1.0047
0.5907	0.0193	299.51	0.9931	302.38	1.0026
0.5922	0.0208	299.96	0.9946		**1.0056**
0.5937	0.0223	299.86	0.9942		
0.5952	0.0238	299.46	0.9929		
0.5967	0.0253	299.06	0.9916		
0.5982	0.0268	299.41	0.9928		
0.5997	0.0283	298.97	0.9913		
0.6012	0.0298	298.77	0.9906		
0.6027	0.0313	298.22	0.9888		
0.6042	0.0328	297.77	0.9873		
0.6057	0.0343	298.37	0.9893		

Sample of Response Data Utilized in Open-Loop Modeling

10) Employed Speed Signal Filtering

The speed signal as utilized employed a filter that averaged every 14 data points. This corresponds with one speed signal for each motor rotation. The Matlab code used to create Figures 34, 35, and 36 is shown below.

```
UF = dlmread('Unfiltered_SS.txt'); %UnFiltered data at Steady-State
%column 1 is time, column 2 is per unit speed

for i=1:(length(UF)/14)
    Avg14(i,1) = UF(1+14*(i-1),1); %time at every 14th data point
    for j=1:14
        speed(j) = UF(j+14*(i-1),2);
        Avg14(i,2) = mean(speed); %avg every 14 speed values
    end
end

%discrete values for speed
%range is 50-70hz, 8-bit
Res = (20/256)/60; %resolution of per unit speed
for i=1:(length(UF)/14)
    Dis(i,1) = Avg14(i,1); %time
    Dis(i,2) = round(Avg14(i,2)/Res)*Res; %discrete speed value
end

hold on
plot(UF(:,1),UF(:,2))
plot(Avg14(:,1),Avg14(:,2),'k')
%plot(Dis(:,1),Dis(:,2))
```

Appendix B: Implementation of the Control System, by Vanessa Esch

Control System for a DC Motor-Generator System for operation as a Shipboard Gas Turbine Generator Model

Vanessa Esch
6.UAP
Spring 2009
at
Laboratory of Electromagnetics and Electronics
Massachusetts Institute of Technology

Abstract

The operation of a U.S. Navy destroyer power system is modeled in this project. The gas turbine generator system has been modeled using a DC motor and generator. The goal of the project is to prove that this model can be extended to act as a scaled GTG system on a TableTop platform to test load faults of the shipboard system. The model was completed first in Simulink and then a physical system to control the model was implemented. The work of the author of this paper was on implementing the physical control system. Although currently the system has power limitations, it can successfully be controlled, and with higher power supplies, can mimic the response of the Navy GTG system.

Acknowledgements

I'd like to thank Professor Steven Leeb and LEES at MIT for allowing me to work on this project for my 6.UAP requirement. U.S. Navy Engineering Duty Officers Jeremy Leghorn and Greg Elkins welcomed me to their project. Their support, encouragement and technical advice throughout the semester was essential. UROP student Jacob Osterberg assembled many of the hardware systems for the project and spent many hours lab testing the system with me. LEES graduate students Warit Wichakool and Chris Schantz gave their insight and support on the system throughout the semester. Also, I'd like to thank my mom for everything she does.

CONTENTS

List of Figures

Appendices

Note: The appendices listed here have been identified in this thesis as C, D, E, and F.

- Greg Elkins

1. Introduction

The purpose of this project is to develop a physical system that operates under reduced scaled characteristics of a U.S. guided missile destroyer (DDG) gas turbine generator set (GTG). The scaled system that has been developed uses a DC motor and generator instead of the gas turbine. The design goal is to use modeling and simulation to find the appropriate control constants for the system such that it behaves as a reduced scale DDG plant would. The control system is then implemented as a software-based feedback system for operation of the DC motor-generator set. Once this scaled system is fully proven and tested via implementation, the next step for the project is to do load and fault analysis in a manner similar to what is demanded of the system a DDG. The modeling and simulation aspect of the project is the work of a U.S. Naval Engineering Duty Officer thesis project. This undergraduate advanced project is to design and implement the actual control loop for the system in software.

This paper presents the technical background and work done toward these goals and the particular contribution of the author. Section two provides a technical overview of the GTG system on a DDG-51 class ship including its method of feedback control and the operating requirements of the shipboard system. Section three provides a similar description of the scaled system developed for testing in the project. This overview description will be followed by an in-depth analysis of the design decisions made for the system in section four. The section will focus on the control system, including the algorithm, physical system, and user interface, as that was the primary work of the author of this project. Section five is a complete explanation of how to use the system and user interface in the hope that it can serve as the foundation for future testing and use of the scaled system. Section six will conclude the paper with a reflection on the project and suggestions for future development of the system.

2. Navy System

2.1 Destroyer Physical System

Power generation of a DDG-51 class ship is provided by three 2500kW gas turbine generator (GTG) sets. The gas turbines are LM2500 engines made by General Electric. Each GTG set produces three-phase 450 VAC 60Hz for shipboard operations.[i] The Allison 501-K34 Gas Turbine Engine is the prime mover on the DDG-51 class ship; it is a single shaft, axial flow gas turbine. For 60Hz output from the generator, the LM2500 operates at 14,340 RPM. Reduction gear translates the engine output to 1800RPM, which correlates with 60Hz output.

2.2 Control System

On the highest level, the control system implemented on DDG GTG systems consists of two elements, a governor and a voltage regulator. These two components are very commonly used in control systems for prime mover and generator sets.[ii] The governor is the element that regulates the output frequency of the system and the voltage regulator controls the amplitude of the voltage produced by the generator. A basic understanding of the design of these elements on the naval system directed the design of the system in the scaled model. The description of these systems is from training documents provided by the Surface Warfare Officers School in Newport, RI.[iii]

On a generator system, real power is related to the prime mover's delivered energy, and therefore the speed of the generator. Reactive power is related to terminal voltage. A generator fails under too great of a real power load due to speed collapse and also fails under too great a reactive load due to voltage collapse.[iv] The system built here attempts to avoid both types of collapse under scaled, rated load application and removal.

2.2.1 Governor

A change in the ship's load is sensed by a load sensor at the output of the generator. When a change in the load occurs, the output voltage and current signals will change both in amplitude and frequency.[v] In order to regulate the frequency of the system, the load sensor measures the frequency of the generator output voltage and calculates a speed error signal for the feedback system by comparing that value to a speed reference value set by the operator, nominally 60 Hz.[vi]

The speed of the prime mover (gas turbine) is regulated by a feedback loop based on this speed error signal. The speed error is sent through both stability and gain amplifiers, "the gain amplifier decreases response time (dampens); the stability amplifier prevents hunting."[vii] In basic control theory, Proportional-Integral-Derivative (PID) control is the common type of control system, and among the three parallel branches of a PID control, integral control is the primary mechanism for avoiding drooping and derivative is the primary mechanism for preventing hunting (ie, oscillate) which occurs which pure proportional control.[viii] A very common method of control for GTG found in literature is PI control (without a derivative branch).[ix] For the naval system, it is appears that PI control is the means used for closed loop feedback in the speed governor. The system used in the model also implements, optionally, a dead band to avoid hunting near the set-point.[x]

There are two modes of frequency control on the DDG, isochronous and droop (ISO and DROOP).[xi] In ISO operation, feedback will try to maintain frequency at the reference speed while in DROOP mode, feedback will not occur and frequency will drop if the load increases. On the ship, DROOP mode is used only for connecting to shore power as shore power is considered an infinite bus supply and if load sharing between it and the shipboard generators takes place, the generators will be pushed beyond their capacity.

The steps required to implement the naval speed control system are more complex than the ones implemented in the scaled version presented here because of the different prime movers. In order to adjust speed, the gas turbine fuel input rate must adjust and temperature bounds must be monitored closely. In the scaled version, all that is necessary to adjust the speed of the DC motor is an adjustment of the DC input voltage to the motor.

2.2.2 Voltage Regulator

The primary purpose of the voltage regulator is to directly adjust the excitation field current applied to the rotor of the generator so that the output voltage of the system has the desired amplitude.[xii] Additional components in the voltage regulation system on the DDGs include a current limiter, an over-voltage limiter, and a failure detection module.

The voltage regulator is supposed to maintain the following operating restrictions on the system;

1. Current over 12,900A on any phase of the generator stator will result in a reduction in field current such that the system voltage (and therefore current) will be reduced.
2. Voltage over 522 VAC for 1.5 seconds or 590 VAC instantaneously will force the field current to drop to the level that correlates to 518 VAC output until an over-voltage protection switch is re-set.

2.3 Navy Operating Requirements

The scaled model developed in this project must operate under the constraints of the GTG system actually deployed on the DDGs. The naval specifications have strict voltage and frequency requirements, these requirements differ slightly between flights (or versions) of the DDG class of ships. Flight I ship, DDG 51-90, have different GTG specifications than Flight IIs,

DDG 91 and later. For Flight I ships, the application and removal of rated load may cause no greater momentary deviation from system frequency than two percent. However, on the Flight I's, this maximum error is two percent for overspeed (application of load) and 2.5 for underspeed (removal of load).[xiii]

On both flights and for load removal and application, the system has 1.5 second to return to within one percent of the normal operating frequency. This final requirement is interpreted to mean that during normal operation, frequency deviation within one percent is acceptable. Also, any added or removed load that does not cause the steady-state load to exceed the rated load should not trip the engine. In order to meet these specifications, a well calibrated control system will be required of the scaled system.

3. Scaled Test System

3.1 Physical System Design

3.1.1 DC Motor

The system controlled in this project consists of two series permanent magnet DC motors that drive a generator. The motors are Leeson 2 HP machines; in series they deliver a total rated capacity of 4 HP. Basic Kirchoff's laws establish the characteristic equation for a DC motor, see equation [1]. The equivalent circuit model of a DC motor is shown in Figure 1.

$$V_{term} = I_a * R_a + V_{emf} \quad (1)$$

Figure 1: Equivalent circuit of DC motor

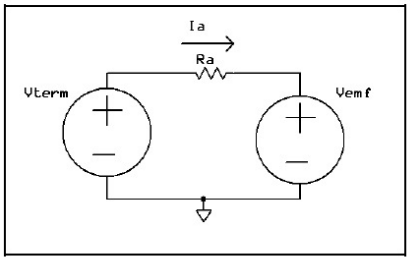

In a permanent magnet motor, the armature current is held constant, therefore there is a linear relationship between speed and back electro-motive force (EMF) (2).[Greg's 1] Torque also exhibits a linear relationship, albeit with armature current (3). Experimentation in the lab determined the motor constant, K, to be .215 Volt-sec for one motor and .217 Volt-sec for the other.[xiv]

$$V_{emf} = K * \omega \quad (2)$$

$$\tau = K * I_a \quad (3)$$

An increase in mechanical load will decrease counter voltage. Since terminal voltage can remain constant under a change of load, this change would force the armature current to become much larger in order to satisfy the Kirchoff's voltage loop. The DC motor shows its inherit stability in this situation because armature current and counter voltage would adjust until, at a lower speed, power could be matched between the motor and load.

Figure 2: Torque-Speed curve of scaled system

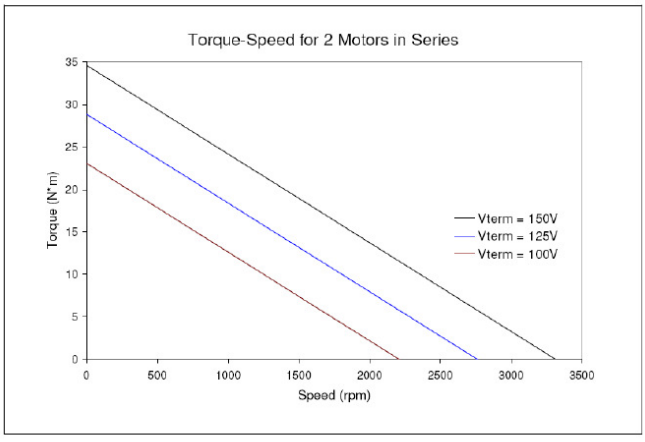

This would be a new steady state for the motor. A change in terminal voltage would have to take place in order to get the speed of the system back to its original level.

The torque-speed curve is the essential operating curve for these operations. Although the two motors in series have a rated speed of 4800 RPM at 240 V, the system limitation is 150 V for terminal voltage. Therefore, torque-speed curve, measured by Greg Elkins, shows terminal voltages of 150V or less. The torque-speed curve is shown in Figure 2.

The generator is a Ming Dong STC-5 series three-phase AC synchronous generator.[xv] The generator has a rotary field and is three-phase Y-connected with a center ground. The generator is a salient pole machine. It has line-to-line and line-to-phase voltages of 400 V and 230 V, respectively. Its rated output is 6.3 KVA or 5KW with a rated current of 9A and power factor of .8 lagging. Rated speed is 1500 r/min. The generator has 4 poles. The prime movers for these generators can be connected directly or via a V-belt, (this system uses a V-belt; its design will be discussed shortly). The generator is designed with a built in voltage regulator, however in system testing, it was found early on that that regulator was not robust enough to control the voltage through the changes in load that the system required.[xvi]

Throughout this project, the exact operating characteristics of the generator have been unverified. The primary reason for the choice of generator was price. The Ming Dong generator was manufactured in China and has very few published specifications; those that are published can be found in Appendix A. The unknown

Figure 3: Adjustable test-bed of loads: This arrangement of loads from 75W per phase to 1125W was created for initial testing.

nature of the generator makes the effectiveness and reliability of the feedback system, as well as system testing, incredibly important.

The load used in this model is a Y-connected arrangement of light-bulbs. Only these resistive loads have been used to test the model system so far. Each line on the Y-connected load has three inserts for light-bulbs that can be switched on or shorted; this arrangement provides a discrete variable load for the preliminary testing done in this project (see Figure 3 for image of the load arrangement). A complete parts list can be found in Appendix B.

3.2 Scaled Control System

In this system there are two independent control loops that mirror the governor and voltage regulator of the DDG plant. They control the frequency and voltage RMS values, respectively.

3.2.1 Governor

DC motor speed control can be implemented in any of three ways, via field resistance control, armature voltage control, and armature resistance control. [xvii] This design controls the motor via armature voltage with proportional and integral control (PI control). With just proportional control, the system feedback is more likely to overshoot the desired frequency beyond the acceptable range of the Navy specifications. Therefore, integral control is also needed. However, the less the relative weight of the integral control constant relative to the proportional control constant, the faster the system will return to 60 Hz after a major disturbance.[xviii]

Ideally, the speed of a DC motor is directly proportional to the input DC terminal voltage. In reality, resistance to increases in torque for upon increased terminal voltage is caused by the back emf, this reduces the slope of the voltage-speed curve at higher voltages.[xix] The most

common means of controlling a DC motor is to use pulse-width modulation control to vary the terminal voltage.[xx] However, for the sake of expediency and simplicity, this system uses a remotely controlled power supply to generate the terminal voltage to the motor at a level calculated by the software based feedback system.

The feedback loop measures the speed of the DC motor against a reference frequency, by default 60Hz. While the actual frequency of the system is from the output of the generator, that value is mechanically tied to the speed of the motor and the turns ratio of the V-belt. A Hall Effect sensor on the output of the motor is a straightforward and acceptably accurate means of reading the speed of the motor, and with equation 1, the frequency of the system.

The software control loop sets the power supply remote control voltage, V_{cr}, between 0-10 V. This value controls the output of power supply, ie, V_{term} of the DC motor. Therefore V_{cr} directly controls output speed and V_{cr} adjustments can remove the error between the DC motor speed and 60Hz. A diagram that includes this loop is shown in Figure 4.

3.2.2 Voltage Regulator

The second control loop of the scaled system provides feedback on RMS values of the output phase voltage of the generator. The voltage regulator for this system is implemented as shown in Figure 4. A PI control loop was chosen for the feedback system. The voltage regulator for this system is based on the error between the sum of the three phase-to-ground RMS voltages and a

Figure 4: Control Loop Diagram

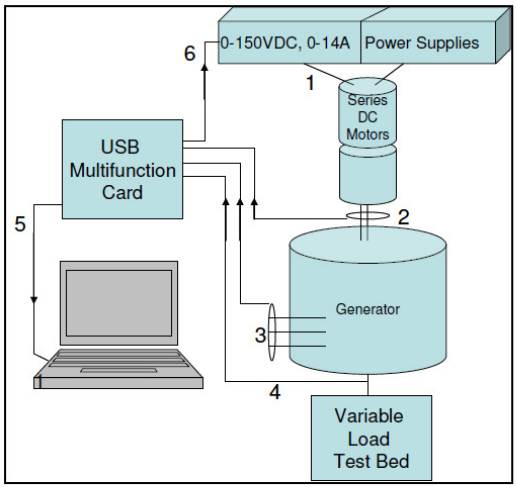

reference voltage. The feedback loop directly adjusts the field current of the generator rotor. The field current is adjusted with a variable power supply that sends a DC voltage through the field resistance (again, a power supply was chosen expediency and simplicity).

The actual control loops are implemented in the LabVIEW development environment. PI control loops were chosen as the control method for both the governor and voltage regulator loops given the popularity of that method of control for motor-generator control loops as published by Stephen Umans[xxi] and Kim et al[xxii].

The details of the signal manipulation will be discussed in the next section. The design of this system was not chosen for power consumption efficiency or practicality in applications. The purpose of the design is a proof-of-concept scaled power generation system for a future laboratory test-bed for the load monitoring system. Therefore the choice of parts for the system was driven by the team's best judgment of what would be effective but the fastest to build and cheapest.

Scaled System Operating Requirements

The performance requirements for the scaled system will be the same as those specified for the destroyer system. Given the responsiveness of the DC motor system compared to a gas turbine system, one concern was that the scaled system would be too responsive to changes in load to be an accurate model for the gas turbine generator. In this case, a time delay would have to be added to slow the feedback system down. Tests, as described in section 6, were done to measure the responsiveness of the system. The physical differences between the scaled system and the naval system are summarized in Table 1.

Table 1: Comparison of Requirements of Naval and scaled systems

	Scaled Model	DDG
Prime Mover	Two parallel DC motors	Allison 501-K34 Gas Turbine Engine
Generator	STC-5 series 3-phase synchronous Mingdong	Allison 501-K34 Gas Turbine Generator set
Rated Voltage	400V/230V	450
Rated Current (A)	9	4009
Power Factor	0.8 (lag)	0.8 (lag)
Output KW	5	2500
Rated Speed	1500 RPM	14,340 RPM
Pole Number	4	2
Exciter	DC power supply	Three phase brushless excited motor

4. Design of Scaled Model

4.1 Software Modeling

In order to prove that the DC motor-generator would suffice as a model for the gas turbine-generator system it was necessary to model the two systems in a software modeling environment. The modeling work and simulations were completed in the theses of two U.S. Navy engineering duty officers, Gregory Elkins[xxiii] and Jeremy Leghorn.[xxiv] They developed models of the motor operation, LCDR Elkins, and the generator, LCDR Leghorn, to prove the system could be used as a scaled DDG model.

A per-unit system was developed in MATLAB Simulink that models the behavior of the physical scaled system in the lab. Power per unit is 5KW as that is the rated real power for the generator. Due to the ratio of the V-belt between the DC motor and generator, the speed per unit is 2880RPM. This motor speed runs the generator at 60Hz.

4.2 Detailed Hardware and Software Implementation

The following section discusses in detail the design choices of the current physical feedback loop. Work on the implementation of this system was done through UROP (Undergraduate Research Opportunity Program) by Jacob Osterberg, and by the author for this 6.UAP (Undergraduate Advanced Project). Circuit diagrams and further details can be found in Appendix C.

The design priorities on the implementation were cost and expediency. Therefore when possible, equipment available in the laboratory and what we thought would be quick, reliable solutions were chosen. In some cases, the actual expediency of the design choices was less than expected. This section includes a discussion of lessons learned and implementation challenges as well as the final design.

4.2.1 Software and I/O Card

The first purchase and defining element of the feedback control project was the software/hardware interface for the control loop. The interface built consists of a hobbyist kit input-output board and the LabVIEW Student Edition software development environment. A software-based control loop was chosen over pulse-width modulated power electronics with the belief that it would provide more flexibility and extensibility for future testing. Hopefully, this system will be the foundation for the streamlined user interface of the future TableTop test-bed. The multifunction input-output card is the connection between system control signals and measurements, it is controlled by the LabVIEW user interface. The card that was chosen has a total of thirty-three digital and analog inputs and outputs, although this is more than necessary, this board is large and flexible enough to incorporate future additions or testing regimes without

additional investment. Additionally, with all inputs and outputs controlled from one central location, data acquisition and analysis will hopefully be easier.

The user interface for the physical model was built in LabVIEW. The primary LabVIEW Virtual Interface (VI) is called the "Panel." The Panel controls and reads physical values through the input-output card which is a Velleman K8061 USB Extended USB interface card (also known as the preassembled VM140 card). The card will be referred to as the I/O card (shown in Figure 5). The I/O card comes with a software driver and a dynamic link library (DLL) with functions that command the I/O card. In LabVIEW, a LabVIEW Library was created as the central location for all functions and code relating to this project, the library is called the User Interface Library (UILib). The I/O card DLL was imported to UILib and every card function (there are twenty-five) was compiled as an independent sub-virtual interface (subVI) that can be run individually within other VIs in UILib. The user manual for the K8061 card can be found online or on the laboratory computer. The Panel was created as a VI in UILib as well; the function subVIs are called from the Panel.

Figure 5: I/O Card. The input/output card for the system was a K-8061 Velleman Hoobyist Kit USB Board.

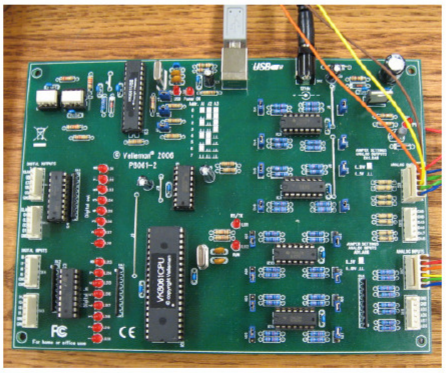

Although the LabVIEW-I/O card arrangement provides flexibility and user-friendliness, there are limitations to the I/O card's capabilities that required an unforeseen increase in the

complexity of signal manipulation between the system and the I/O card. The I/O card has both analog and digital inputs and outputs, however, it translates all signals to either 8 (for output) or 10 (for input) bit digital values on either a 0-5V or 0-10V scale. Precision is lost. Furthermore, the channels are specified as DC voltage channels by the manufacturer. The reason for this specification is that calls to read or write to a channel on the card are discrete and only return or set a voltage one time when they are called. These specifications for the I/O card have required increased complexity in software and hardware for this loop.

The hardware adjustments necessary for use of the I/O card were to translate both the motor speed (approx. 2880 RPM) and the phase-to-ground RMS voltages (approx. 120 V) to DC voltages between 0-10V that can be read into the I/O card. The circuits for both of these translations were built primarily by Jake Osterberg (see Appendix D). An 8-bit PIC18F4620 microcontroller was used to translate the motor speed to a DC value and LTC1966 Precision Micropower RMS-to-DC Converter chips were used to read the RMS voltage levels of the output phase voltages. The chip translates the RMS voltage to a DC value between 0-10V. Although the addition of these circuits has added complexity to the system, complexity itself is not a problem. However, it has increased the likelihood that a small error or noise in any part of the system will magnify and propagate to the voltages read by the software. To counter the uncertainty added by these parts, control system constants have been adjusted. The frequency reading is very consistent during steady state. Figure 8 shows stead state frequency readings. The discrete jumps are the difference between the 8-bit digital values that voltage is converted into from the I/O board.

Figure 6: Steady state frequency during feedback. The variations are discrete and caused by rounding between 8-bit input values from the I/O board.

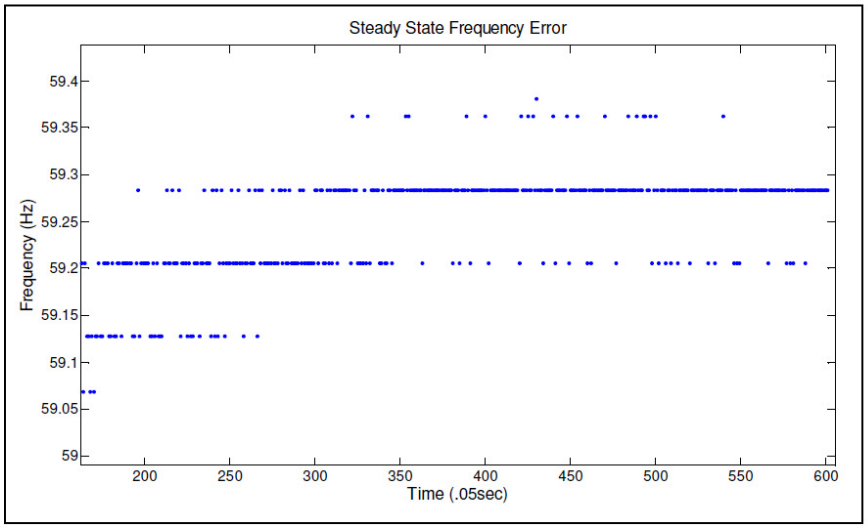

4.2.2 Power Supplies

Sources of DC voltage for this system are needed to power the DC motor and the field current in the generator. We decided to use power supplies for both of these sources as they would be the simplest to implement from the board as long as the supplies have analog voltage-based remote control and provide enough power. The initial goal for the optimal terminal voltage power supply for the motor voltage was 200V and 10A. However, when two 150V, 7A supplies that could be paralleled to provide 150V and 14A were found in the lab, they were used instead.[xxv] Given that researching the price for a controllable supply with these high power ratings made it clear that one would not be purchased for less than $2000, these power supplies were the best choice.

These supplies are 1000W series XHR 150-7s made by Xantrex (see Appendix E). The power supplies are remote controllable and when placed in a master-slave configuration, they should produce 14A and 150V. This power output fits the specifications for system power with

an adjustment in the motor to generator pulley.[xxvi] The lower power at the input of the system requires a lower terminal voltage to be able to drive the generator at rated frequency, 60 Hz. The pulley adjustment allowed a lower motor speed to correspond with a higher generator speed.

The XHR 150-7 output can be remotely controlled with a 0-5V or 0-10V DC voltage that will linearly correspond to an output voltage of 0-150V. We set the system to run on a 0-10V DC input from the I/O card. Each discrete voltage level specified by the 8-bit I/O card analog output is a jump of .58 volts on a scale of 0-150V. The implications of this constraint are discussed in the following section. The voltage-speed curve of the motor is shown in Figure 6.

Figure 7: Speed-Voltage Curve of Motor

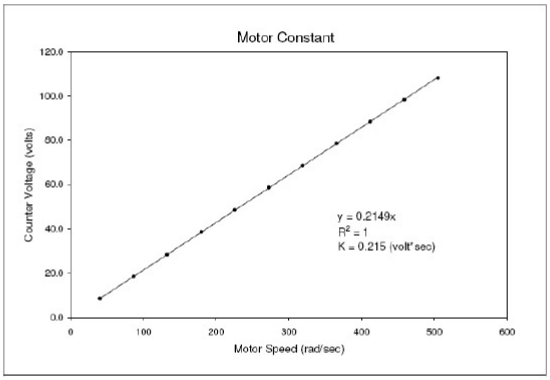

The field current power supply was purchased very late due to the high cost of the supply needed. It is calculated that we will need a power supply that provides simultaneously 3A and 50V. Currently, there is manually controlled power supply that fits these specifications in use in the system. The purchase delays were because no analog signal control supply could be found for less than $1000. However, an economical supply operated by serial port was found, and has been purchased though not incorporated into the system. It is an Instek PSP-603 60V/3.5A supply. This supply can be integrated into the LabVIEW Panel using the control functions through the USB serial port instead of analog control through the I/O card.

4.2.3 Pulley System

The physical connection between the motor and generator is a V-belt. The sizing of the pulley between the two is essential to meeting the operating requirements of the system under loads given the restrictions of power from the XHR 150-7s. Initially, the pulley had 32 teeth. To calculate the speed requirements for this system we can use equation [2]. We know our maximum voltage and current is 150V and 14A respectively. Also, from characterizing the motor we know K and R from the voltage-speed plot shown in Figure 6. The pulley was adjusted to one that has 22 teeth so that rated speed would be reached at approximately 125 V unloaded.

4.2.4 Summary of System Operation

The first step in the system is when LabVIEW (either through automated feedback or manual user control) designates a terminal voltage and, in future, a field current level that will drive the motor and generator, respectively. These voltage levels will be translated to 8-bit values and then outputted as the corresponding voltages between 0-10V on the I/O card. The terminal voltage 0-10V DC voltage is inputted to the back of the master XHR 150-7 power supply and commands the output voltage of the power supplies.

The terminal voltage is applied to the armature of the DC motors and produces mechanical torque in the series motors. The shaft of the DC motors is connected via V-belt to the rotor of the generator. Mechanical power is transferred to the generator via V-belt. The speed of the motors determines generator frequency. In a separate loop, the field current determines generator output voltage amplitude. In order to control the terminal voltage and field current, the frequency and RMS system voltage are feedback to the software to calculate the appropriate next value for these signals.

5. System testing and Analysis

The graduate theses on this system were to test whether the physical system, as modeled in software simulations could theoretically represent a scaled version of a DDG gas turbine generator. The purpose of this undergraduate project was to prove or disprove the physical ability of the system to operate as a scaled version of the DDG system. The answer to whether this physical system can be used in future testing as a reduced scale version of the DDG plant is yes, with a caveat. The present arrangement has major limitations in two areas, some can be improved upon, some can not. The first source of limitations is the power supply rating. The second problem that hinders the successful replication of the successfully simulated model in the physical system is the imprecise nature of both the input and output signals of the control loop.

In testing, the control loop constants had to be adjusted to fit the time and accuracy limits of the physical system. The optimal control constants for the physical system are very different than those of the Simulink system. One major difference between the two is that the physical system has a delay time between iterations of the feedback loop. This component was not considered in the more complex mathematical models in Simulink. The equations used for feedback in the physical system are shown below. The variables are defined as follows, e is the error, f_{set} is the desired system frequency, f_{system} is the frequency read in for the system.

$$e = f_{set} - f_{system} \tag{4}$$

$$V_{term\,(n)} = 150V + \left(K_p * e + \int_{n-30}^{n} K_i * e * dt \right) \tag{5}$$

Although it is not in use now, the secondary loop, for RMS voltage and field current is set up in LabVIEW. If the inheritors of the project have access to a 0-10V remote controlled

power supply to power field current, all that will be necessary is a tuning of the gains in LabVIEW. A serial-port controlled power supply will require additional work simply to add the control methods to the UILib and call those instead of I/O card DLL functions to set the voltage. Data acquisition is already running for RMS voltage and will be able to run through the board as set up. Another channel can be used to record the field current power supply voltage if desired.

In development of this project, major errors were recorded during testing related to magnetic field interference. These errors produced erratic frequency readings. An example of the incorrect data is shown in Figure 7. After debugging, the problem was discovered and physical layout changed. The changes removed the error. After that improvement, tuning could take place.

Figure 8: Data Run with Data Errors. Red is where unexpected and extreme frequency values were read into the system.

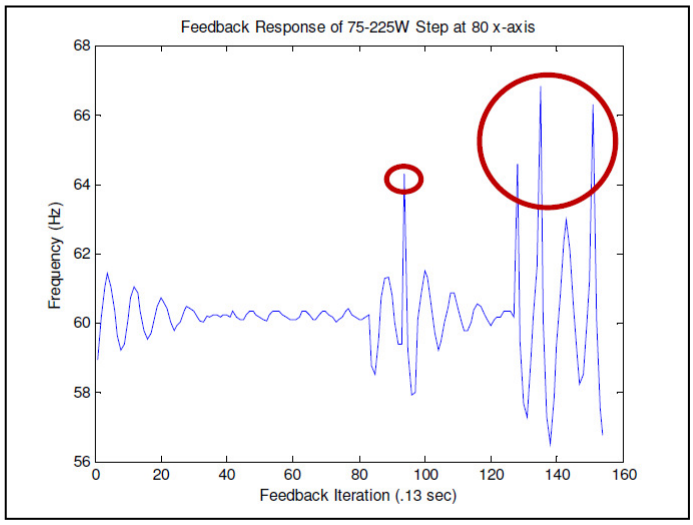

Instability invariably occurred when the physical system was put under the control conditions found in the Simulink model. The reason for this instability is that the simulated governor is built to correct frequency to within 0.15 Hz. In the physical system, the use of the relatively large PI constants developed for this precise control causes extreme oscillation. Using these constants demands the system operate more precisely than it can measure. The feedback control is trying to maintain an error less that 0.15 Hz and the speed reading is oscillating occasionally more than that. See Figure 8 for an example of the steady state error in

frequency. The error is mainly due to rounding errors of the 8-bit digital representation of the frequency in the software. This limitation is caused by the I/O card. Instead of stabilizing frequency, with this error, the simulated constants cause the governor to alternately force the terminal voltage to zero and maximum, 150 V. It was found that an initial $K_p = 0.01$, $K_i = 0.0$, and feedback loop period = .1 sec could control the system stably and near Navy regulations. These values are very far from the Simulink values of $K_p = 1.8$, $K_i = .23$ and feedback period = nearly continuous.

After tuning, the optimal constants were found to be $K_p = .0012$, $K_i = .0012$, time delay = .08 seconds and no dead band. The results from a load change from 225W to 675W is shown in Figure 9. The relationship between the K-values and time delays is not mathematically known and needed to be tuned manually. It was roughly found that the faster the feedback operates, the lower the K-values needed to be to avoid overshoot. The optimal response is the best fit for the

Figure 9: Good Feedback Data. Example of good feedback occurring under a change of load from 75W to 225W per phase.

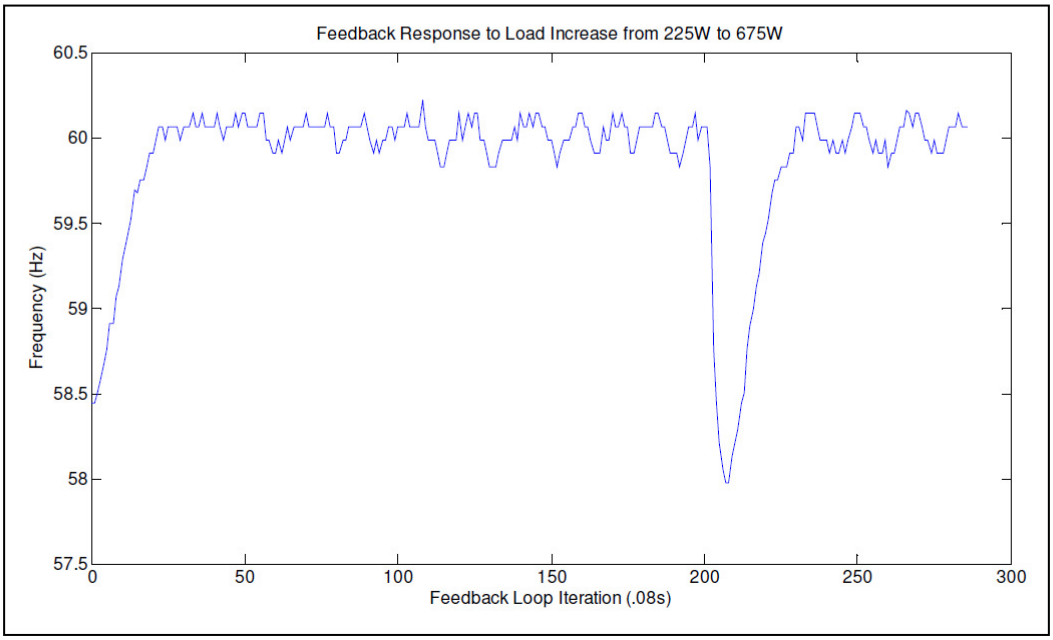

Simulink model because it doesn't overshoot and it also smoothly returns to steady frequency like the GTG system.

A major limitation of the current system is that the power supply simply can't deliver high enough power for full-load operation. When the maximum load of the current load platform, 1125W, is applied the system saturated. The effect on the frequency can be seen in Figure 10. This figure shows an application of the 1125W load at approximately 50 iterations and 150 iterations. The response to the application of the load, as well as observation of power supply operation, show that the power supplies were current limited during the response. In order to handle rated load for the system, actually 5kW, a much more powerful power supply is needed. The actual response of the GTG system is shown in Figure 11 for comparison.[xxvii]

Figure 10: Largest Applied Load. 1125W applied and removed from system with Ks = .0012 and time delay = .08 sec.

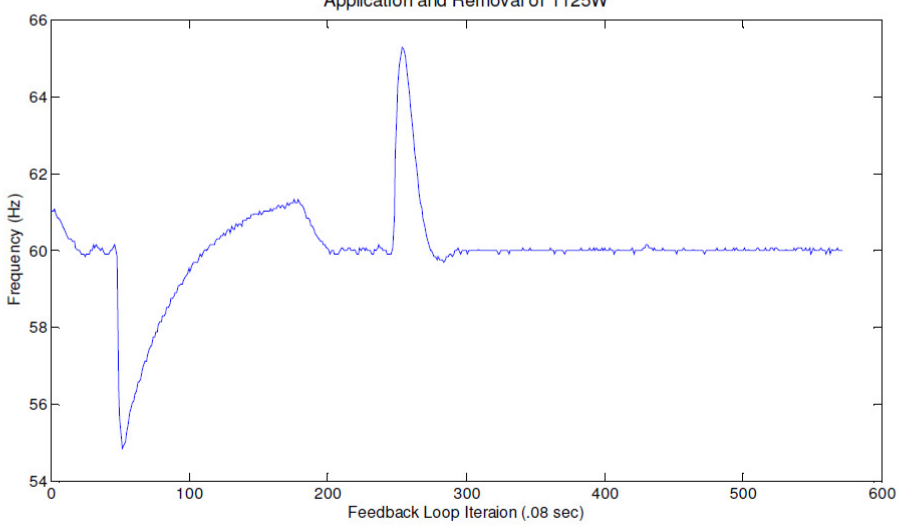

Another place where imprecision is added to the system is where the I/O card sets commands the terminal voltage level. Output analog voltages from the card are 8-bit values. Every step in the 8-bit value corresponds to a change of .58 V in the terminal voltage. This

Figure 11: Response of the actual GTG system to application and removal of its rated load.

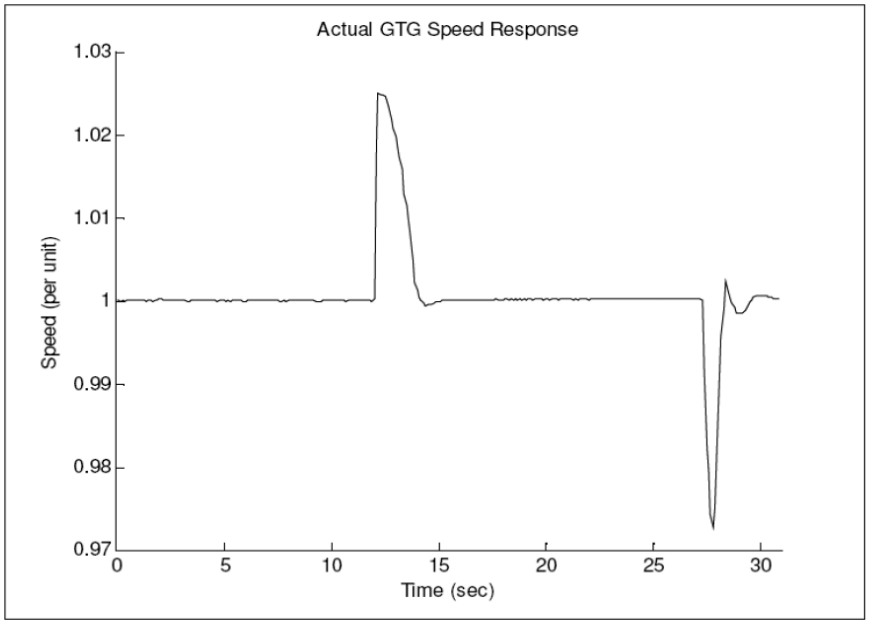

problem, though not conveniently solved due to the limitations of the board, can be improved. A simple improvement would be to split the 0-10 V power supply remote control signal between two analog outputs between 0-5 V and then use an operational amplifier to sum these two voltages. The resulting terminal voltage control signal would be precise to 512 partitions of 0-10 V instead of only 256. This circuit is built and is an easy extension for the project if more precision is found to be necessary.

Despite the improvement that can and should be made to this system, it is currently set to operate as close as possible to the GTG operating characteristic. For instance, when a smaller load that does not saturate the power supplies is applied, the model's response is the closest it can be to the GTG model. The response shown in Figure 12 is similar to the actual GTG model. The response of the scaled model was tuned to fit this response as best as possible.

Figure 12: The response of the system to less than rated load (225W to 675W and back to 225W). This is the closest the scaled system can come to the GTG model.

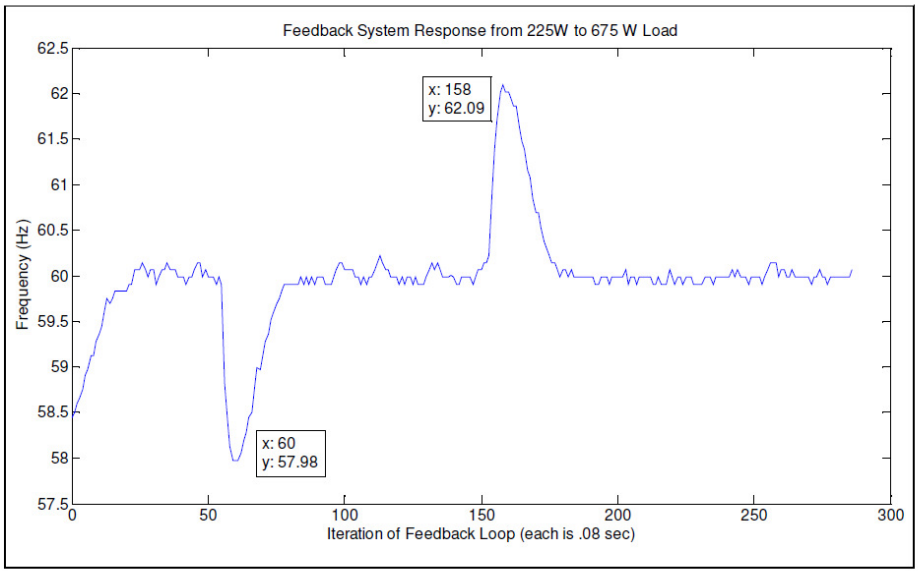

6. User Interface User Manual

The user interface for the model is implemented in LabVIEW. Front panel testing can be done easily for manual, step, or variable feedback control. The Panel is shown in Figure 13. Operation from this screen is straightforward. However, editing the code for the interface is much more complex. Both operations will be discussed in this section.

6.1 Panel Control

The Panel is designed to provide some flexible testing and control options. Iterations of testing for the software and for the system models drove an interface design that has multiple operating methods, the user must designate the operating method prior to running the control software. There are three options that are available for operation;

Figure 13: The Panel User Interface

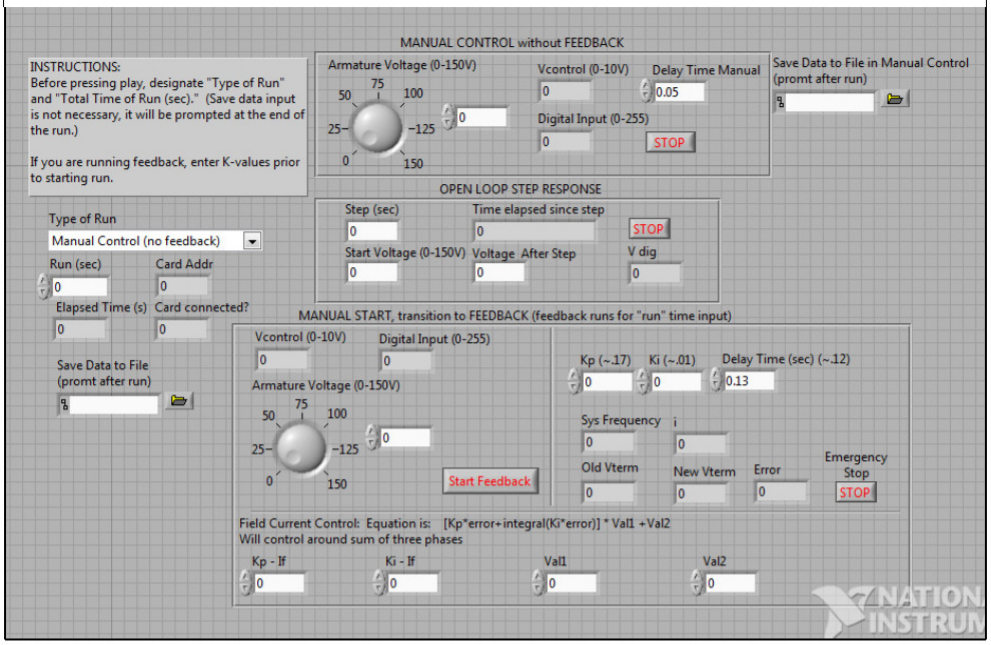

1. Manual control of DC motor input voltage and generator field current without feedback. This set-up was designed for preliminary testing. It remains on the user interface so that it is easily accessible if new elements are integrated into the system and manual control is necessary for testing.
2. Open-loop step response of motor input voltage provides an easy set up for open-loop step response testing.
3. A feedback system. In this option manual control of V_{cr} is allowed for an undesignated amount of time so that the operator can put the motor in whatever steady state condition they wish to start the test in, operations during this time are not saved or timed. When ready, the operator presses the 'Start Run' button and the feedback loop takes over V_{cr} control. The feedback loop will run for either the pre-designated run time or until the 'Emergency Stop' button is pressed.

6.1.2 Running

After opening Panel and before hitting the LabVIEW run button, the user must designate the run type. They also must designate the total run time. For open-loop step response and control, further test variables should be set before the program is run. However, these values are adjustable during operation – especially for feedback control prior to pressing the 'Start Feedback' button.

When the runs LabVIEW, the Card Address should change to 0 and 'Card Connected?' should be one, representing true. If this is not the case, the USB is not plugged in, or there is a major problem with the block diagram. The next step will likely to be to adjust the voltage manually (for manual and feedback control). Voltage input can be controlled by dial or by typing into the textual prompt to the left of the "Armature Voltage" dial. The input value to this controller will be exactly the output of the power supply.

For feedback, there are important settings to pay attention to. The K_p and K_i values as well as the time delay need to be set on the Panel. Also, the dead band size will by default be .08 multiplied by the average of the gains and then by 150. This can be adjusted in the block diagram if desired.

6.1.3 Saving

Data is recorded at discrete time intervals from every analog input on the I/O board. The saving time interval is the same as the feedback interval during feedback, it can be set on the Panel in the other settings. At the end of a run, the Panel will automatically prompt the user for a file path to save the data. The data is saved in vertical columns. Table 2 provides a list of the column headers. The Panel saves all analog inputs to the files it creates. Even though some columns are empty under the current set-up, this saving method provides allows for easy extension of data acquisition. The data can be imported to excel or MATLAB for analysis.

Table 2: Column Headers in a Panel data acquisition file

COLUMN	MEASUREMENT	RANGE /UNITS
1	Time	Time Delay (seconds)
2	System Frequency	50-70 Hz
3	Terminal Voltage	0-150V
4	V_{RMS} Φ_A	0-250 V
5	V_{RMS} Φ_B	0-250 V
6	V_{RMS} Φ_C	0-250 V
7	Frequency Error	Voltage
8	Integrator Sum	Voltage
9	Dead Band Indicator	Boolean

6.2 The LabVIEW Block Diagram

The code for the Panel is graphically designed a block diagram. A snapshoot of part of the block diagram is shown in Figure 14. Future operators of the system can adjust the design of the control system by editing this code. The basic format is a sequential loop that commands the I/O card. The card must first be opened before it can be controlled. Then, depending on the user's choice of operating scheme, an operating loop, usually a while loop, will execute until the time is expired or a stop button is pressed. As the while loop executes, board data is read into an array that builds indexes every time the loop executes. At the end of the loop, the data array is saved. After saving, the card is cleared of data commands and then closed. Sub-VIs that execute data conversions, control methods, and the actual feedback have been designed to simplify the highest level loop for the system.

Figure 14: Part of the LabVIEW Panel Block Diagram. LabVIEW Panel has many layers of block diagrams to simply the graphical code.

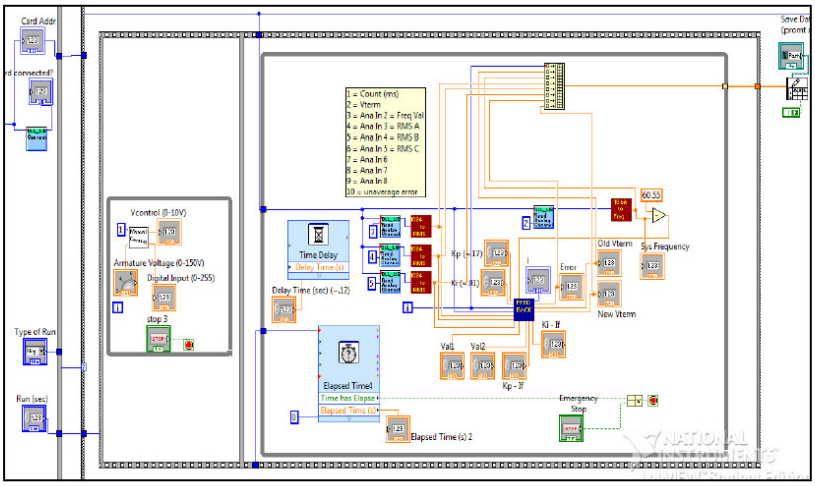

The I/O card commands are in the form of sub-VIs and are stored in the 'VIs' folder within the UILib. Depending on whether the operating system of the computer uses 32 or 64 bits, there are different DLL libraries that must be used. To switch between the two, one must recompile the library and replace each sub-VI. There is also a small but major bug in the DLL library in the 'ReadAnalogChannel' function. This essential function does not return the data in as written in the DLL library, however, the operator can fix this problem by editing the header file and ensuring that the data is returned manually during the LabVIEW compilation of the functions.

7. Conclusion

The results from this project show that a future Table Top test bed is most likely possible with the addition of more powerful power supplies. It may be possible to more closely approximate the GTG response on this system if these supplies were larger. Also, improvements

could be made in the control loop with a possible inclusion of a derivative term for a smoother return to steady state. Maximum load could not be applied in these samples due to both the limitations of the power supply and the load test-bed. However, Figure 13 shows a summarizing image of load application and removal with working feedback. The load changes from 225W to 675W in this run.

Many lessons were learned in this project. The use of LabVIEW was central to this project and the programs strengths and weaknesses became clear to the author, strengths being power and depth of the National Instruments systems, and weaknesses dominated by the inconvenience of not using National Instruments hardware and Toolboxes for implementing the interface. Despite this, I still believe that LabVIEW has provided a very user friendly user-interface and easy incorporation of the third party DLL library.

Although magnetic interferences delayed the project and testing for many days, the effect of this phenomenon was a good lesson to have hammered home. The first few reactions were that the problem was in hardware, software, or the generator itself. However, it is important to always check physical connections and influences on the system. These major, game-stopping problems were quickly fixed once the cause was found.

In order for this problem to move forward, the software will be placed on a computer in lab. The drivers for the I/O card and LabVIEW will be stored in the lab. Also, for the aid of those who continue this project, the appendices of this paper will include more details on hardware and software operation. A file will be saved to the lab computer that includes these files as well as additional background information.

[i] "Governor/Voltage Regulator: Assignment Sheet Number 64B9-302." Surface Warfare Officer Student Guides from Newport, RI Surface Warfare Officers School.
[ii] Sheldrake, Alan. "Gas Turbine Driven Generators." Handbook of Electrical Engineering: For Practitioners in Oil, Gas, and Petrochemical Industry. 2003. John Wiley and Sons, Ltd.
[iii] Information about naval system provided by assignments from SWOS in Newport, RI and personal conversation with Carderock division of the Naval Surface Warfare Center. See graduate thesis, "Hardware Model of a Shipboard Generator" by Greg Elkins.
[iv] Boldea, Ion. Synchronous Generators. "6: Control of Synchronous Generators in Power Systems." 6-1. Taylor and Francis. 2006.
[v] Drury, Bill. Control Techniques Drives and Controls Handbook. Institution of Engineering and Technology. 2001.
[vi] "Governor/Voltage Regulator" pg. 7. See reference 1.
[vii] Drury, Bill. Control Techniques Drives and Controls Handbook. Institution of Engineering and Technology. 2001.
[viii] VanDoren, Vance. "The Three Faces of PID." Control Engineering International. March 7, 2007. http://www.controleng.com/article/ca6420825.html?nid=2361&rid=4606141
[ix] Ibid.,
[x] http://books.google.com/books?id=98-HDQ9GuBoC&pg=PA66&lpg=PA66&dq=pid+control+prevent+hunting&source=bl&ots=gqQWyoOPml&sig=MK8W-S3kjFfWtP2_UqyOl536asQ&hl=en&ei=ezUCSruWMMOMtgfr3KiIBw&sa=X&oi=book_result&ct=result&resnum=2
[xi] Ibid, 1.
[xii] Ibid. 7.
[xiii] Purchase Specifications for Allison 501-K34 used in naval system. Curtosy of NSWC, Carderock. See "Hardware Model of Shipboard Generator" thesis by Greg Elkins.
[xiv] Elkins, Greg. "Hardware Model of a Shipboard Generator." MIT Department of Mechanical Engineering Thesis, Spring 2009.
[xv] Online specifications for the STC-5 generator. "STC Series Three Phase A.C. Synchronous Generators. Accessed May 7, 2009. http://en.ccmotor.cn/myjh/showproduct.asp?id=7403&mylb=sell
[xvi] Leghorn, Jeremy. MIT Deparment of Mechanical Engineering Thesis, Spring 2009.
[xvii] Chapman, Stephen. Electric Machinery Fundamentals. McGraw-Hill. 2004.
[xviii] Ibid, 5.
[xix] Ibid, 17.
[xx] Ibid, 17.
[xxi] Umans, Stephens. "Transinet Performance of a High-Temperature-Superconducting Generator." Provided by Prof. James Kirtley.
[xxii] Y. T. Kim & *S.* H. Back, "The Speed Regulation of a DC Motor Drive System with a PI, PID, and Command Matching Controllers", Dongguk Journal, Vol. 29, 1990, pg. 525-541.
[xxiii] Ibid, 14.
[xxiv] Iblid, 16
[xxv] Ibid, 14.

Appendix C: Additional Generator Information, by Vanessa Esch

Appendix A: Additional Generator Information

Generator Specifications were found at the following website from the manufacturers in China. The generator was bought off eBay.

Details | Company | Contact

STC generators are to be used in town, the countryside, worksites, mountain and pasture lands as a electric power source for lighting purpose, It can also be used as a reserved power source for emergent case.

The generators are of drip-poof with rotary field type and with the adoption of harmonic excitation system, that allow your easy operation and simple maintenance. The generators are of three-phase four-wire type, making use of star connection with neutral point. The rated line voltage is 400V. phase voltage 230V. frequency 50Hz. power factor 0.8(lag). It can provide 60Hz and the other voltage's generator according to necessary.

They can be coupled with a prime mover directly or through V-belt making right or reverse continuous rotation at the rated speed. when the revolution slip of prime mover is 3% and load varies in the range of 0 100% cos 1.0-0.8 they give food constant voltage. After sudden change (increase or decrease)of load. the generators will soon return to their normal working state. without any starting devices the generator can directly start an unloaded squirrel cage induction

Type	Output		Mounting Dimension (mm)									Overall Dimension				
	KVA	kW	H	A	B	C	D	E	F	G	g	k	a	b	h±h	L1	L2
STC-5	5.8	5	132	216	178	89	328	80	10	27	54.8	12	542	260	184	00	480	270
STC-6	6.3	6	160	254	254	108	388	80	10	330	40.8	15	605	10	264	66	680	326
STC-7.5	9.4	7.5	160	254	254	108	388	80	10	33	40.8	15	605	10	264	66	680	326
STC-8	10	8	160	254	254	108	388	80	10	33	40.8	15	605	10	264	66	680	326
STC-10	12.5	10	180	279	203	121	421	10	12	37	44.8	15	605	39	264	96	610	366
STC-12	15	12	180	279	203	121	421	10	12	37	44.8	15	605	39	264	96	610	366
STC-15	18.8	15	200	318	228	133	481	10	14	42.5	61.8	19	605	78	306	40	660	400
STC-20	25	20	200	318	228	133	481	10	14	42.5	61.8	19	605	78	306	40	660	400
STC-24	30	24	200	318	228	133	481	10	14	42.5	61.8	19	605	78	306	40	660	400
STC-30	37.5	30	225	356	286	149	560	140	18	53	64	19	664	21	326	10	770	462
STC-40	50	40	225	356	286	149	560	140	18	53	64	19	664	21	326	10	770	462
STC-50	62.5	50	225	356	311	149	560	140	18	53	64	19	664	21	326	10	810	462

Type	Output		Voltage (V)	Current (A)	Power factor (cos)	Speed (r/min)	Ferq (Hz)	Pole Number
	KVA	KW						
STC-5	5.8	5	400/230	8.4	0.8	1500	50	4
STC-6	6.3	6		9				
STC-7.5	9.4	7.5		13.5				
STC-8	10	8		14.4				
STC-10	12.5	10		18.1				
STC-12	15	12		21.7				
STC-15	18.8	15		27.1				
STC-20	25	20		36.1				
STC-24	30	24		43.3				
STC-30	37.5	30		54.1				
STC-40	50	40		72.2				
STC-50	62.5	50		90.2				

Type	T2X-10	T2X-12	T2X-16	T2X-20	T2X-24	T2X-30	T2X-40	T2X-50	T2X-64	T2X-75	T2X-90	T2X-120	T2X-150	T2X-200	T2X-250
Rated output	10	12	16	20	24	30	40	50	64	75	90	120	150	200	250
Rated current	18.1	21.7	28.9	36.1	43.3	54.1	72.2	90.2	115	135	162	217	271	361	451

(http://en.ccmotor.cn/myjh/showproduct.asp?id=7403&mylb=sell)

Appendix D: Parts List, by Vanessa Esch

Appendix B: Parts List

Terminal Voltage Power Supply: (2 x) Xantrex XHR 150-7 Power Supply

Field Current Power Supply: Instek PSP-603 Programmable DC Power Supply, 60V/3.5A

Input/Output Card: Velleman K8061 Hobbyist Board (also called, preassembled, a VM140)

DC Motor: (2 x) Leeson Direct Current Permanent Magnet Motor. Model: C42D34OT7A, Volts: 120V, RPM: 4800 RPM, Current: 14A, 2 H.P.

Pulley: McMaster-Carr Drive Pully, L-series, 22 teeth, ½", Bushing bore, Part Number 6495K213

Generator: STC-5 Ming Dong Generator, 5KW, 4 pole machine

Speed-to-DC Converter: (See Appendix C)

RMS-to-DC Converter: (See Appendix C)

Note: Converters are shown in Appendix F of this thesis. Addition to the parts list made below.
- Greg Elkins

Addition

Parts listed below were purchased through McMaster-Carr (www.mcmaster.com) unless otherwise specified.

5KW 3-Phase Generator: listed above, Purchased through Georgia Generator on ebay (stores.shop.ebay.com/Georgia-Generator) operated by Tom Osborne (478-457-5524)

Motor Pulley: listed above

Motor Pulley Quick-Disconnect Bushing: Style JA, 5/8" Bore, Part # 6086K112

Generator Pulley: Timing Belt Pulley, L Series, 32 Teeth, OD 4.06", Bushing Bore, Part # 6495K218

Generator Pulley Quick-Disconnect Bushing: Style SDS, 1-1/2" Bore, Part # 6086K324

Timing Belt: Trapezoidal Tooth, Neoprene, L-Series, 1/2" Width, 39" Outer Circle, 3/8" Pitch, Part # 6484K157

Motor Coupling (connects 2 motors): Steel One-Piece Set-Screw Coupling, 5/8" Bore, 2" Length, 1-1/4" OD, Without Keyway, Part # 6412K15

Gearbox (for future consideration): Howse Gearbox for M60 Rough Cut Mower, 55HP, 1.47 Gear Ratio, Model # 45PRC30147-N, available at Northern, Tool + Equipment (www.northerntool.com)

Appendix E: Pictorial, by Vanessa Esch

Appendix C: Pictorial Walk-Through System

1. The first step in the control of the system is setting the Terminal Voltage and Field Current from the LabVIEW software interface. The laptop is shown as arranged during testing.

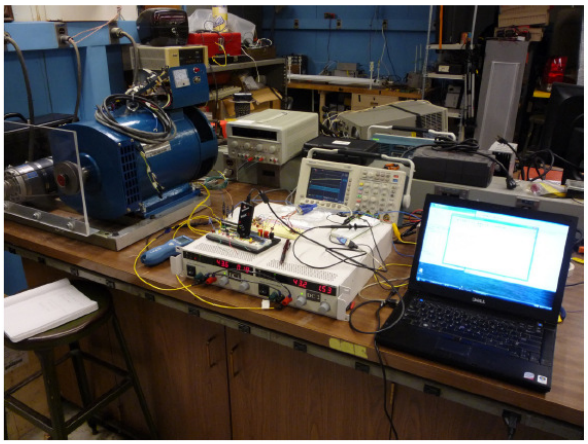

2. A USB connects the laptop and K8061 card.

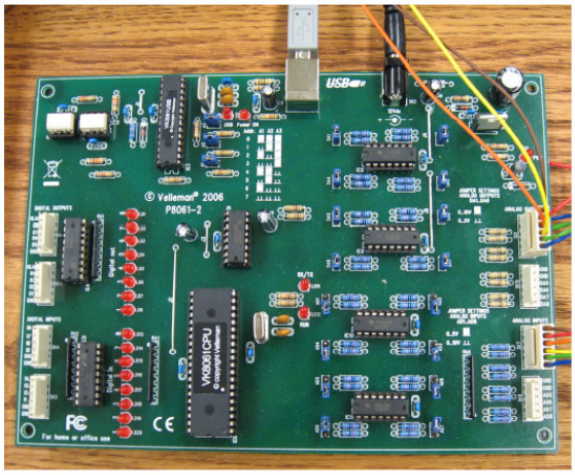

3. The output from the K8061 card and ground go directly to the back of the Power Supply (red and black) to command its output voltage. Current out of the terminal voltage power supply is not actively controlled but is a function of the load on the system.

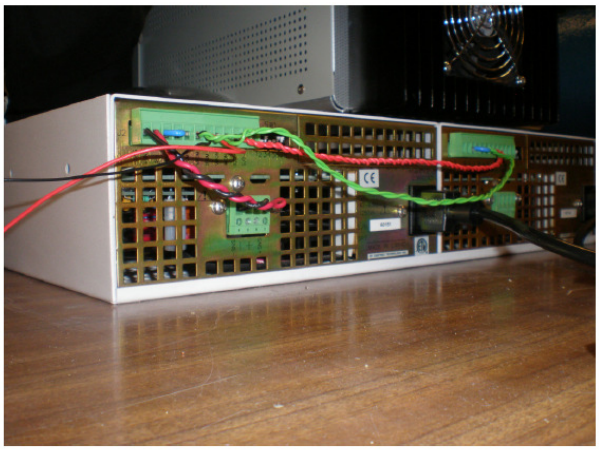

4. Terminal voltage from the power supply is applied to the prime mover DC motor rotors in series. (Yellow wires)

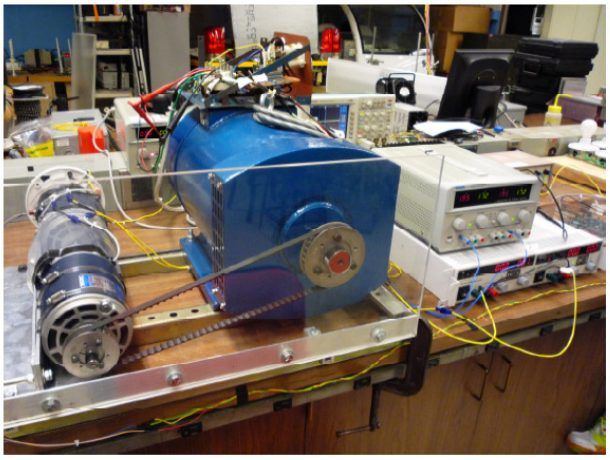

5. A Hall Effect Sensor reads the speed of the prime movers. (See previous picture, far side of motors.)

6. The digital output of the Hall Effect Sensor is sent to a conversion board that outputs an analog voltage between 0-10 V that corresponds to the frequency of the system. Board on the left.

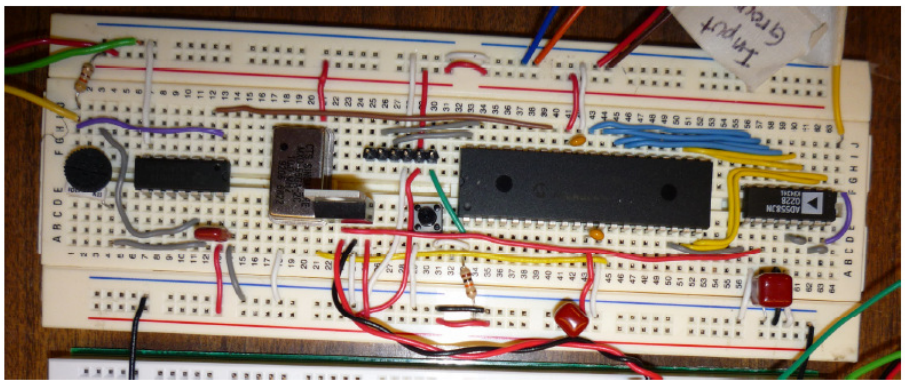

7. The prime mover mechanical torque is transferred to the generator via V-belt.

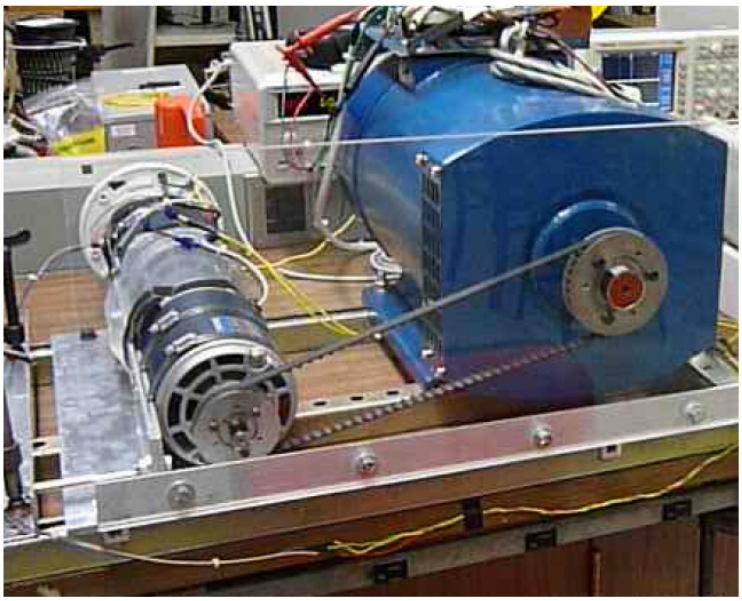

8. The output voltage from the generator goes to the load bed

9. The output from the generator is stepped down and then applied to the RMS-to-Analog conversion board. The output of this board is set to the K8061 board and then to the software feedback loop.

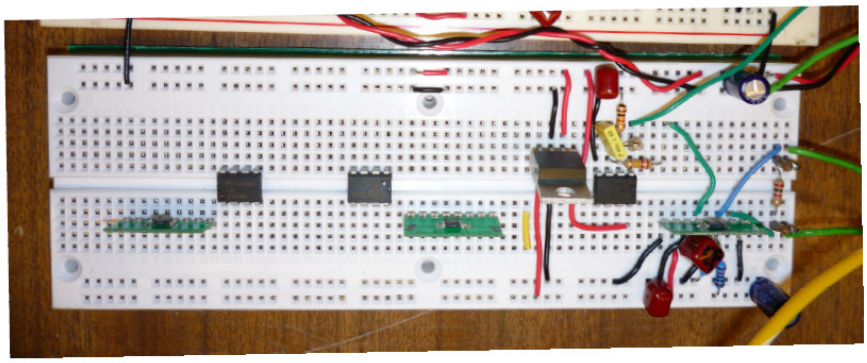

Appendix F: Signal Conditioning, by Jacob Osterberg

Generator Feedback Electronic Hardware Specifications

Jacob Osterberg
Spring 2009

Overview:

Two additional circuits were necessary beyond the Velleman Extended USB Interface Card in order to interface the generator system and the measurement computer. Both speed and voltage measurements of the system were necessary. Since the extended USB interface card did not have input hardware interrupts, it would have been difficult to accurately measure the TTL input pulse from the Hall Effect speed sensor on the motor. Therefore the frequency converter circuit was created to convert this TTL pulse into an analog voltage easily readable by the USB interface card. The generator voltage measurement may have been possible through fast sampling with the USB interface card, but an outside RMS conversion would be less taxing on the card, provide a more accurate measurement, and reduce the software complexity in Labview. For this reason a RMS converter circuit was built to measure, amplify and filter the generator voltage. Finally a modified version of the frequency converter was designed as a PCB with some additional capabilities.

RMS Converter:

Function:

This circuit receives an AC voltage waveform with an amplitude of up to 350V and converts it into a RMS value scaled from 0 to 10V.

Details:

Three identical circuits (one for each phase voltage) use a resistor divider to scale down an AC input waveform from a maximum amplitude of 350V to a 1V maximum AC input to the Linear Technology LTC1966 RMS chip. Since the LTC1966 does not have a negative voltage supply it was necessary to insure the input AC waveform does not fall below 0V. This is accomplished by using a simple resistor divider creating a reference voltage of 2.5V for the 1V AC waveform to oscillate around. The output of the LTC1966 is then averaged by a 1uF capacitor on its output. Next a passive filter with a cutoff frequency of 15.4 Hz further smoothes the waveform. Finally the signal is amplified by an AD358 op-amp resulting in a final output voltage of 10V for a 350V peak AC input. As currently configured a RMS voltage of 208V corresponds to an 8.2V output from the circuit and a RMS voltage of 120V corresponds to a 4.8V output.

Discussion:

When selecting resistors for the circuit it is essential that great care be taken in measuring and noting the actual value of the resistances and

not their stated value. Most resistors have tolerances of 5-10%. This variation of 5-10% can greatly affect the resistor dividers and the op-amp amplification circuit. While it is possible to purchase resistors with smaller tolerances, the higher tolerance resistors can work fine. Through direct measurement, only resistors with values close to the desired value will be selected. Also in the final circuit calculation actual measured values should be used instead of the ideal printed values on the resistor.

An averaging capacitor of 1uF was selected for the output of the LTC1966 RMS chip as recommended by the datasheet. An additional passive filter with a cut off frequency of 15.4 Hz was also added to smooth the output waveform. These act as a significant delay to the voltage measurement, but greatly reduce the noise. The passive filter may have to be changed for future measurements depending on the acceptable delay and noise when using the RMS signal.

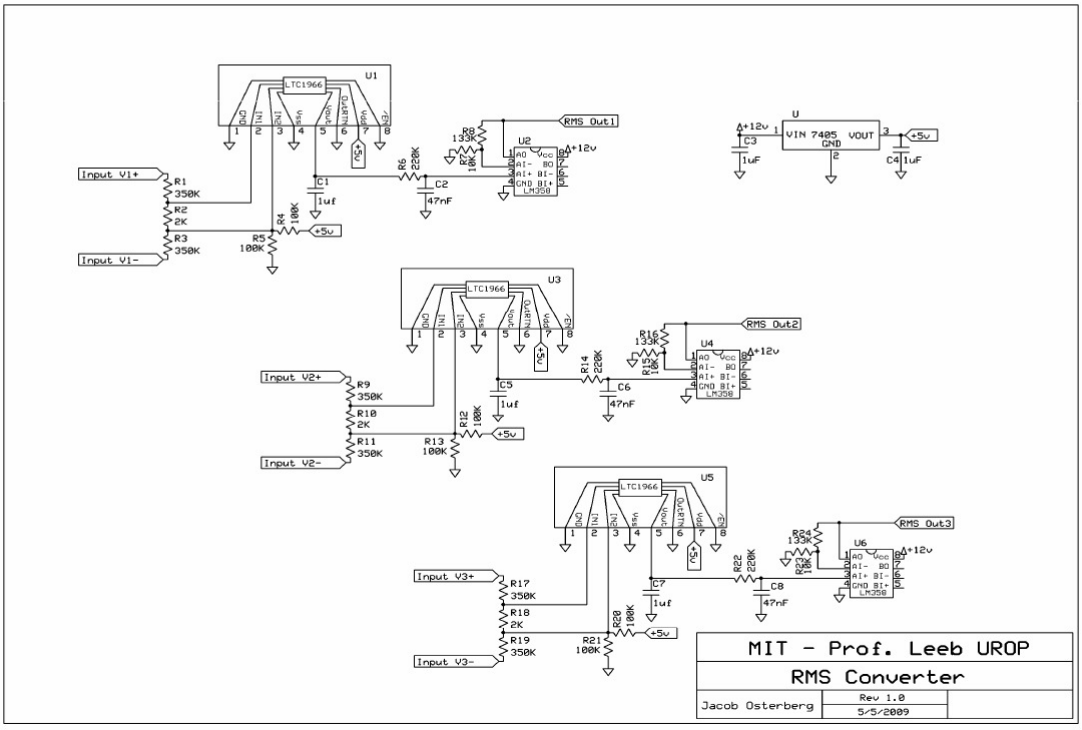

Figure 1: RMS Converter Schematic

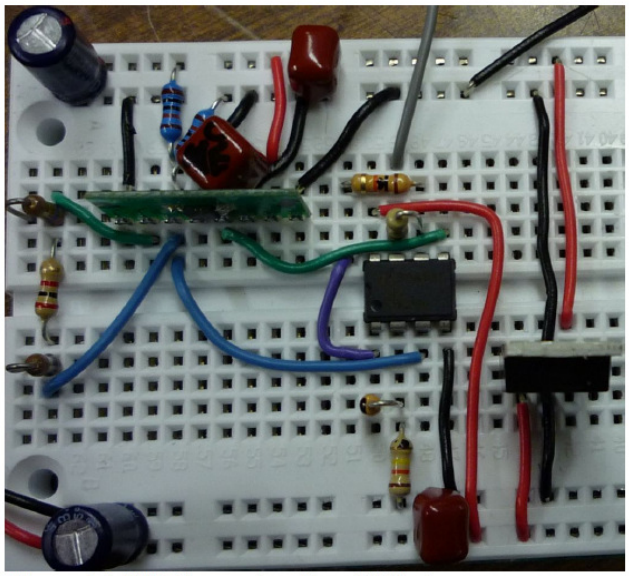

Figure 2: RMS Converter Circuit Photo

Frequency Converter:

Function:

This circuit receives a TTL square wave pulse input and converts the frequency of that pulse within a specified range to a 0 to 10V analog output with 256 discrete values.

Details:

A TTL square wave input ranging from 40Hz to 2500Hz is input into a 74HC14. The signal is then sent to a PIC18F4620 microcontroller. Depending on constants set in internal code the microcontroller outputs a scaled 8 bit value to an AD558 DAC. The result is an analog voltage which corresponds to the input frequency. The maximum output voltage is 10V with a minimum of 0V. There are 256 possible steps in the analog output voltage.

Discussion:

Currently the input pulse is received from a Hall Effect sensor connected to the motor driving the generator. The sensor triggers 14 times for every revolution of the motor. At an output frequency of 60Hz from the generator this corresponds to a 611Hz signal from the sensor. This circuit is set to output 0V from 0-509Hz (there is a slight glitch at 38.147Hz from the internal timer overflowing, but it has a very small <0.1Hz bandwidth and should not effect the general operation of the circuit). The sensor frequency of 509Hz corresponds to a generator

voltage frequency of 50Hz. At 611Hz (a generator voltage frequency of 60Hz) the output will be 5V and at 713Hz (a generator voltage frequency of 70Hz) the maximum output voltage of 10V will be reached. All measurements from the sensor at greater than 713Hz will result in a 10V output.

The frequency conversion can be easily changed in the PIC software by modifying the constant values in "frequency.h". This allows for an easy change from 509-713Hz to anything desired within the 40-2500Hz range of the current setup. Since there are only 256 values available from the DAC this range should be modified to suit the needs of the system. A larger 10bit DAC could also be substituted with minor additional programming in order to increase the resolution of the system to 1024 values.

The 74HC14 Schmitt Trigger may seem redundant in this circuit, but it provides a buffer between any inputs and the microcontroller. Also if the input signal is not perfect the 74HC14 will ensure a nice edge delivered to the microcontroller interrupt. The 74HC14 also has an oscillator circuit built on it with a potentiometer in order for quick circuit testing to be preformed without the aid of a function generator.

The PIC18F4620 is overkill for this application, but it was familiar and available at the start of the project and provided the easiest microcontroller option. It also gives future flexibility for the entire feedback control loop to be moved into the microcontroller. For programming, I recommend using the PICkit 2 (http://www.microchip.com/stellent/idcplg?IdcService=SS_GET_PAGE&nodeId=1406&dDocName=en023805). It is a cheap programming option for PIC microcontrollers. For software, I used the MPLAB ICD software, available free from Microchip (http://www.microchip.com/stellent/idcplg?IdcService=SS_GET_PAGE&nodeId=1406&dDocName=en019469&part=SW007002), with the free student MPLAB C18 C complier also available from Microchip (http://www.microchip.com/stellent/idcplg?IdcService=SS_GET_PAGE&nodeId=1406&dDocName=en010014&part=SW006011).

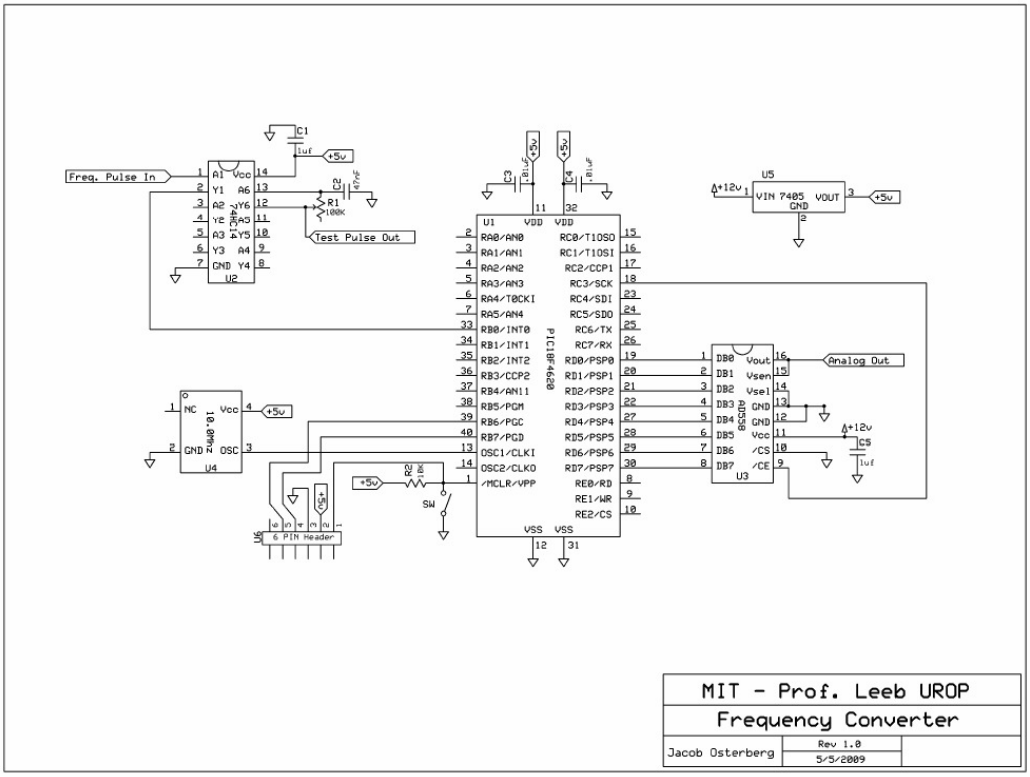

Figure 3: Frequency Converter Schematic

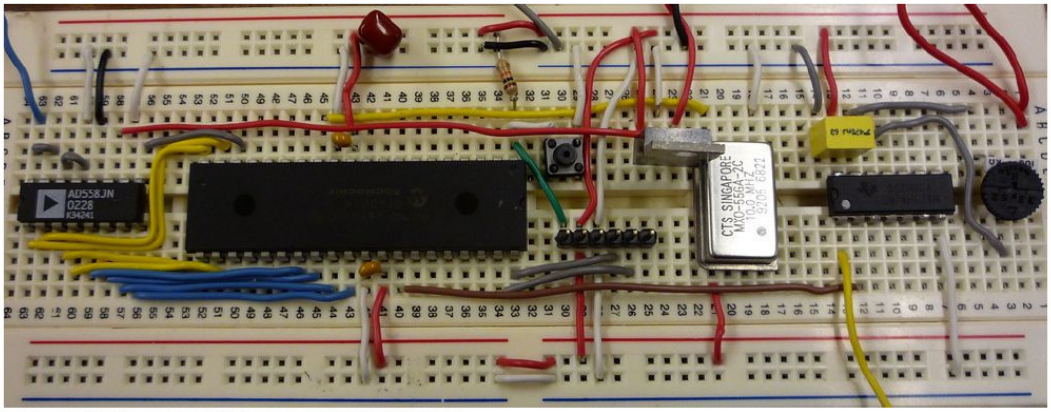

Figure 4: Frequency Converter Circuit Photo

Frequency Converter PCB:

Function:

This printed circuit board functions very similar to the previous frequency converter built on the prototyping breadboard, but it supports additional inputs and outputs including a serial port.

Details:

The same basic hardware is all present from the original frequency converter circuit. It has the ability to sense a TTL input and output a corresponding analog voltage. Additional features include access to more inputs and outputs and the ability to communicate to a computer through a serial port. Also switches and LEDs have been added for user functionality. Although all these features may be useful, it is not necessary to populate the entire board for it to perform the frequency conversion function. The MAX3221, DB9 and supporting capacitors are not required for the frequency function of the circuit. Take care to ensure that the correct pins are connected (by a jumper connector) on the AD558 for either 2.56V operation or 10V operation. When programming ensure that the white triangle on the PICkit 2 programming port lines up with pin 1 on the connector (also pin 1 on the PIC18F4620).

Discussion:

The functionality of this version of the frequency conversion circuit is much more than a simple measurement, calculation, and output. This circuit is capable of containing the entire feedback loop for the generator system. In addition, data can be sent to and from a computer connected through the serial port. The RMS voltage may also be measured by a built in 10bit analog to digital converter in the microcontroller. The possibilities of this circuit are also not confined to the generator system. This board provides many inputs and outputs useful for additional applications. When used with the PICkit 2 programmer from Microchip, this board becomes a very powerful tool to quickly measure and respond to many different signals.

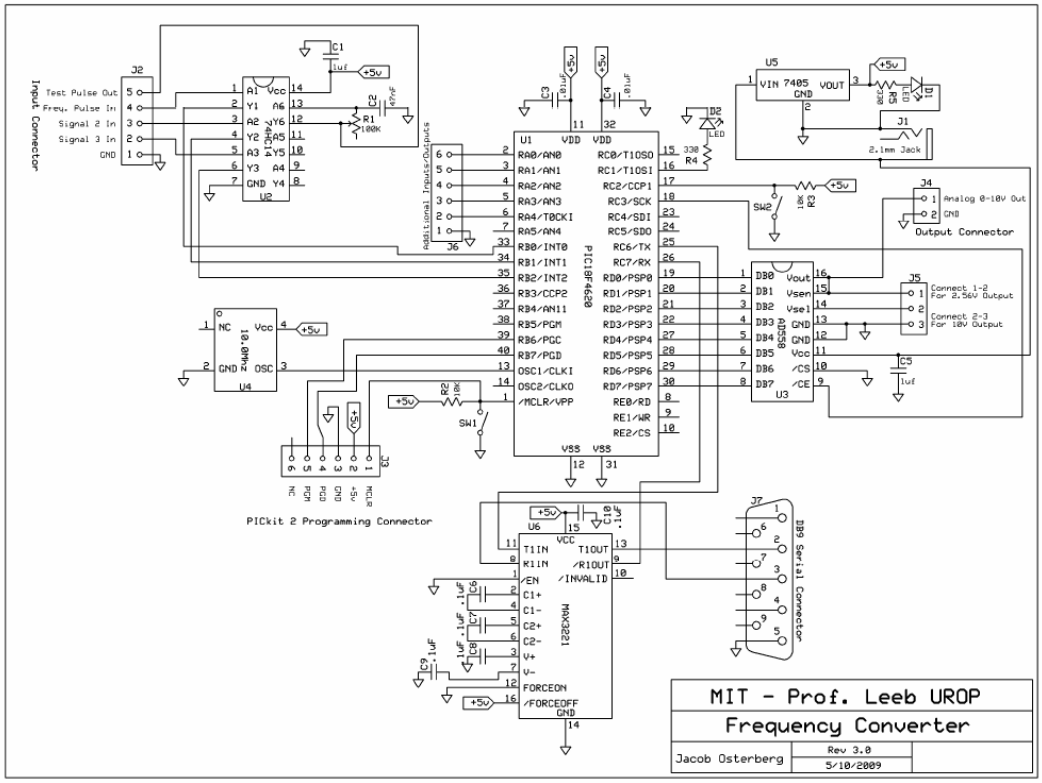

Figure 5: Frequency Converter PCB Schematic

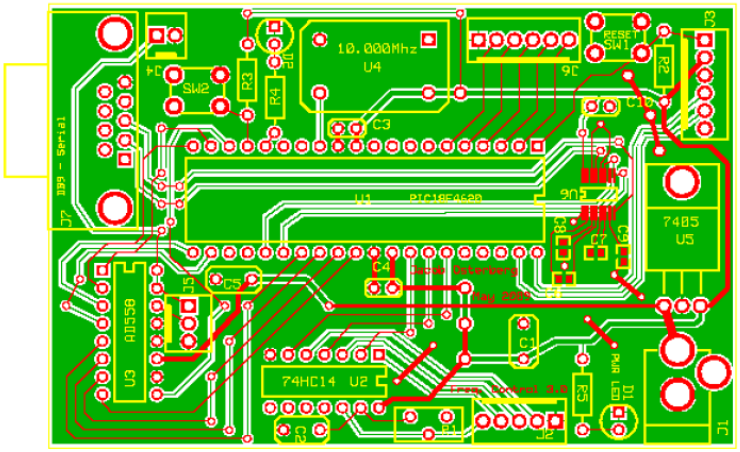

Figure 6: Frequency Converter PCB Board

Parts List for Frequency Converter PCB:

C1	1uf Through Hole
C2	47nF Through Hole
C3	.01uF Through Hole
C4	.01uF Through Hole
C5	1uf Through Hole
C6	.1uF 603 Surface Mount
C7	.1uF 603 Surface Mount
C8	.1uF 603 Surface Mount
C9	.1uF 603 Surface Mount
C10	.1uF Through Hole
D1	Red LED
D2	Red LED
J1	2.1mm Jack
J2	5 Pin .1" Spacing Header
J3	6 Pin .1" Spacing Header
J4	2 Pin .1" Spacing Header
J5	3 Pin .1" Spacing Header
J6	6 Pin .1" Spacing Header
J7	DB9 Right Angle Through Hole Connector
R1	100K Pot Through Hole
R2	10K Through Hole
R3	10K Through Hole
R4	330 Through Hole
R5	330 Through Hole
SW1	Momentary Push Button Switch SW403-ND
SW2	Momentary Push Button Switch SW403-ND
U1	PIC18F4620 (40pin DIP)
U2	74HC14 (14pin DIP)
U3	AD558 (16pin DIP)
U4	10.000Mhz Crystal Oscillator Full Size
U5	7405 5V Regulator (T0-220)
U6	MAX3221 (16pin SSOP)

Frequency Converter PIC18F4620 C Code:

```
//Jacob Osterberg
//Spring 2009
//Frequency Converter
//freqMain.c

//**Remember to set the configuration bits
//****Oscillator -- HS-PLL enabled freq=4xFosc1
//****PORTB A/D Enable -- PORTB<4:0> configured as digital I/O on RESET
//****Low Voltage Program -- Disabled

#include <p18f4620.h>
#include "frequency.h"

void low_isr(void);
void high_isr(void);

#pragma code high_vector=0x08
void interrupt_at_high_vector(void)
{
  _asm GOTO high_isr _endasm
}
#pragma code /* return to the default code section */

#pragma interrupt high_isr
void high_isr (void)
{

        if(INTCONbits.INT0IF){
                FREQ_ISR();
        }

}

#pragma code low_vector=0x18
void interrupt_at_low_vector(void)
{
  _asm GOTO low_isr _endasm
}
#pragma code /* return to the default code section */

#pragma interruptlow low_isr
void low_isr (void)
{

  if(INTCONbits.TMR0IF){
        Timer0_ISR();
        }

}

void main(){
```

```
        Function_Init();

        INTCONbits.GIE = 1;     //global enable
        TIMER_0_RUN = 1;        //start the timer

        while(1){

                FreqToDAC();
        }

}

-----------------------------------------------------------------------------------------
//Frequency.h

#ifndef __FREQ
#define __FREQ

#include <delays.h>
#include <timers.h>
#include <math.h>

#define HIGH 1
#define LOW 0
#define INPUT 1
#define OUTPUT 0
#define TRUE 1
#define FALSE 0
#define ON      1
#define OFF 0

#define TIMER_0_RUN   T0CONbits.TMR0ON
#define TIMER_0_FLAG INTCONbits.TMR0IF
#define TMR0_CONST 2500000. // 1/2500000 = seconds per timer increment

//*****************************************************************
//Constants
#define MAX_FREQ 713            //Freq Value (Hz) resulting in maximum DAC output (<2500Hz)
#define MIN_FREQ 509                    //Freq Value (Hz) resulting in minimum DAC output (>40Hz)
#define FREQ_SCALE 60                   //Set largest with MAX_FREQ*FREQ_SCALE < 65535
#define DATA_OUTPUT_COUNT 14    //# of values averaged before output - (between 1-30)
#define DAC_MAX_VAL 255                 //# of DAC Values
//*****************************************************************

#define MAX_VAL (unsigned) MAX_FREQ*FREQ_SCALE
#define MIN_VAL         (unsigned) MIN_FREQ*FREQ_SCALE
#define FREQ_STEP (unsigned) ((MAX_FREQ*FREQ_SCALE)-
(MIN_FREQ*FREQ_SCALE))/DAC_MAX_VAL

void Function_Init();
void FreqToDAC();
void FREQ_ISR();

void Timer0_ISR();
void Timer0_Init();
```

```
void Write_DAC(char);
void Delay10();

#endif
```

```
//Frequency.c

#include "frequency.h"

unsigned int FREQ_L = 0;
unsigned int FREQ_H = 0;
unsigned int FREQ = 0;
unsigned int ave_FREQ = 0;
unsigned long total_FREQ = 0;

char Data_Flag = FALSE;
char Overflow_Flag = FALSE;
char Data_Count = 0;

//Initialization Function for interrupts, inputs, outputs and timer0
void Function_Init(){

        //Interrupts
        RCONbits.IPEN = ON;  //enable interrupt priority levels
        INTCONbits.PEIE = ON;  //peripheral interrupt enable

        //Setup INT0
        TRISBbits.TRISB0 = INPUT;  //RB0 INT0 is an input
        INTCON2bits.INTEDG0 = HIGH; //trigger interrupt on rising edge
        INTCONbits.INT0IF = FALSE; //clear the INT0 flag
        INTCONbits.INT0IE = ON; //enable INT0

        //setup DAC OUTPUT
        TRISD = OUTPUT;         //set D port as output
        PORTD = 0;  //initialize as 0
        TRISCbits.TRISC3 = OUTPUT;  //set C3 as output for DAC latch
        PORTCbits.RC3 = 0; //initialize as 0


        //Initialize Timer Zero
        Timer0_Init();

}

//Initialization of timer0
void Timer0_Init(){

        //timer 0 register setup
        //16 bit internal clock timer with 2x scalar
        //initially turned off
        T0CON = 0b00000001;
        INTCONbits.TMR0IE = ON;         //enable timer 0 interrupt
        INTCONbits.TMR0IF = FALSE;    //make sure the time 0 overflow flag not set
        INTCON2bits.TMR0IP = LOW;     //low priority interrupt

        //set timer to 0
```

```
        TMR0H = 0x00;
        TMR0L = 0x00;
}

//Sets the overflow flag if the timer overflows
void Timer0_ISR(){

        INTCONbits.INT0IE = OFF; //disable INT0 - don't let it harware interrupt while
                                                        //resetting the timer

        //notify system of overflow
        Overflow_Flag = TRUE;

        //clear the interrupt flag
        INTCONbits.TMR0IF = FALSE;

        //stop the timer
        TIMER_0_RUN = OFF;

        //enable INT0
        INTCONbits.INT0IE = ON;
}

//Takes an 8 bit value and writes it to the DAC
void Write_DAC(char data){

        PORTD = data;           //write data
        Delay10();
        PORTCbits.RC3 = 0;      //open latch for write
        Delay10();
        PORTCbits.RC3 = 1; //latch in data
}

//Runs when interrupt tiggers - gets the value of the timer, averages over DATA_OUTPUT_COUNT
//values, resets the timer, checks for overflow, and signals for output after
//DATA_OUTPUT_COUNT values
void FREQ_ISR(){
        unsigned int Time_L;

        if(Overflow_Flag == FALSE){

                TIMER_0_RUN = OFF;  //stop the timer

                //read the timer (have to read low byte first)
                Time_L = TMR0L;

                FREQ = TMR0H;
                FREQ <<= 8;
                FREQ |= Time_L;

                //Reset Timer
                TMR0H = 0x00;
                TMR0L = 0x00;

                //run the timer
                TIMER_0_RUN = ON;
```

```
                //These conditional statements only signal valid data for output
                //(by setting the Data_Flag) when the number of measured frequency values
                //is greater than DATA_OUTPUT_COUNT <-set in frequency.h
                if(Data_Count < DATA_OUTPUT_COUNT){
                        total_FREQ += FREQ;
                        Data_Count++;
                }
                else{
                        ave_FREQ = total_FREQ/DATA_OUTPUT_COUNT;
                        total_FREQ = 0;                 //reset the frequency sum
                        Data_Count = 0;                 //reset the data count
                        Data_Flag = TRUE;                       //set flag to output data
                }


                //reset the interrupt
                INTCONbits.INT0IF = FALSE;
        }
        else{
                //reset timer
                TMR0H = 0x00;
                TMR0L = 0x00;

                //TIMER OVERFLOW OUTPUT
                Write_DAC(0);
                Data_Flag = FALSE;

                //reset the freq interrupt
                INTCONbits.INT0IF = FALSE;
                //start the timer again
                TIMER_0_RUN = ON;
                //clear the overflow
                Overflow_Flag = FALSE;
        }

}

//Watches for new data and outputs to the DAC when data is available
void FreqToDAC(){
        long value = 0;
        unsigned data = 0;


        //if there is new data
        if(Data_Flag){

                //find the scaled frequency value
                value = TMR0_CONST*FREQ_SCALE/ave_FREQ;

                //see if the freqency is less than the allowed minimum
                //if so output 0 to the DAC
                if(value <= (MIN_VAL)){
                        Write_DAC(0);
                }
                //if the frequency is greater than the maximum value output
```

```
                //set the output to the maximum DAC output value
                else if(value >= (MAX_VAL)){
                        Write_DAC(DAC_MAX_VAL);
                }
                //if the frequency is within the correct range output it to the DAC
                else{
                        data = (value - MIN_VAL)/((unsigned) FREQ_STEP);
                        if(data < 255 && data > 0)
                                Write_DAC((char) data);
                }
        Data_Flag = FALSE;  //reset the new data flag
        }

}


//Delays for 10 cycles
void Delay10(){
        Delay1TCY();
        Delay1TCY();
        Delay1TCY();
        Delay1TCY();
        Delay1TCY();
        Delay1TCY();
        Delay1TCY();
        Delay1TCY();
        Delay1TCY();
        Delay1TCY();
}
```